ABSTRACT

WALKER, BRANDON RAY. Synthesis and Characterization of Orthogonally Self-Assembled Nanoparticle Heterodimers. (Under the direction of Christopher B. Gorman.)

This project involved the synthesis of novel bifunctional linear linker molecules that were used to bind gold and platinum nanoparticles using orthogonal self-assembly. These heterodimers were created as a model for the possibility of using similar bimetallic structures as molecular electronic components.

The binding affinities of the terminal thiol and isonitrile functional groups on planar surfaces and nanoparticles were analyzed using surface and transmission Fourier-transform infrared spectroscopy. It was found, qualitatively, that the binding affinity of the binding groups differed significantly depending on whether the functional group was binding to a planar surface or a nanoparticle.

The linking of two nanoparticles to form a heterodimer was also studied using transmission electron microscopy (TEM) and size-exclusion chromatography (SEC). While unable to provide quantitative results on heterodimer formation, TEM provided a straight-forward, though limited, method for demonstrating that some heterodimer formation did occur. The main limiting factor of TEM was the relative size difference of the particles in the heterodimer. SEC provided a more quantitative view of the heterodimer sample, but this technique introduced many variables that control the separation of nanoparticles and heterodimers. Results from the SEC experiments support the formation of heterodimers, but many of the variables inherent to the technique must be overcome for it to become a viable technique for routine analysis of nanoparticle arrays.

SYNTHESIS AND CHARACTERIZATION OF ORTHOGONALLY SELF-ASSEMBLED NANOPARTICLE HETERODIMERS

by
BRANDON RAY WALKER

A thesis submitted to the Graduate Faculty of
North Carolina State University
in partial fulfillment of the
requirements for the Degree of
Master of Science

CHEMISTRY

Raleigh, North Carolina
2007

APPROVED BY:

_____
Dr. Christopher B. Gorman
Chair of Advisory Committee

_____ _____
Dr. David A. Shultz Dr. Edmond F. Bowden

SYNTHESIS AND CHARACTERIZATION OF ORTHOGONALLY SELF-ASSEMBLED NANOPARTICLE HETERODIMERS

by
BRANDON RAY WALKER

A thesis submitted to the Graduate Faculty of
North Carolina State University
in partial fulfillment of the
requirements for the Degree of
Master of Science

CHEMISTRY

Raleigh, North Carolina
2007

APPROVED BY:

_____
Dr. Christopher B. Gorman
Chair of Advisory Committee

_____ _____
Dr. David A. Shultz Dr. Edmond F. Bowden

DEDICATION

This is dedicated to “My Girls.”

None of this would have been possible without the loving support of my wonderful wife, Shirley, or my beautiful daughters, Susannah and Isabelle.

BIOGRAPHY

Brandon Ray Walker was born on April 15, 1975 in Durham, NC to Susan Ray and Michael Walker. He spent his early childhood in Hillsborough, NC and then moved to Rocky Mount, NC when his mother remarried. He went to high school at Northern Nash Senior High where he was involved with track, theater, marching band, and winterguard. He graduated in 1993 and pursued his undergraduate studies at the University of North Carolina at Chapel Hill where he graduated with a Bachelor of Science degree in Chemistry in 1997. From there, he spent four years as a pharmaceutical analytical chemist in Research Triangle Park, NC before deciding to pursue an advanced degree at North Carolina State University in the fall of 2001. Also, in that time, he met his future wife, Shirley Robinson, through a mutual friend, and they were married on April 28, 2001. Their first daughter, Susannah Constance Walker, was born on November 14, 2004 and quickly became the one thing their world revolved around. Isabelle Ione Walker followed on October 4, 2006 and has been equally as precocious as her older sister.

ACKNOWLEDGEMENTS

First and foremost, I'd like to thank my wife, Shirley. Without her love, understanding, and support, I would not have been able to accomplish this. Second, I would like to thank my parents for their guidance in making the person I am today. I would like to acknowledge Dr. Christopher B. Gorman for his guidance and knowledge and thank him for the chance to work on this interesting project. I would especially like to thank Dr. Chris Cameron, Dr. Tyson Chasse, and Dr. Young-Rae Hong for their tremendous help when I first started with the group as a lowly "First Year." Their synthetic experience, as well as group procedures, were invaluable to me acquiring a solid foundation for my graduate work. Finally, I would like to thank Jennifer Ayres, Dr. Kusum Chandra, Dr. Drew Wassel, and Dr. Sheng Zhang for their assistance on many aspects of this project.

TABLE OF CONTENTS

LIST OF FIGURES

Chapter 1

Chapter 3

Chapter 4

LIST OF TABLES

Chapter 2

Chapter 4

LIST OF SCHEMES

Chapter 2

CHAPTER 1

Towards Synthesis of a Molecular Transistor

1.1 INTRODUCTION

1.1.1 Limitations of Current Silicon Techniques

The first computer was built in the 1940's and occupied 1800 ft^2, containing almost 17,500 vacuum tubes. Since that time, scientists have managed to reduce the size of computer components from centimeters to nanometers using solid-state technology. As predicted by Gordon Moore in 1968, the density of devices on a chip has doubled approximately every 18 months. This trend has come to be known as Moore's Law (Figure 1.1).[1] Unfortunately, deviation from this trend is expected to happen within the next decade as devices are scaled down out of the bulk regime and quantum effects begin to dominate electronic behaviors. Because of this expected bottom limit of silicon devices, molecular electronics is becoming an increasingly important area of research.

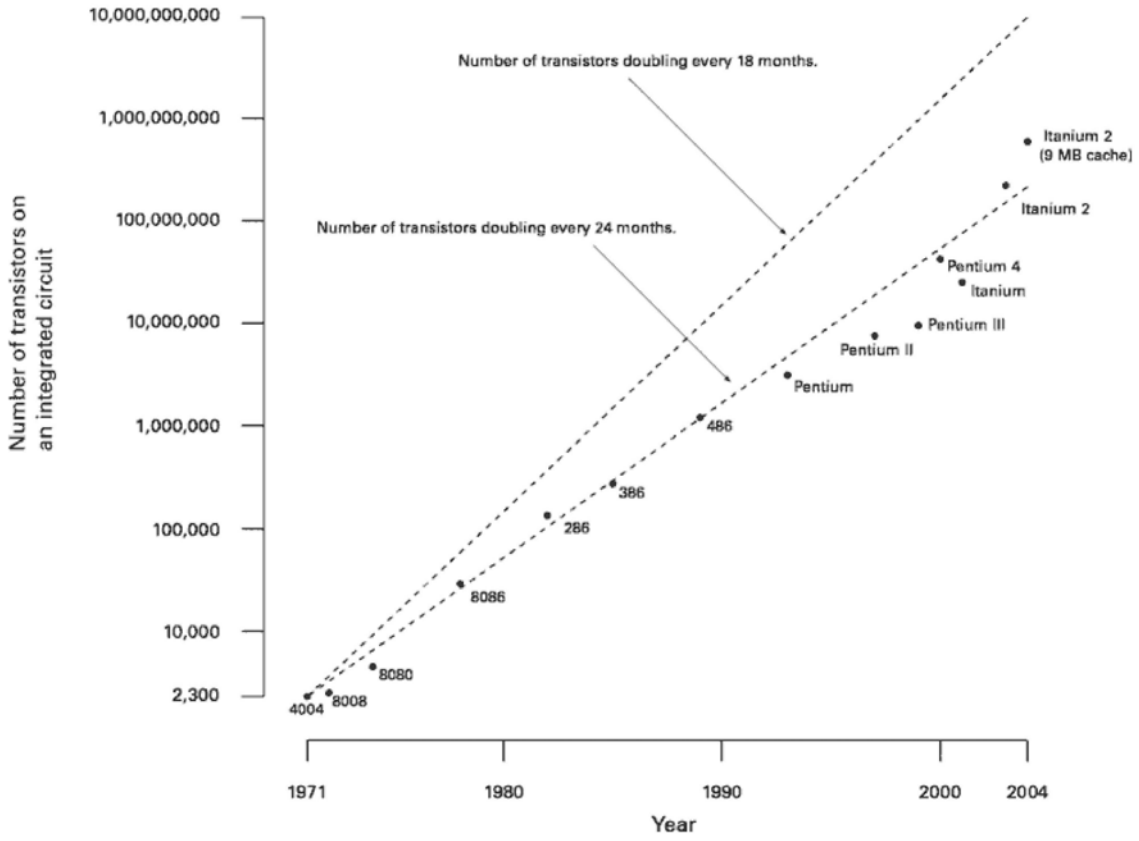

Figure 1.1. Growth of transistor counts for Intel processors (dots) and Moore's Law (upper line=18 months; lower line=24 months) [image from http://en.wikipedia.org/wiki/Moores_law].

While silicon technology has worked very well up to the present, there are several difficulties to overcome to allow further miniaturization of electronic components, specifically, the transistor. Aside from issues in scaling down the sizes of electrical devices, manufacturing silicon components in itself has some drawbacks. Numerous steps are required to create one wafer of field effect transistors, as shown in Figure 1.2. Because of this lengthy process, a significant amount of manufacturing waste is generated. A breakdown of the materials required to produce silicon chips as well as the cost is shown in Figure 1.3.[2]

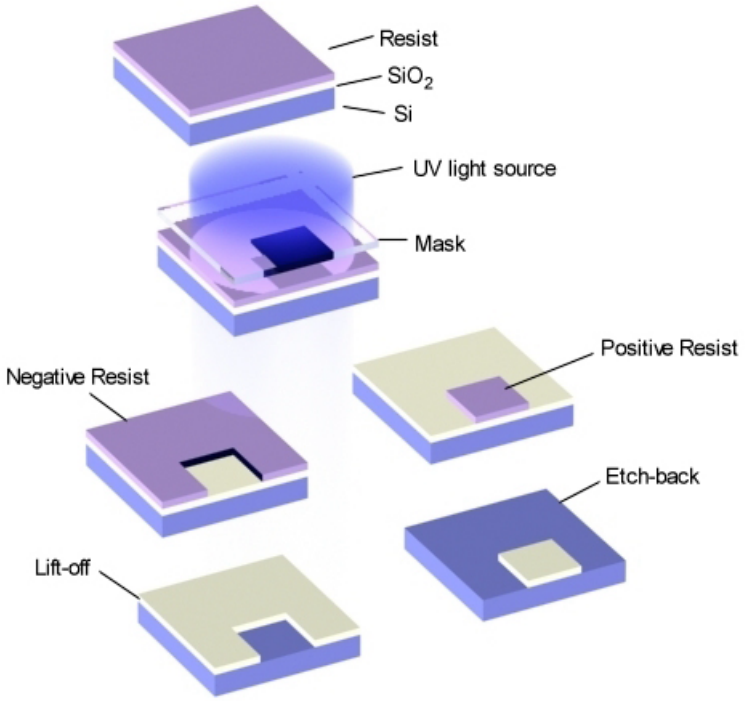

Figure 1.2. The main processes in photolithography [image from http://britneyspears.ac/physics/fabrication/photolithography.htm].

SEMICONDUCTOR MATERIALS

Moderate revenue growth is expected again for 2006

$ MILLIONS	SALES 2004	2005[a]	2006[a]
Silicon wafers	$7,554	$8,314	$9,118
Other substrates	640	670	720
Photomasks	2,775	3,045	3,183
Photoresists	876	916	946
Photoresist ancillaries	852	834	876
Wet chemicals	815	825	857
Gases	2,039	2,051	2,103
Sputtering targets	402	434	464
CMP slurries & pads	611	676	767
Other new materials	275	300	336
TOTAL	**$16,839**	**$18,064**	**$19,370**
GROWTH		7%	7%

NOTE: Individual figures may not add to total due to rounding. **a** Estimate. **CMP** = chemical mechanical planarization.
SOURCES: SEMI, Techcet Group (sputtering targets)

Figure 1.3. Costs of manufacturing semiconductor chips.[2]

In addition to manufacturing drawbacks, there are several obstacles involved with scaling down present silicon technology. A major concern for transistors is charge leakage across the gate oxide. As the transistor size is reduced, the overall thickness of the insulating gate is compromised. Once the thickness of the oxide reaches a minimum limit, it can no longer insulate the gate from the channel of the transistor and thus the transistor no longer possesses discrete on-off states. This behavior has resulted in an intensive search for gate materials with higher dielectric constants. One alternative that Intel has explored is use of hafnium compounds for the gate oxide.[3] Hafnium compounds have a higher dielectric constant allowing for thinner insulating layers. Intel's current 65 nm transistor has a gate insulator that is 1.2 nm. By switching to hafnium compounds it is hoped that the feature size of the transistor can be reduced to 45 nm with a 90% reduction in charge leakage. The main drawback of this approach is that the hafnium compounds are not compatible with current silicon gate electrodes requiring new metal electrodes to be examined.

Another obstacle to scaling down silicon electronics is the resolution of the photolithographic techniques employed to make them. Since photolithography is a major tool for processing electronic components, the size of these reduced components is limited to the resolution of the photolithography technique. Once the size of the feature being created is reduced below the wavelength of the light employed for the photolithography, more complicated lithography techniques are needed such as phase shifting photolithography, x-ray lithography, or interferometric lithography. Another difficulty is that as components are scaled down, their bulk properties (which are well known) begin to vanish and quantum effects (which are not as well known) begin to have increased importance.

1.1.2 Molecular Electronics

Aviram and Ratner proposed the idea of molecular electronics in 1974 as a way of allowing further miniaturization of electronics.[4] One advantage is that these components can be made using bottom-up manufacturing. Instead of starting with a large section of silicon and removing what is unwanted, the bottom-up approach builds up the necessary structure from atoms and molecules. Along with this is the added advantage of precisely controlling the structure of the device using well-known synthesis techniques. While there are many advantages of molecular electronics over silicon technology, several challenges still remain to be overcome before molecular electronics can be a viable replacement for silicon components.

A major challenge, after the synthesis of the molecular components, is establishing a method for insertion of these devices into patterned circuits. There is a definite need to be able to place the electronic device into a circuit and measure its electronic properties. Some of the current methods for measuring a molecule's electronic properties include: break junctions (Figure 1.4),[5] scanning tunneling microscopy (STM) addressing (Figure 1.5),[6] and self-assembled monolayers with a evaporated metal top contact.[7] One problem with these techniques is the nature of the contact between the molecules and the electrodes is not fully known. Also, it is difficult to verify if the property being measured is due to a single molecule or a collection of molecules.

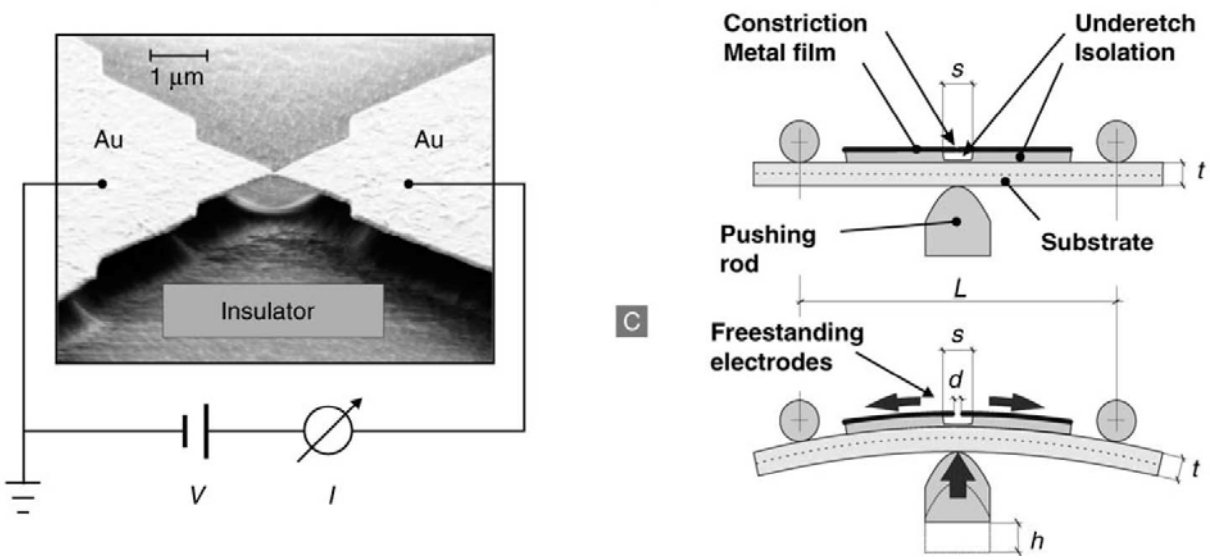

Figure 1.4. Schematic of a break junction designed to trap and electronically measure a single molecule.[5]

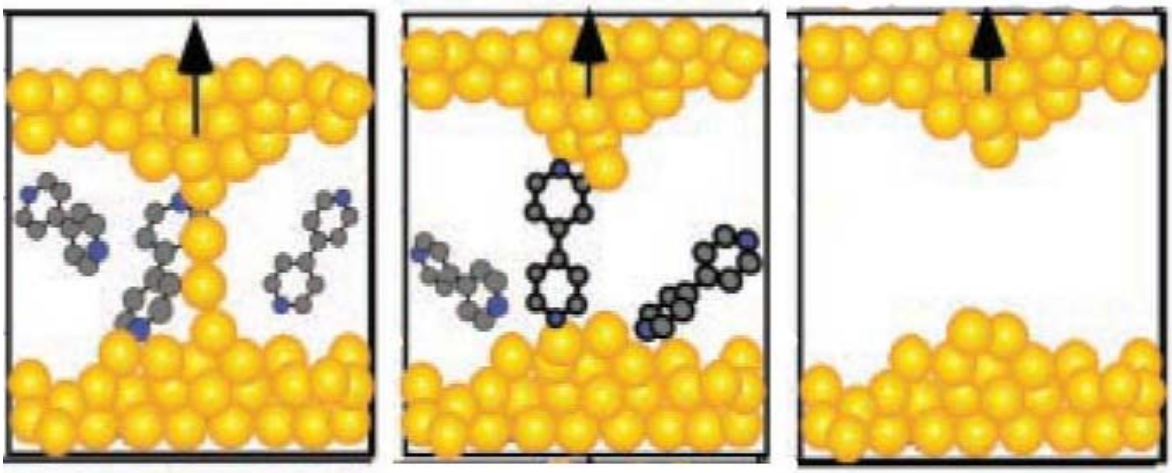

Figure 1.5. Diagram of a STM tip used to trap a single molecule for electronic measurement.[6]

Another technique receiving extensive research in the literature is the use of DNA to connect nanoparticles together. Mirkin et al.[8] have developed a method to selectively functionalize Au nanoparticles with DNA to allow the formation of nanoparticle arrays of controlled shape (Figure 1.6). Although this method is very selective, in molecular electronics, one is forced to tunnel through the binding groups and, for this reason, DNA is not attractive. Another drawback of using DNA is the inability to have a discrete length for

the linker molecule. Also, the DNA is not conductive, which would be a requirement of any molecular electronic device.

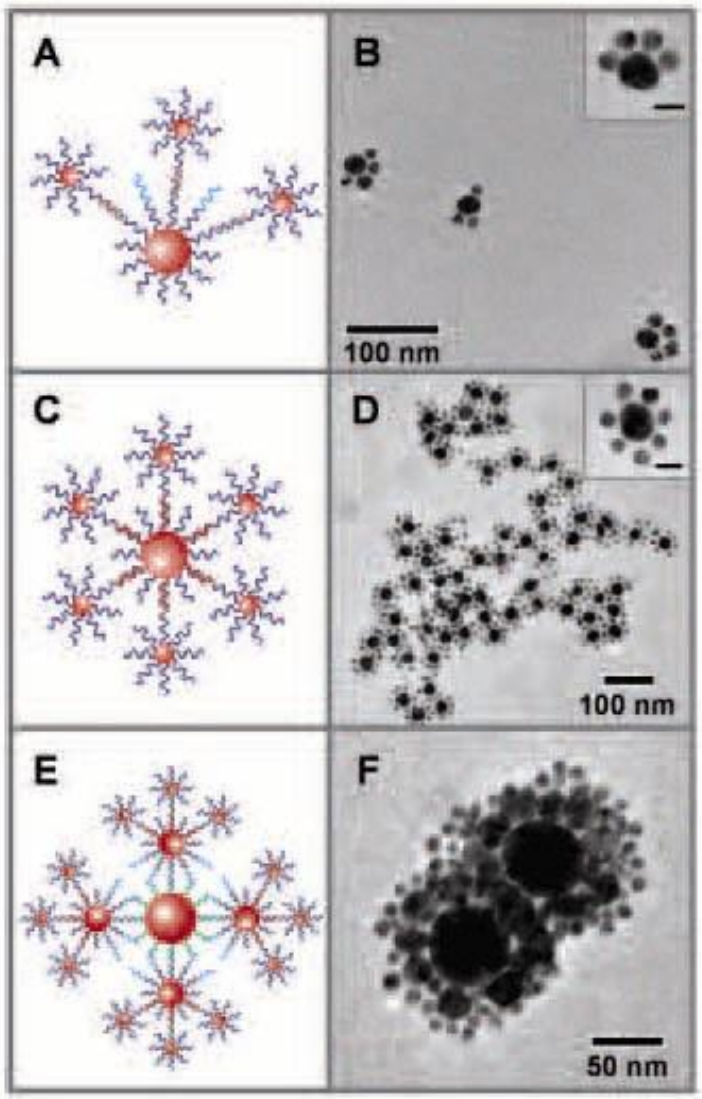

Figure 1.6. Assembly of DNA-functionalized, Au nanoparticle into (A, B) cat paw, (C, D) satellite, and (E, F) dendrimer-like structures.[8]

1.1.3 Orthogonal Self-Assembly

An alternative technique to what was described above is to employ orthogonal self-assembly to allow for precise placement of the molecule of interest into a circuit for measurement. Orthogonal self-assembly, first proposed by Wrighton and Whitesides in 1989,[7] utilizes the preference of one adsorbant to bind to a specific substrate over another

(Figure 1.7). In this way, it is possible to selectively bind different types of molecules to discrete regions on a chemically heterogeneous substrate. This concept provides a unique way to install molecular components into devices in a specific orientation. Prior research involving covalent binding of molecules to substrates for molecular electronics measurements has either involved a molecule with one terminus bound to a metal and the other contact made mechanically, [9-11] or used molecules with two identical binding groups.[12-15]

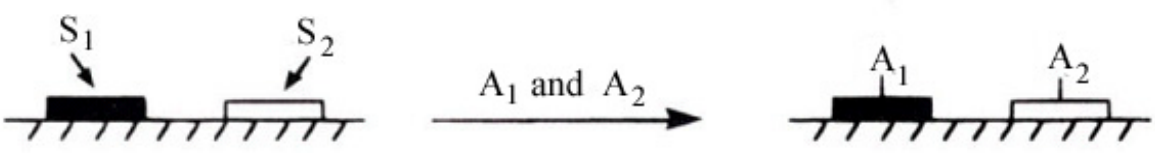

Figure 1.7. Visualization of orthogonal self-assembly where A_1 binds preferentially to S_1 and A_2 binds preferentially to S_2.[7]

Wrighton and Whitesides[7] first studied the binding of alkanethiols to gold and carboxylic acids to alumina (Figure 1.8). In their experiments, a heterogeneous surface consisting of Au and Al_2O_3 containing regions was exposed to an equimolar solution of alkanethiol and alkane carboxylic acid (~1 mM) in isooctane. The surfaces were then examined by x-ray photoelectron spectroscopy (XPS), which showed pure monolayers of alkanethiol on the gold regions and alkane carboxylic acid on the alumina regions.

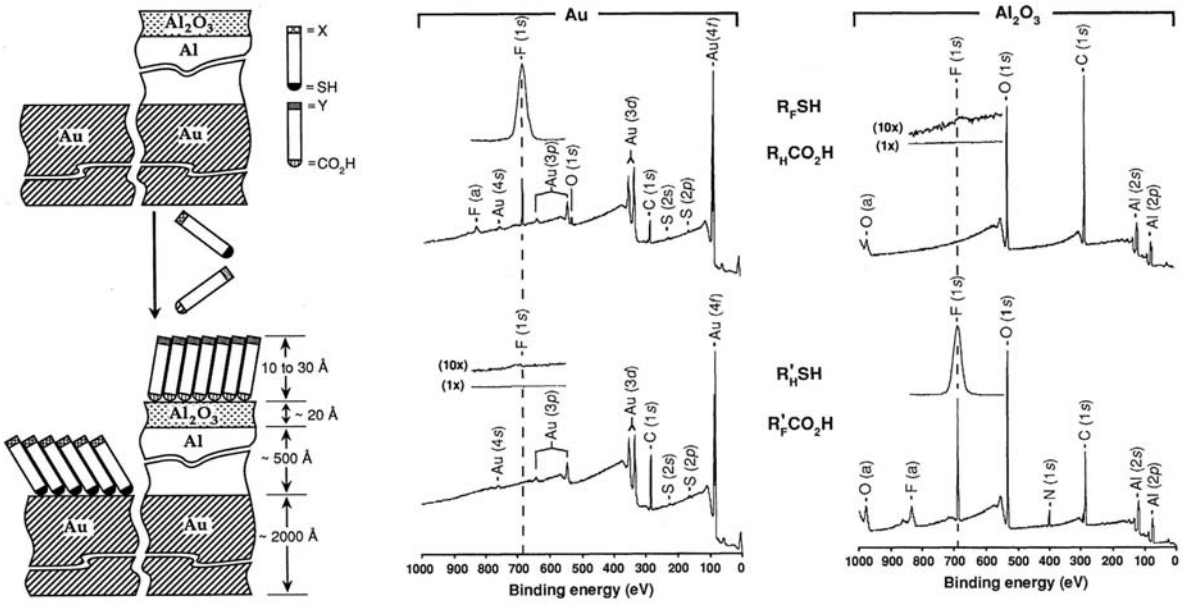

Figure 1.8. First example of orthogonal self-assembly demonstrated by Wrighton and Whitesides et al. [7]

The next set of adsorbants and substrates examined by Whitesides were disulfides on gold and isocyanides on platinum (Figure 1.9).[16] While the previous results using gold and alumina were promising for orthogonal self-assembly, gold and platinum were chosen for their usefulness as electrodes where Al_2O_3 is an insulator. The disulfide molecule contained an alkylferrocenyl headgroup, while the isocyanide molecule had an acylferrocenyl headgroup. The electroactive ferrocene groups allowed the respective surface concentrations to be calculated by cyclic voltammetry (CV) due to the 300-mV difference between the $E_{1/2}$ of the two headgroups. The initial results using an equimolar solution of disulfide and isonitrile showed an 8:1 preference of the Au towards isocyanide versus disulfide. The preference for Pt depended on the initial pretreatment of the surface, oxidized or reduced. Oxidized platinum showed a 200:1 preference of isocyanide over disulfide, while the reduced platinum showed a preference of 20:1. By using a concentration ratio of 40:1 disulfide:isocyanide, it was possible to form a monolayer with an isocyanide:disulfide ratio of 1:10 on Au and 10:1 on Pt.

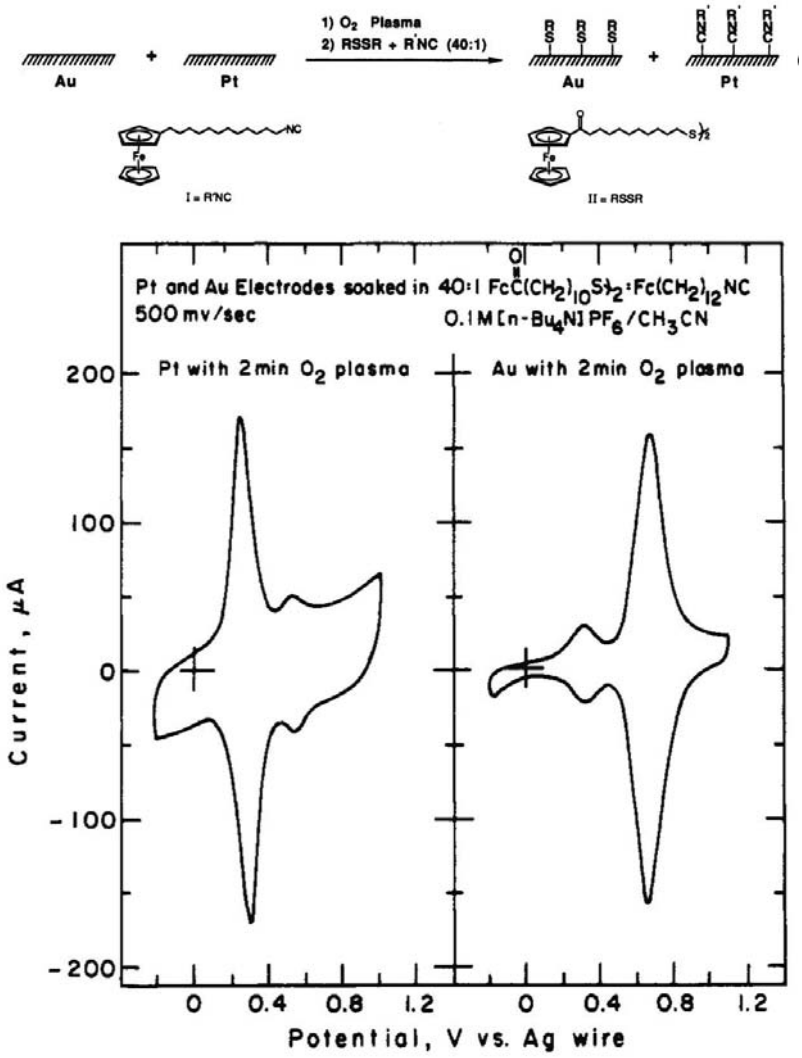

Figure 1.9. Examination of orthogonal self-assembly on Au and Pt by Wrighton and Whitesides.[16]

Wrighton also studied a third group of adsorbants and substrates, thiols on gold and carboxylic/phosphonic acids on indium tin oxide (Figure 1.10).[17] The shift away from the isocyanides/Pt couple was due to the inability to form orthogonal self-assembled monolayers with an equimolar solution of disulfides and isocyanides. As in the study above, alkylferrocenyl and acylferrocenyl headgroups were used to allow for surface concentration calculations via cyclic voltammetry. Using an equimolar solution of thiol and carboxylic acid, the coverage ratio of thiol:carboxylic acid on Au and ITO was 100:1 and 1:45, respectively, after a 30-minute incubation period. By switching to an alkyl phosphonic acid,

it was possible to increase the coverage ratio on ITO to 1:100, but the ratio on Au was reduced to 30:1.

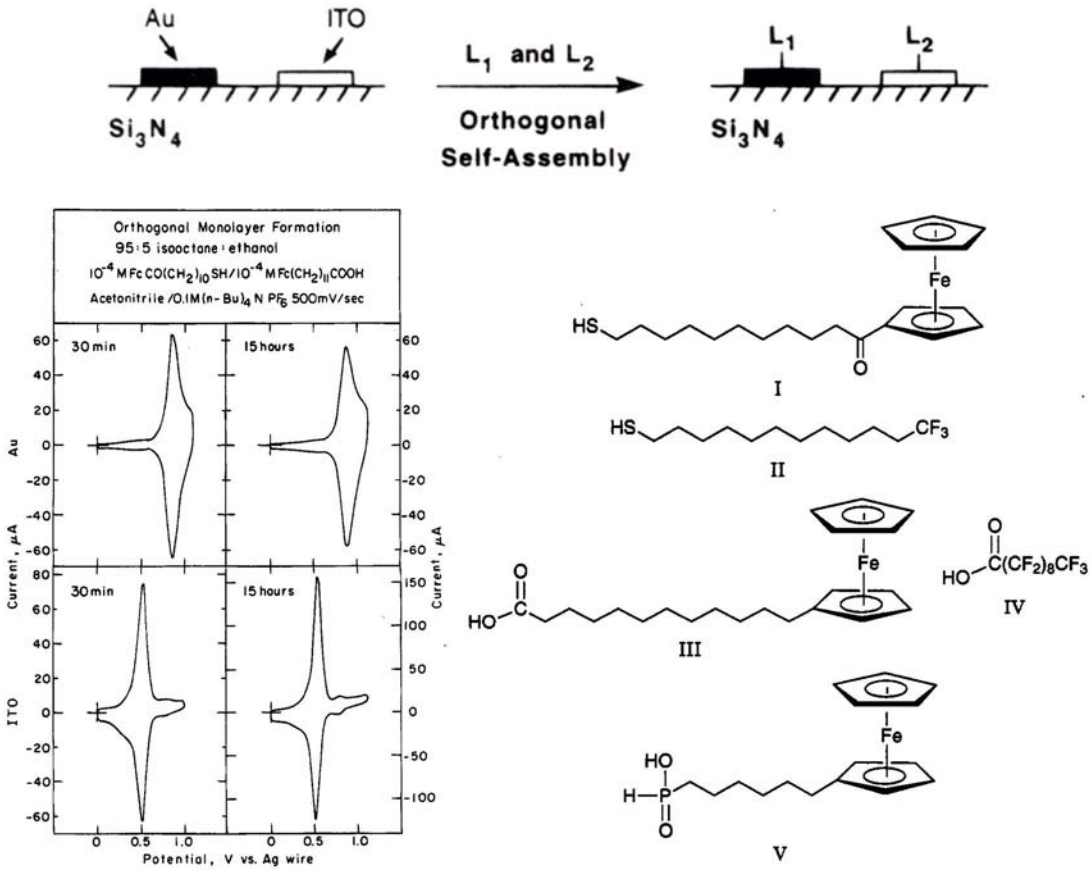

Figure 1.10. Demonstration of orthogonal self-assembly of thiols and acids on Au and ITO respectively published by Wrighton et al.[17]

Mallouk et al.[18] synthesized segmented Au/Pt/Au nanorods and demonstrated that selective functionalization of the Au segments with thiol and the Pt segment with isonitriles could be achieved (Figure 1.11). The rods were exposed to a butyl isonitrile solution, which assembled on both the Au and Pt sections. The rods were then placed in a solution of mercaptoethylamine (MEA), which displaced the isonitrile groups on the Au sections due to its higher affinity for that metal. The displacement was verified by attaching a fluorescent tag to the amine-terminated thiol, which allowed examination by fluorescence spectroscopy.

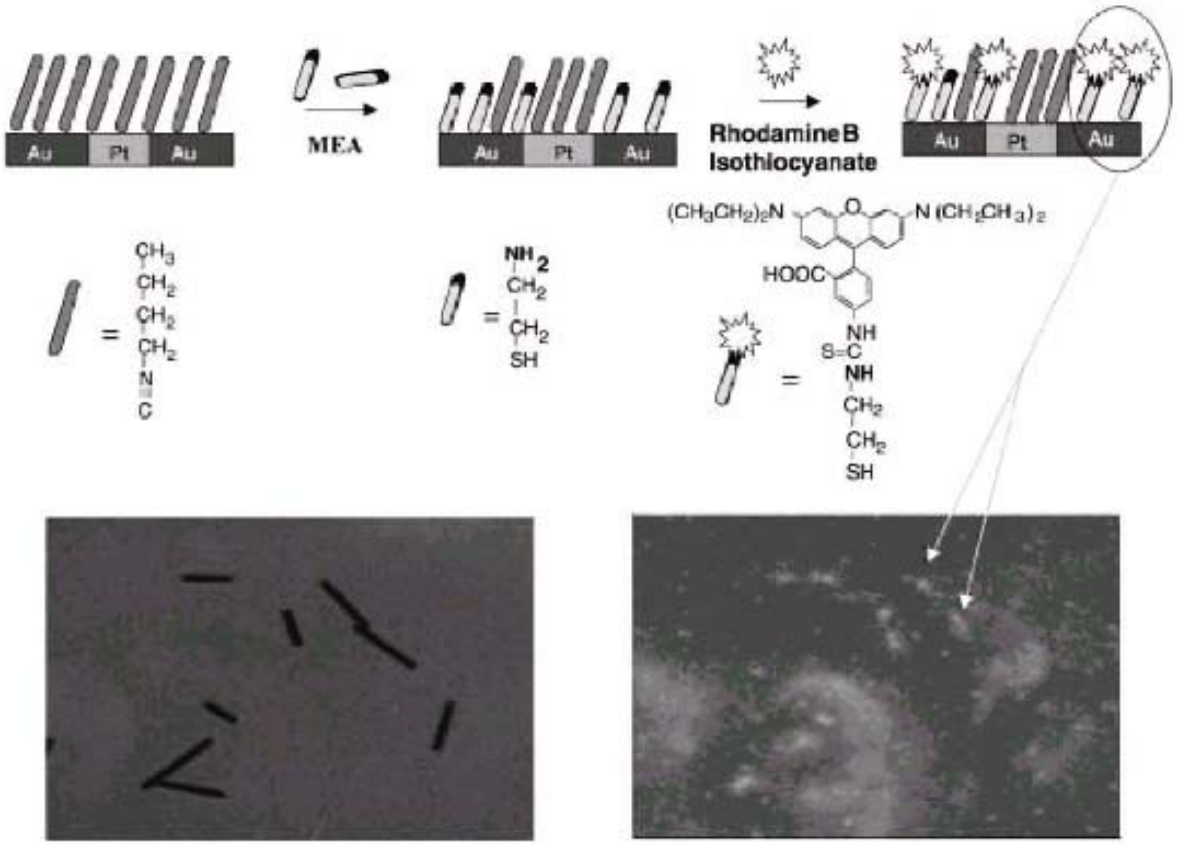

Figure 1.11. Segmented nanorods as published by Mallouk et al.[18]

Using segmented Au and Ni nanorods, Meyer at el.[19] were able to selectively coat the rods with a thiol-terminated molecule on the Au segment and a carboxylic acid-terminated molecule on the Ni segment (Figure 1.12). By using an amine terminated carboxylic acid molecule, they were able to label the acid molecules on the Ni segment with a fluorescent tag and show that the carboxylic acid molecules had only weak interactions with the Au segments. Meyer and coworkers rationalized the preference for one metal over the other was based on hard-soft acid-base (HSAB) theory. Previous research has shown that since thiols are soft bases, they would preferentially bind to Au (a soft metal) over Ni (a hard metal).[4] In contrast, the carboxylate anion is a hard base and thus prefers the hard metal, Ni.

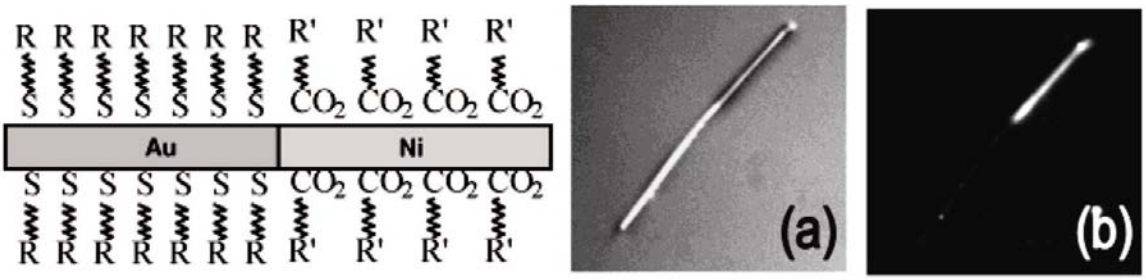

Figure 1.12. Demonstration of a functionalized nanorod by Meyer et al.[19]

A simple extension of the orthogonal self-assembly concept is to employ molecules that contain terminal groups with different functionalities. This type of orthogonal self-assembly could then be useful in the installation of molecules into metallic junctions where the molecule in question should only be inserted "one way". In this case, the two junctions and the chemistries used to bind to them should not be the same.

The key to this differential binding is elucidating which types of linking groups (e.g., headgroups) on a molecule will bind to one surface while avoiding (or eventually becoming displaced from) a different surface. Despite the obvious usefulness of this idea in nanometer-scale construction, only a few reports[18-23] provide synthetic aspects relevant to orthogonal self-assembly. Little information is available as to which chemical functional groups can be employed in the presence of others (e.g., the relative tolerance of one chemical functional group for another). Moreover, the relative affinity of a given substrate for one functional group over another is not well understood in the general case.

1.2 Project Goals

The ultimate goal of this project was to lay a solid foundation for the synthesis of a molecular transistor that could be installed in an electronic feature using orthogonal self-assembly. This goal influenced many of the initial decisions for the direction and choices that were made over the course of the project. In order for a molecule to function as a transistor, it is necessary for it to have three discrete sections: source, drain, and gate. In a transistor, charge flows from the source to the drain with control of the flow being provided by the gate. An example of this is shown in Figure 1.13. For this reason, a three-armed molecule was chosen with two arms having the same terminal groups (source and drain) and

a different third arm (gate). Also, a conjugated phenyl-acetylene backbone was chosen for reasons which are explained in Chapter 2.

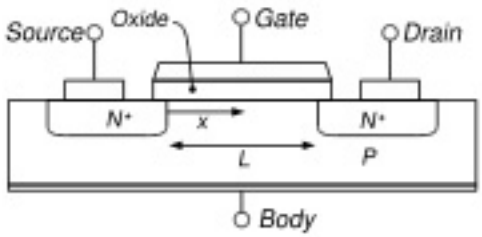

Figure 1.13. Cross-section diagram of a n-channel metal-oxide-semiconductor field-effect transistor (nMOSFET) [image from http://en.wikipedia.org/wiki/MOSFET].

The second part of the project involved controlling the orientation of the molecule as it was inserted into a circuit feature. To this end, the terminal groups were specifically chosen so that orthogonal self-assembly could be employed. Following the initial work of Wrighton and Whitesides, thiols and isocyanides were used as the binding groups to Au and Pt respectively. It was decided to bind nanoparticles to the linker molecule to bridge the distance between molecular and lithographic length. By binding the linker molecule to nanoparticles, it allowed for several spectroscopic techniques to be used to analyze the binding efficiency of the molecule. Also, it allowed for larger circuit features to be used in the interim since the size of the attached nanoparticles could be changed depending on the size of the electronic feature. A schematic of the proposed three-armed linker molecule attached to nanoparticles and inserted into a trench can be seen in Figure 1.14.

Some examples of nanoparticles connected by linker molecules have been presented in the literature, but those examples involved using only one type of functional group and nanoparticle type and are not examples of orthogonal self-assembly. Novak and Feldheim used thiol-terminated phenyl acetylene molecules to link Ag nanoparticles to form dimers and Au nanoparticles to form trimers and tetramers as shown in Figure 1.15. [24] Dadosh and Gordin also linked Au nanoparticles to form dimers and electrostatically trapped them to measure their electronic properties (Figure 1.16).[25]

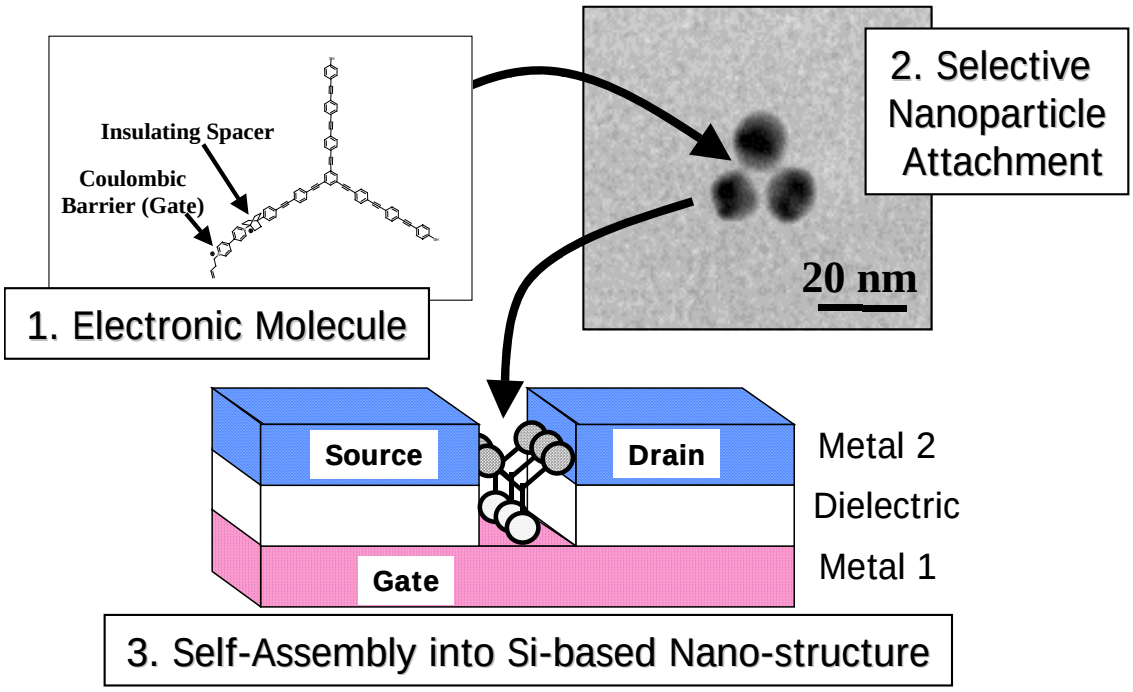

Figure 1.14. Proposed vertically patterned test structure (nanoparticle heterotrimer and silicon structure drawn to scale) for three-terminal molecular electronic analysis.

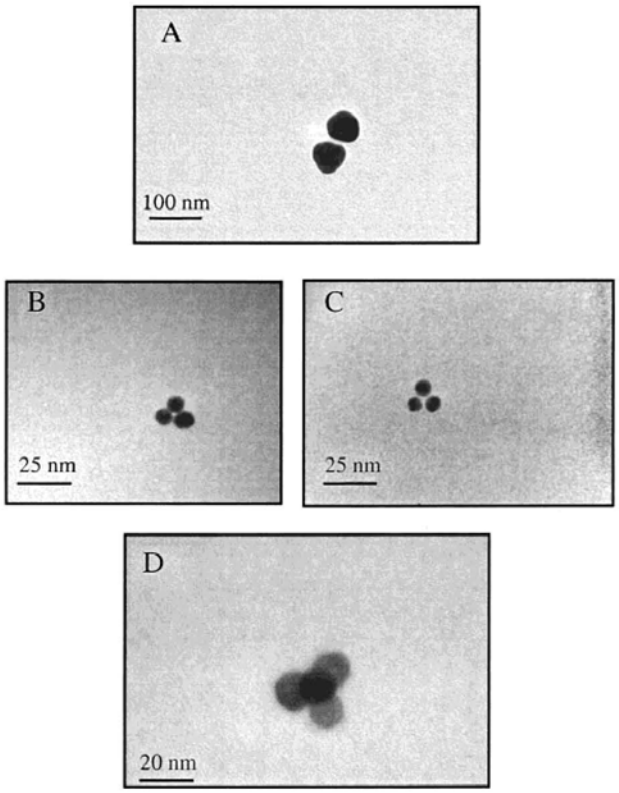

Figure 1.15. TEM images of a Ag dimer (A), Au trimers (B, C), and Au tetramer (D) as published by Feldheim and Novak.[24]

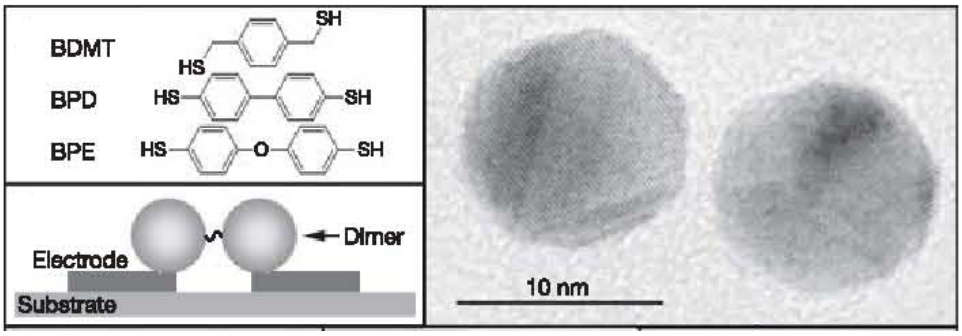

Figure 1.16. Electronic measurements of a Au dimer published by Dadosh et al.[25]

Before attempting to synthesize the three-armed molecule and attach nanoparticles, it was decided to synthesize a small test molecule that had differing terminating functional groups. This would allow for synthetic difficulties to be resolved early as well as allow for easier testing of nanoparticle binding conditions. An example of this test molecule is shown in Figure 1.17.

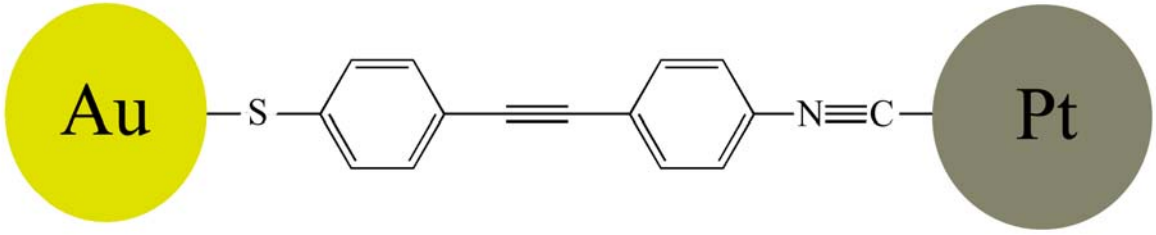

Figure 1.17. Proposed molecule and nanoparticles for initial synthesis and testing.

1.3 REFERENCES

(1) Moore, G. E. In *International Electron Devices Meeting*, 1975, pp 11-13.

(2) Tullo, A. H. In *Chem. Eng. News*, 2006; Vol. 84, pp 30-32.

(3) Tullo, A. In *Chem. Eng. News*, 2007; Vol. 85, p 9.

(4) Aviram, A.; Ratner, M. A. *Chem. Phys. Lett.* **1974**, *29*, 277-283.

(5) Lortscher, E.; Ciszek, J. W.; Tour, J.; Riel, H. *Small* **2006**, *2*, 973-977.

(6) Xu, B. Q.; Tao, N. J. J. *Science* **2003**, *301*, 1221-1223.

(7) Laibinis, P. E.; Hickman, J. J.; Wrighton, M. S.; Whitesides, G. M. *Science* **1989**, *245*, 845-847.

(8) Xu, X. Y.; Rosi, N. L.; Wang, Y. H.; Huo, F. W.; Mirkin, C. A. *J. Am. Chem. Soc.* **2006**, *128*, 9286-9287.

(9) Kushmerick, J. G.; Naciri, J.; Yang, J. C.; Shashidhar, R. *Nano Lett.* **2003**, *3*, 897-900.

(10) Ramachandran, G. K.; Tomfohr, J. K.; Li, J.; Sankey, O. F.; Zarate, X.; Primak, A.; Terazono, Y.; Moore, T. A.; Moore, A. L.; Gust, D.; Nagahara, L. A.; Lindsay, S. M. *J. Phys. Chem. B* **2003**, *107*, 6162-6169.

(11) Cygan, M. T.; Dunbar, T. D.; Arnold, J. J.; Bumm, L. A.; Shedlock, N. F.; Burgin, T. P.; Jones, L.; Allara, D. L.; Tour, J. M.; Weiss, P. S. *J. Am. Chem. Soc.* **1998**, *120*, 2721-2732.

(12) Price, D. W.; Dirk, S. M.; Maya, F.; Tour, J. M. *Tetrahedron* **2003**, *59*, 2497-2518.

(13) Tour, J. M. *Accounts of Chemical Research* **2000**, *33*, 791-804.

(14) Robertson, N.; McGowan, C. A. *Chemical Society Reviews* **2003**, *32*, 96-103.

(15) Kushmerick, J. G.; Holt, D. B.; Pollack, S. K.; Ratner, M. A.; Yang, J. C.; Schull, T. L.; Naciri, J.; Moore, M. H.; Shashidhar, R. *J. Am. Chem. Soc.* **2002**, *124*, 10654-10655.

(16) Hickman, J. J.; Laibinis, P. E.; Auerbach, D. I.; Zou, C. F.; Gardner, T. J.; Whitesides, G. M.; Wrighton, M. S. *Langmuir* **1992**, *8*, 357-359.

(17) Gardner, T. J.; Frisbie, C. D.; Wrighton, M. S. *J. Am. Chem. Soc.* **1995**, *117*, 6927-6933.

(18) Kovtyukhova, N. I.; Mallouk, T. E. *Chem. Eur. J.* **2002**, *8*, 4355-4363.

(19) Bauer, L. A.; Reich, D. H.; Meyer, G. J. *Langmuir* **2003**, *19*, 7043-7048.

(20) Flatt, A. K.; Yao, Y. X.; Maya, F.; Tour, J. M. *J. Org. Chem.* **2004**, *69*, 1752-1755.

(21) Pollack, S. K.; Naciri, J.; Mastrangelo, J.; Patterson, C. H.; Torres, J.; Moore, M.; Shashidhar, R.; Kushmerick, J. G. *Langmuir* **2004**, *20*, 1838-1842.

(22) Mohaddes-Ardabili, L.; Martinez-Miranda, L. J.; Silverman, J.; Christou, A.; Salamanca-Riba, L. G.; Al-Sheikhly, M.; Bentley, W. E.; Ohuchi, F. *Applied Physics Letters* **2003**, *83*, 192-194.

(23) Keren, K.; Berman, R. S.; Buchstab, E.; Sivan, U.; Braun, E. *Science* **2003**, *302*, 1380-1382.

(24) Novak, J. P.; Feldheim, D. L. *J. Am. Chem. Soc.* **2000**, *122*, 3979-3980.

(25) Dadosh, T.; Gordin, Y.; Krahne, R.; Khivrich, I.; Mahalu, D.; Frydman, V.; Sperling, J.; Yacoby, A.; Bar-Joseph, I. *Nature* **2005**, *436*, 677-680.

CHAPTER 2

Synthesis and Characterization of Bifunctional Molecules Capable of Orthogonal Self-assembly

2.1 INTRODUCTION

Linear phenylacetylene oligomers were synthesized with different end groups to allow for binding to nanoparticles. These nanoparticle assemblies could then be used for molecular electronic applications. It was initially decided to employ a thiol/isonitrile combination to bind to gold/platinum nanoparticles, respectively. The study of these functional groups binding to metals[26] and the nanoparticle synthesis is very well documented in the literature.[27] To allow for more possible combinations, a carboxylic acid binding group was also explored which could bind to metal oxides, nickel, etc.[28]

A phenylacetylene backbone was chosen for the target molecule for several reasons. First, the chemistry involved is straightforward and well established.[29] Second, the structure is rigid and has a known conformation. Finally, the molecule is conjugated which is desirable for molecular electronics. Previous reports of the synthesis of functionalized oligophenylethylenes (OPEs) largely involved the generation of molecules with the same functional groups at each end,[29-31] with very few literature publications of bifunctional molecules.[32] To create molecules with different functional groups at each end, it is necessary to address some synthetic challenges. The most difficult problem was synthesizing one functional binding group (i.e. isonitrile) in the presence of another (i.e. thioacetate) without damaging either group. To this end, it was decided to generate several small, bifunctional molecules with a synthesis scheme involving the fewest steps possible yet encompassing all of the transformations necessary in the synthesis of molecules of arbitrary length, before attempting to synthesize the larger trifunctional Y-shaped molecules.

2.2 RESULTS AND DISCUSSION

The first route examined to synthesize the thioacetate-isonitrile bifunctional molecule (**4**) is shown in Scheme 2.1. Commercially–available bromothiophenol (**1**) was treated with acetic anhydride and imidazole to yield the protected bromothioacetate (**2**). Next, a palladium-catalyzed Sonogashira coupling was used to attach trimethylsilylacetylene (**3**). This reaction did not proceed satisfactorily under the attempted conditions, resulting in low yields and a large amount of unreacted starting material. This result may have been due to

the unintentional deprotection of the thioacetate to give free thiol, which could then deactivate the Pd-catalyst.[33]

Scheme 2.1. Attempted route for the synthesis of a thioacetate-isonitrile bifunctional molecule

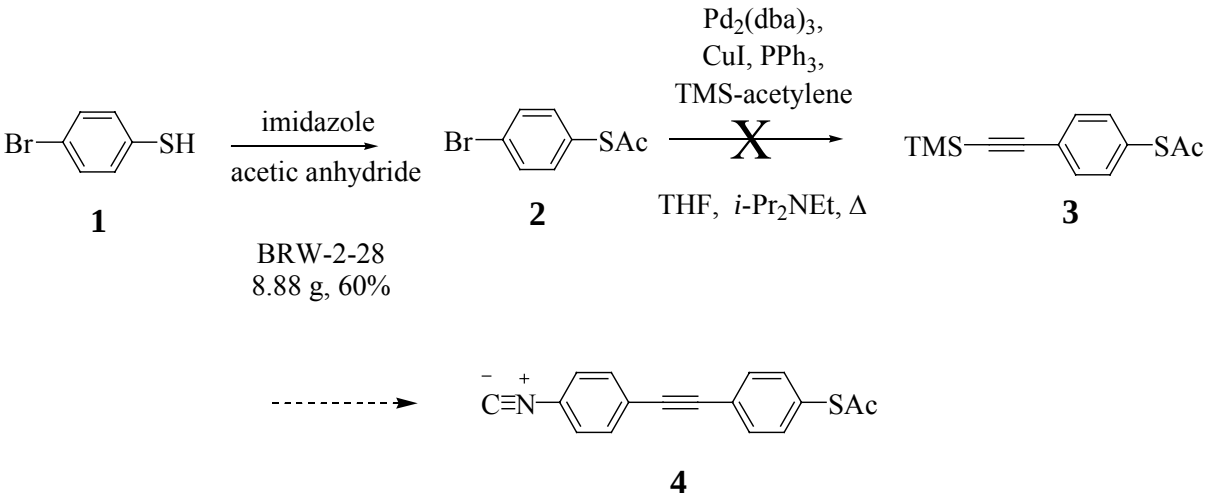

1 **2** **3** **4**

Since Sonogashira couplings with aryl iodides proceed much faster and at lower temperatures than those with aryl bromides,[34] it was decided to use iodothioacetate (**10**) to perform the Sonogashira coupling. To limit the exposure of the thioacetate (**10**) to the Pd-catalyst, the formamide side of the bifunctional molecule (**8**) was synthesized first. As shown in Scheme 2.2, iodoaniline (**5**) was reacted with trimethylsilylacetylene in the presence of a Pd-catalyst to give **6**. Desilylization of **6** with MeOH and K_2CO_3 afforded **7**. Acetic anhydride and formic acid were then heated together to form a mixed anhydride, which was subsequently reacted with **7** to give the formamide (**8**). Another Sonogashira coupling of **8** and **10** yielded the protected bifunctional molecule (**11**). To generate the isonitrile, a phosgene-mediated dehydration was performed to yield **4**. This five step sequence was successful with a 12% overall yield.

While the Sonogashira coupling of TMS-acetylene to the iodoaniline (**6**) proceeded with minimal problems, it was difficult to determine if the reaction had gone to completion because the starting material and the product coeluted on the TLC plate. Since it is known that ring substituents on the iodobenzene will affect the Pd-catalyzed coupling,[35] the order of the reactions was modified in an attempt to increase yield and ease purification of the intermediate compounds.

Scheme 2.2. Initial successful route for the synthesis of a thioacetate-isonitrile bifunctional molecule

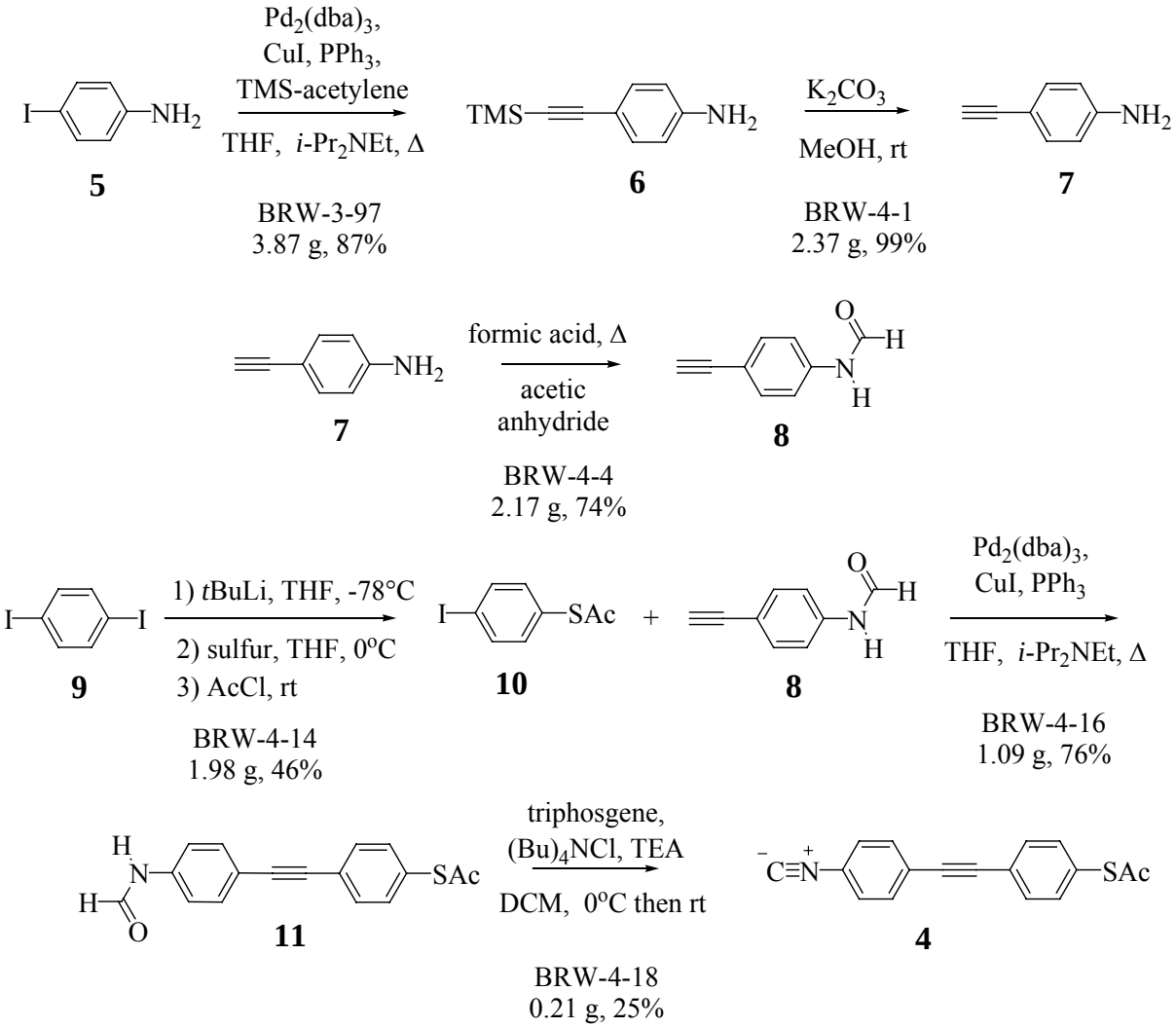

In the modified scheme (Scheme 2.3), iodoaniline (**5**) was reacted with the mixed anhydride of acetic anhydride and formic acid to yield **12**. This reaction proceeded extremely well even on large scales and allowed the product to be purified by recrystallization instead of flash chromatography. The next step involved a Sonogashira coupling of **12** with TMS-acetylene to yield **13**. Again, this reaction performed much better using the iodoformamide (**12**) as compared to the iodoaniline (**5**). Desilylization of **13** with MeOH and K_2CO_3 afforded **8** in higher yields as compared to Scheme 2.3. At this point, the reaction route was the same as described in Scheme 2.2. A Pd-catalyzed coupling of **7** and **9** yielded the protected bifunctional molecule **10,** followed by a phosgene-mediated dehydration to generate the isonitrile **11**. The overall yield of the five-step synthesis was

22%. This increase in overall yield can be attributed to the increase in yield and scale of the first three steps.

Scheme 2.3. Final route for the synthesis of a thioacetate-isonitrile bifunctional molecule

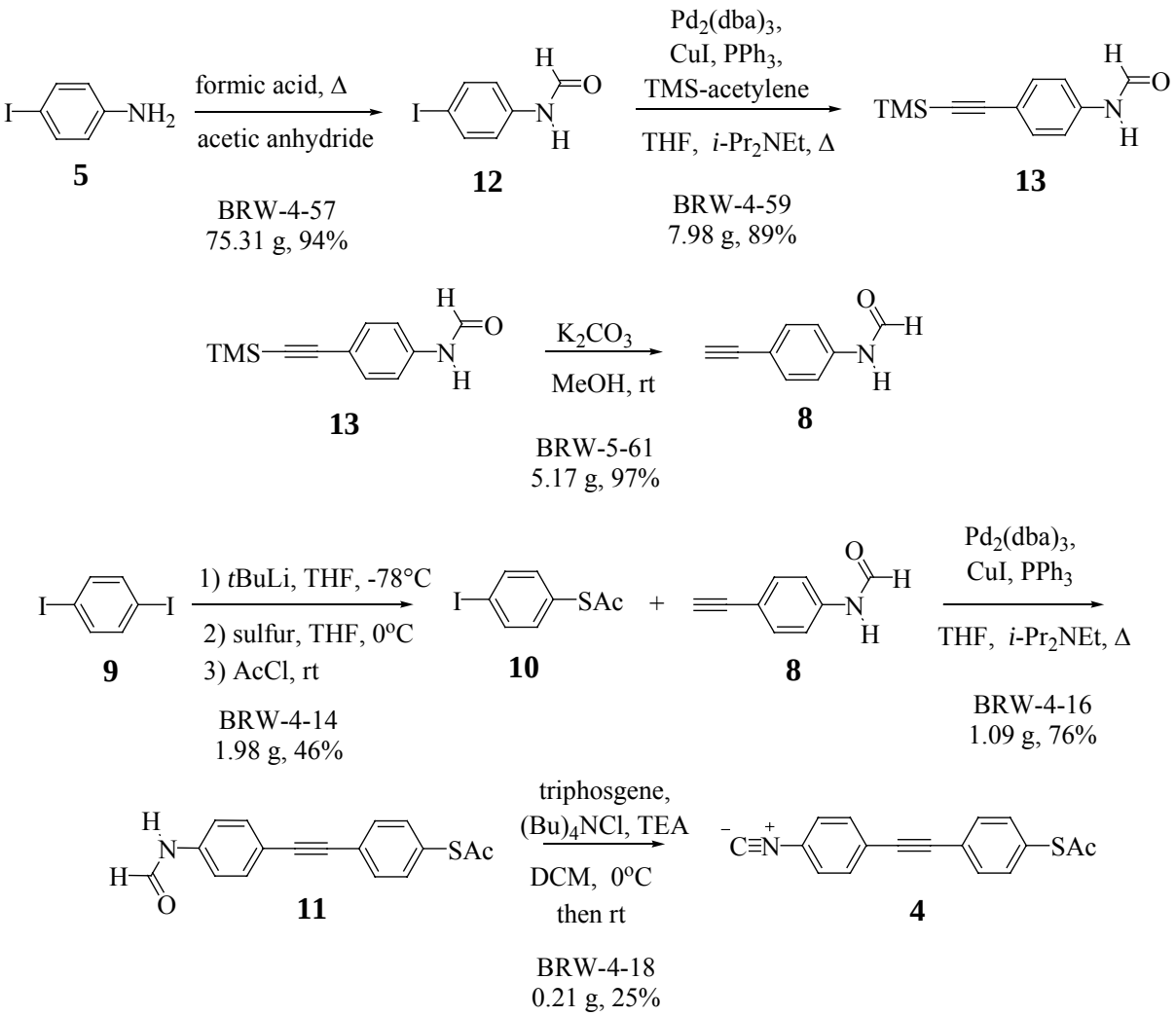

The second bifunctional molecule (**17**) was synthesized in a similar manner (Scheme 2.4). Commercially available methyl-4-iodobenzoate (**14**) was used in a Sonogashira reaction with **8** to yield the protected molecule **15**. The formamide group was then dehydrated using triphosgene to give the free isonitrile (**16**). Several reaction conditions were tried to deprotect the methyl ester in the presence of the isonitrile (Table 2.1). Exposure to LiOH for 2 days was found to be the best reaction conditions to give the free carboxylic acid, **17**. The overall yield of the three-step synthesis was 24%.

Scheme 2.4. Synthesis of an isonitrile-carboxylic acid bifunctional molecule

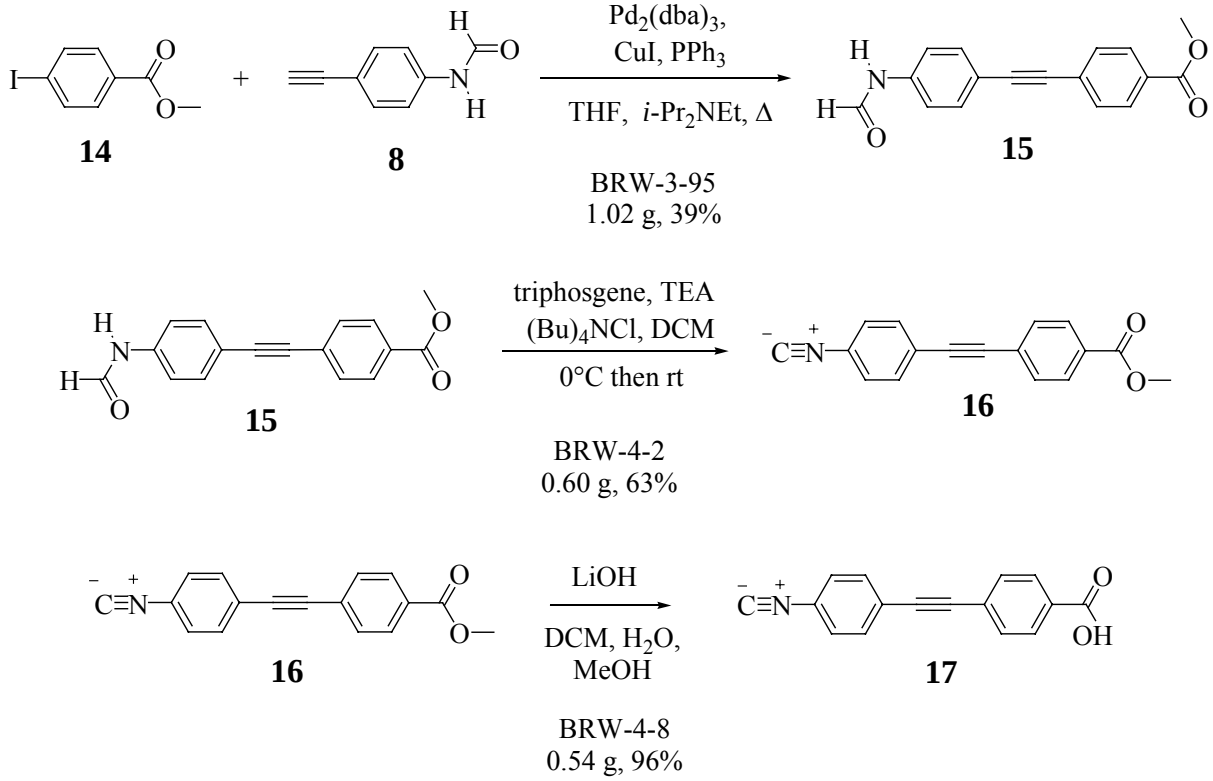

Table 2.1. Reaction Conditions for Methyl Ester Deprotection

Reactants/Solvent	Time	Results
TMSI in THF		Starting Material
NaOH in THF		Regenerated Formamide
8 eq LiOH in MeOH, DCM, H_2O	4 hours	Dirty Product
4 eq LiOH in MeOH, DCM, H_2O	4 hours	Mostly Starting Material
4 eq LiOH in MeOH, DCM, H_2O	24 hours	Starting Material/Product
4 eq LiOH in MeOH, DCM, H_2O	48 hours	Product

A third bifunctional molecule (**21**) was synthesized using similar chemistry as compound **17** (Scheme 2.5). Commercially available methyl-4-iodobenzoate (**14**) was used in a Sonogashira reaction with TMS-acetylene followed by desilylization with MeOH and K_2CO_3 to yield **19**. Reaction of **19** with **10** in the presence of a Pd catalyst gave the protected bifunctional molecule **20**. Unlike molecule **17**, exposure to LiOH also deprotected the thioacetate and did not give **21**. The overall yield of the three-step synthesis of compound **20** was 13%.

Scheme 2.5. Synthesis of a thioacetate-carboxylic acid bifunctional molecule

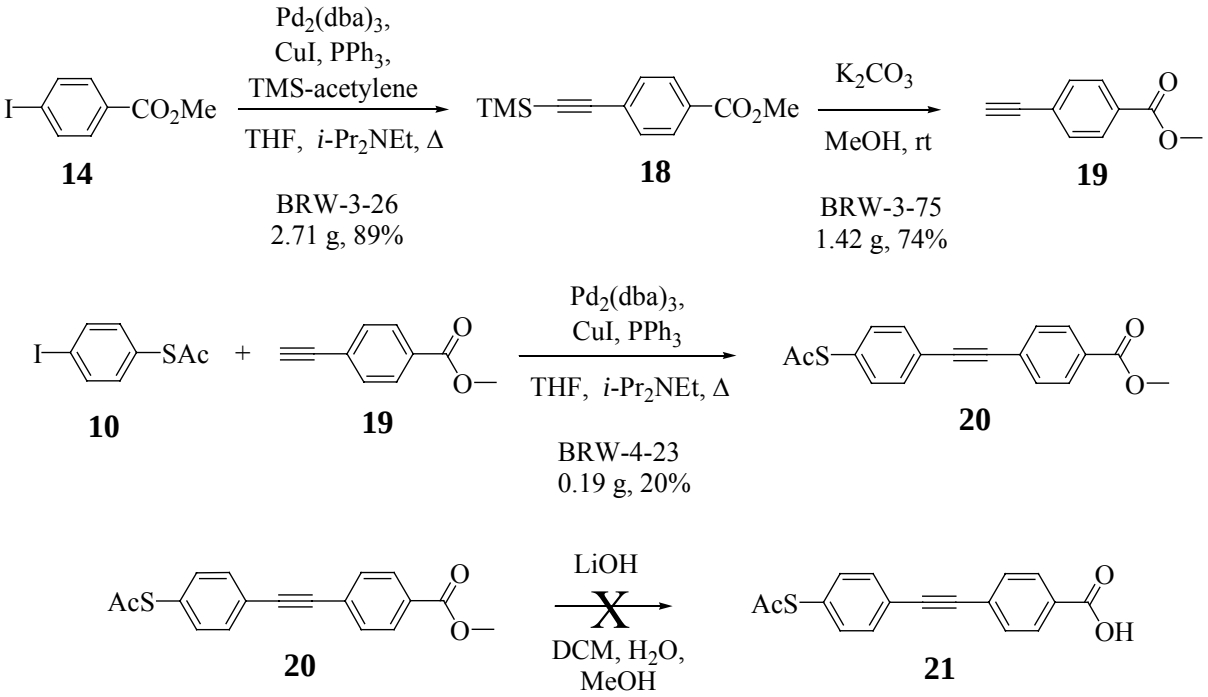

In an effort to understand several of the binding properties of the bifunctional molecules to metals, it was necessary to synthesize several molecules that mimicked the structure of the bifunctional molecules, but only had a single functional group for binding (Schemes 2.6-2.8). Phenyl acetylene (**22**) was coupled to **10** via a Pd-catalyzed reaction to give **23** (Scheme 2.6). Similarly, compound **25** was synthesized by a Sonogashira reaction of phenyl acetylene (**22**) with **12** to give **24** in an overall yield of 24%, which then could be dehydrated using triphosgene (Scheme 2.7). The final monofunctional molecule was generated by coupling phenylacetylene (**22**) with methyl 4-iodobenzoate (**14**) to yield **26.**

This molecule was then deprotected by LiOH to give **27** in 64% overall yield for the two-step synthesis (Scheme 2.8).

Scheme 2.6. Synthesis of a thioacetate-terminated control molecule

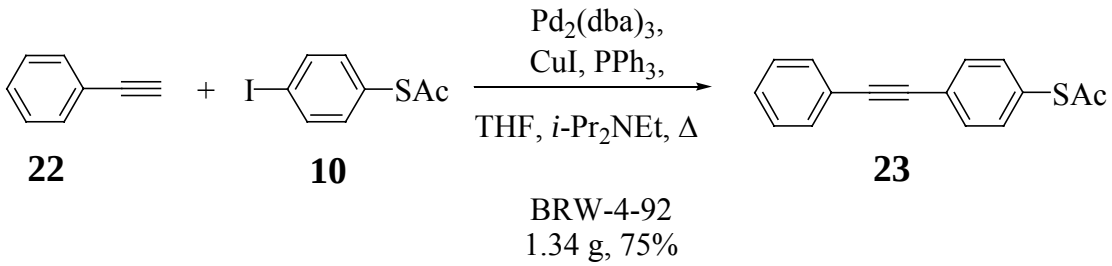

Scheme 2.7. Synthesis of an isonitrile-terminated control molecule

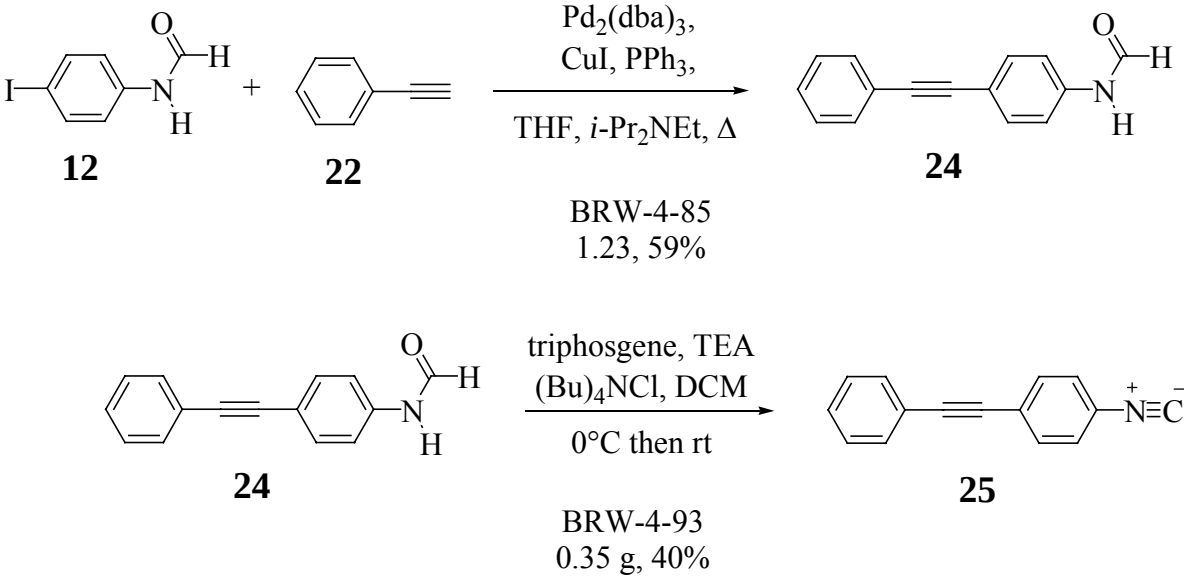

Scheme 2.8. Synthesis of a carboxylic acid-terminated control molecule

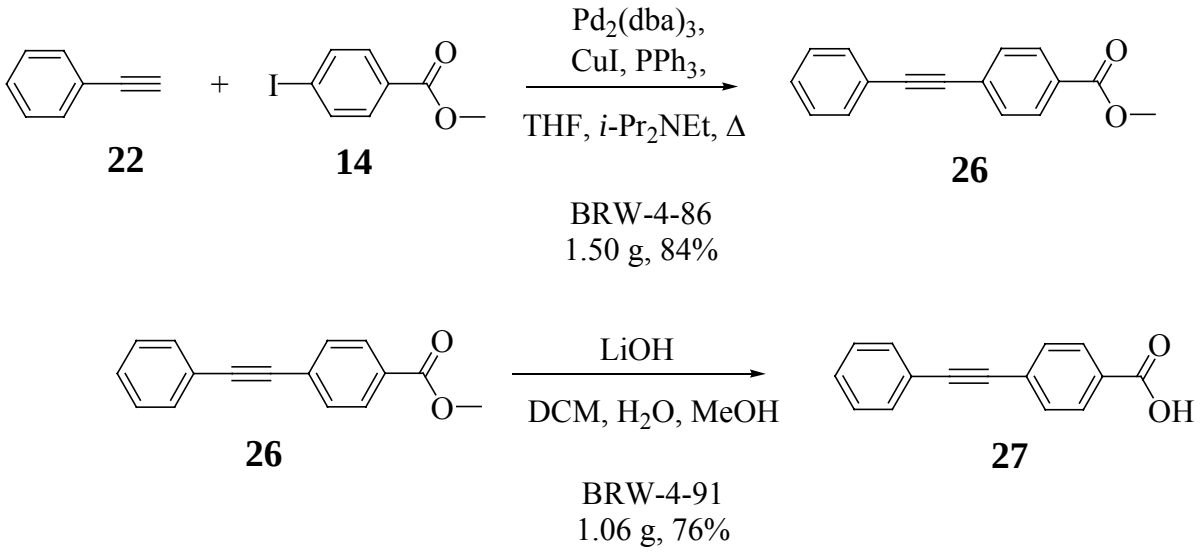

Progress has also been made towards the synthesis of trifunctional, Y-shaped molecules. Similar Pd-coupling chemistry (as above) was utilized to synthesize generic phenyl-acetylene molecules that could be used for any arm of the trifunctional molecule or to generate longer bifunctional oligomers. As shown in Scheme 2.9, a modified Sandmeyer reaction was performed to convert bromoaniline (**28**) to 4-N, N-diethyltriazene, -bromobenzene (**29)**. Subsequent reaction with trimethylsilylacetylene in the presence of a Pd-catalyst gave **30**. The triazene group of **30** could then be converted to an iodide using methyliodide to yield **31**. Alternatively, compound **30** was desilylated using MeOH and K_2CO_3 to generate **32**. Coupling of **31** with **32** was achieved with a Sonogashira reaction to yield **33**. The triazene protecting group was then converted to an iodide using methyl iodide to give **34**. The five-step process produced compound **34** in an excellent overall yield of 64%.

Further reaction of compound **34** proved to be difficult. The coupling of **34** with **7** yielded **35** in small yield (Scheme 2.10), but purification of the product was problematic due to its low solubility in common organic solvents. Since this low solubility would cause complications in subsequent reactions, an attempt was made to synthesize phenyl-acetylene molecules with side chains to enhance solubility.

Scheme 2.9. Synthesis of longer phenyl-acetylene molecules

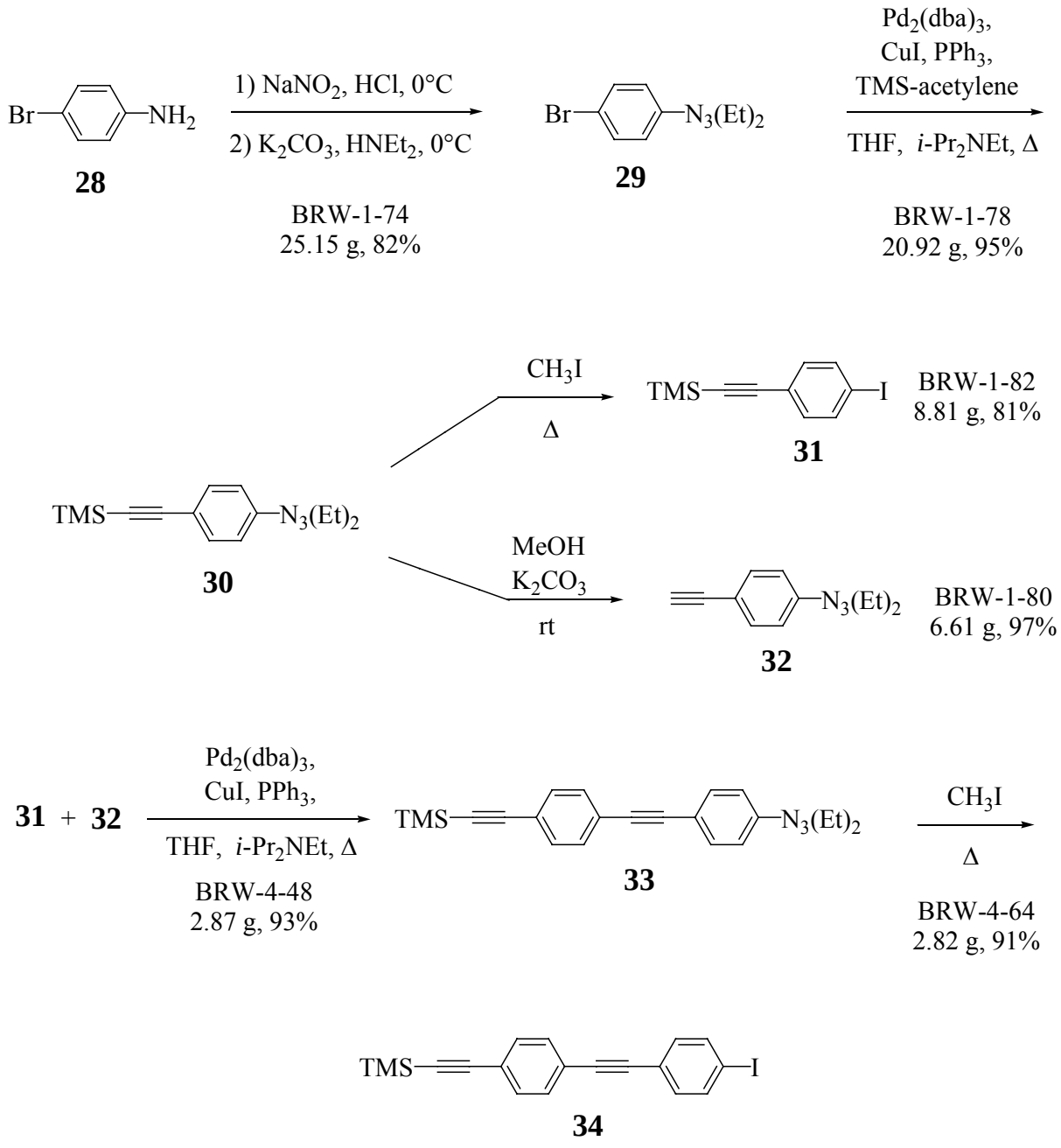

Scheme 2.10. Functionalization of longer phenyl-acetylene molecules

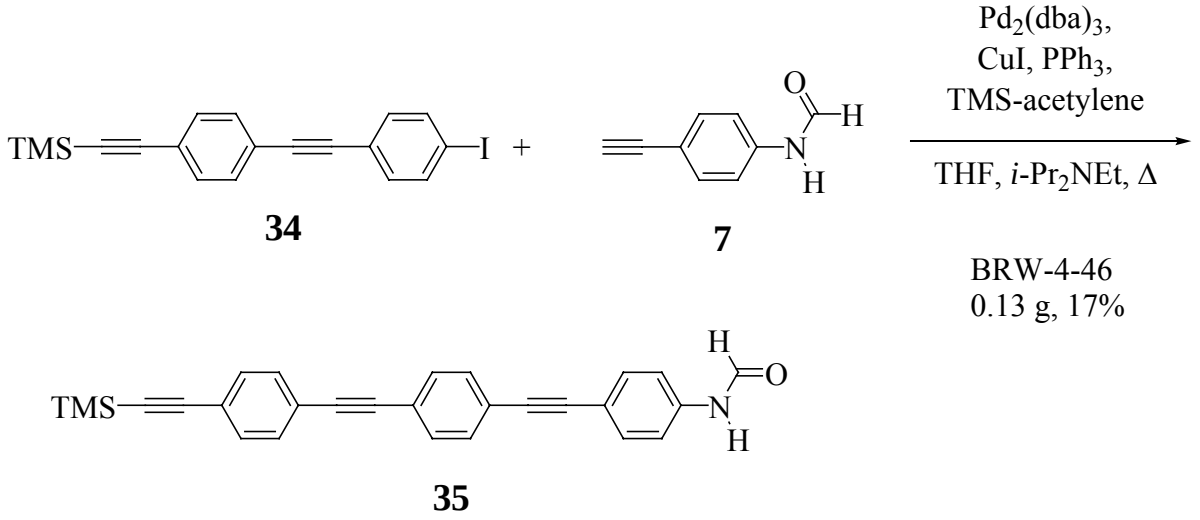

The first attempt to synthesize phenyl acetylene molecules with side chains is shown in Scheme 2.11. Diethylbenzene (**36**) was reacted with iodine and periodic acid to give **37**. The reaction of **37** with TMS-acetylene via Sonogashira coupling to give **38** did not proceed to completion. Visualization by TLC showed mostly starting material and no isolatable product.

Scheme 2.11. Synthesis of longer phenyl-acetylene molecules with solubilizing ethyl side chains

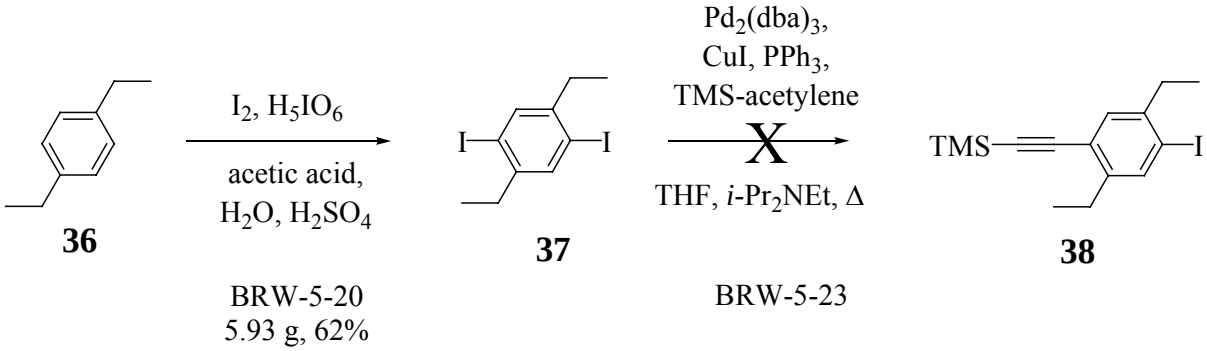

An alternate reaction was tried to generate phenyl acetylene molecules with hexyloxy side chains (Scheme 2.12). Hydroquinone (**39**) was reacted with bromohexane to give **40**, which could then be iodinated by exposure to iodine and periodic acid to yield **41**. Again, further reaction of **41** with TMS-acetylene via Sonogashira coupling to yield **42** proved to be problematic. The NMR spectrum of the crude product did not show the expected TMS peak

indicating that the reaction did not proceed. Other attempts to couple the bishexyloxy diiodobenzene (**41**) with a phenyl acetylene formamide (Scheme 2.13) and with (triisopropylsilyl)acetylene (Scheme 2.14) were also unsuccessful.

Scheme 2.12. Synthesis of longer phenyl-acetylene molecules with solubilizing bis-hexyloxy side chains

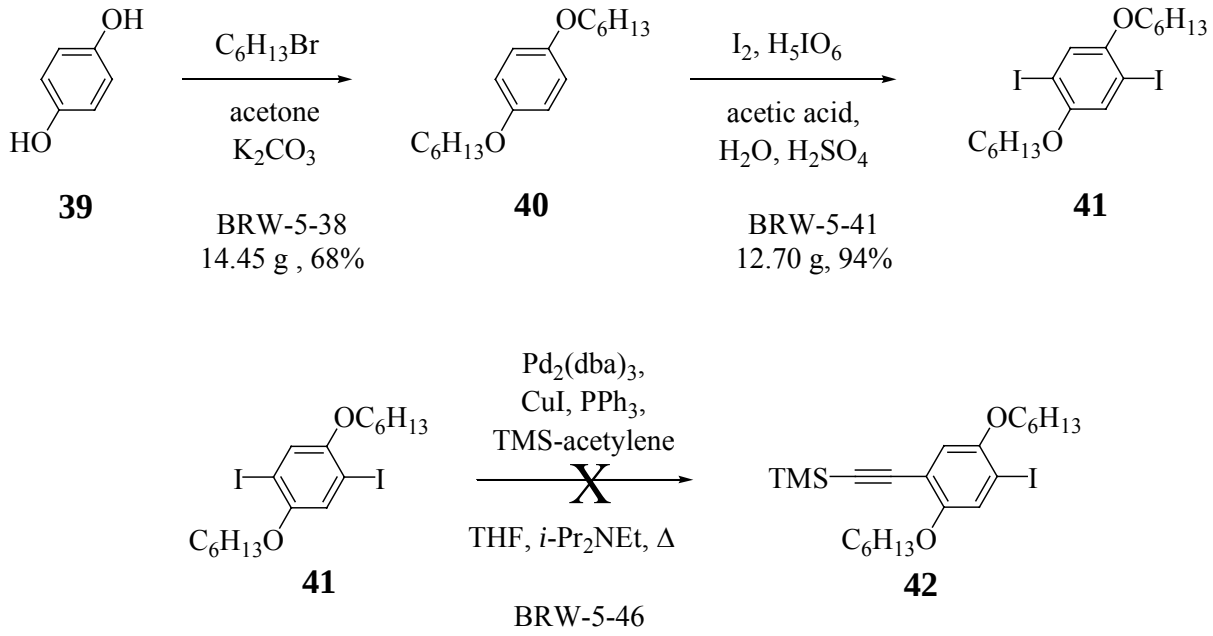

Scheme 2.13. Synthesis of longer phenyl-acetylene molecules with solubilizing bis-hexyloxy side chains

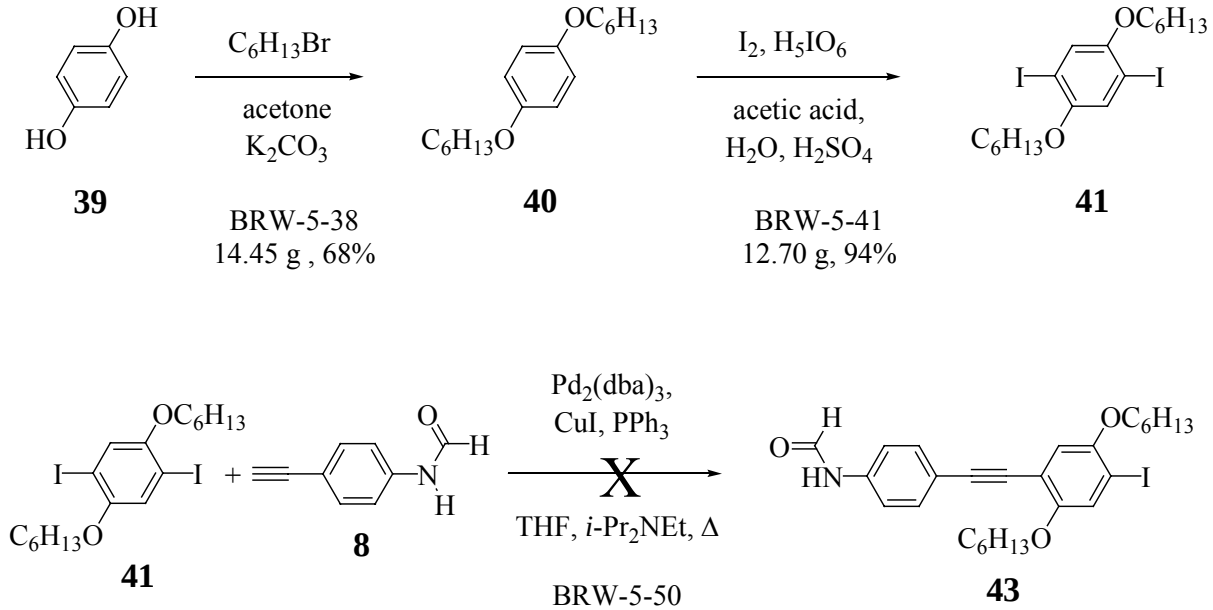

Scheme 2.14. Synthesis of longer phenyl-acetylene molecules with solubilizing bis-hexyloxy side chains

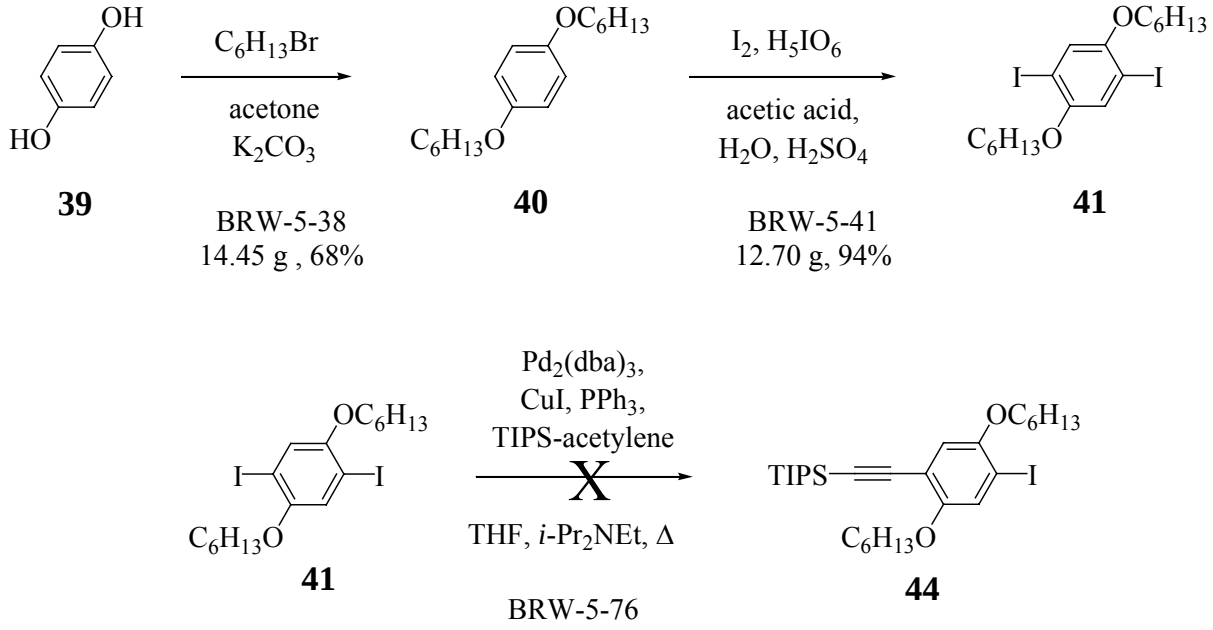

2.3 CONCLUSION

Developing a synthesis that could generate one side of the linker without destroying the other represented a large step in the goal of this project. The synthesis of novel molecule **4** allowed for verification of the synthetic methodologies for creating a bifunctional linker as well as providing a test molecule for binding studies of the linker to metals. Before extensive synthetic efforts were made to synthesize bifunctional three-armed linkers or longer bifunctional linkers, it was decided to examine the binding characteristics of the shorter monofunctional and bifunctional molecules (**4**, **23**, and **25**). Thus, the remainder of the project was spent characterizing the binding of functional groups to metal surfaces as well as developing analytical methods for verifying that heterodimers could be formed using orthogonal self-assembly.

2.4 EXPERIMENTAL

General Considerations:

The following compounds were commercially available and were used as is: bromothiophenol (**1**), 4-bromoaniline (**5**), 4-iodoaniline (**4**), p-diiodobenzene (**9**), methyl-4-iodobenzoate (**14**), phenyl acetylene (**22**), 4-bromoaniline (**28**), diethylbenzene (**36**), and hydroquinone (**39**). Tetrahydrofuran (THF) was purchased anhydrous from ACROS and stored inside the dry box. Diisopropylethylamine was purchased from ACROS, distilled over potassium hydroxide, and stored in the dry box. Methyliodide was purchased from ACROS and distilled over calcium chloride. Dichloromethane (DCM) was distilled over calcium hydride. Tris(dibenzylideneacetone) bispalladium (0) – $CHCl_3$ was synthesized as described below. NMR data was collected at 300 or 400 MHz for ^1H NMR and at 75 MHz for ^{13}C NMR on Varian spectrometers. Column and flash chromatography was performed using silica gel 60Å, 32 – 63 μm (Sorbent Technologies, Atlanta, GA).

Tris(dibenzylideneacetone) bispalladium (0) – $CHCl_3$

Palladium chloride (2.01 g, 11.36 mmol), dibenzylideneacetone (4.01 g, 4.01 mmol), and sodium acetate (7.90 g) were added to a round-bottomed flask and dissolved in methanol (300 mL). The flask was then fitted with a reflux condenser and the solution heated to 60°C for 6 hours. The solution was then filtered and the resulting black solid was recrystallized from chloroform with ether. The solution was filtered, washed with water and acetone, and then vacuum dried.

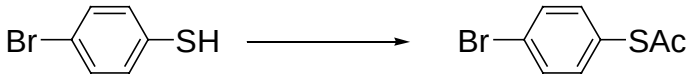

1 **2**

4-bromophenylthioacetate (2) Bromothiophenol (**1**) (12.03 g, 63.65 mmol), acetic anhydride (7.28 g, 71.37 mmol), and imidazole (6.57 g, 96.62 mmol) were added to a round-bottom flask and dissolved in DCM (180 mL). The solution was stirred at room temperature for 2 days then the solvents were removed on a rotatory evaporator. The residue was dissolved in petroleum ether, washed with water, dried with magnesium sulfate, filtered, and the solvents removed on a rotatory evaporator to yield a yellowish crystalline solid. The

solid was filtered through a silica plug with hexanes followed by DCM. The combined organics were taken and the solvents removed using a rotary evaporator to yield the desired off-white crystalline solid (8.88 g, 60%). ^{1}H NMR (400 MHz, $CDCl_3$) δ (ppm) 7.54 (d, J = 8.0 Hz, 2H), 7.27 (d, J = 8.4 Hz, 2H), 2.42 (s, 3H).

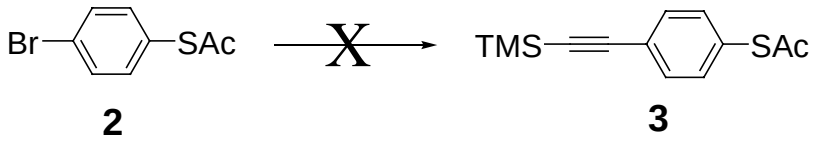

2 **3**

Attempt at 1-thioacetyl-4- (trimethylsilylethynyl)benzene (3) 4-bromophenylthioacetate (**2)** (0.56 g, 2.39 mmol), tris(dibenzylideneacetone) bispalladium (0) (0.19 g, 0.18 mmol), triphenylphosphine (0.11 g, 0.44 mmol), and copper iodide (0.11 g, 0.58 mmol) were added to an oven-dried Schlenck flask. The flask was evacuated and backfilled with argon three times. Under high argon pressure, the stopper was loosened and then THF (15 mL), diisopropylethylamine (3 mL), and trimethylsilylacetylene (1 mL, 7.14 mmol) were added. The flask was purged with argon, sealed, and heated to 80°C with stirring for 72 hours. The flask was cooled to room temperature and the solvents were removed on a rotatory evaporator. The remaining residue was dissolved in ethyl ether and filtered through a Celite plug. The filtrate was dried and checked by TLC. A large amount of unreacted starting material was still present as determined by TLC thus the synthesis was not pursued further.

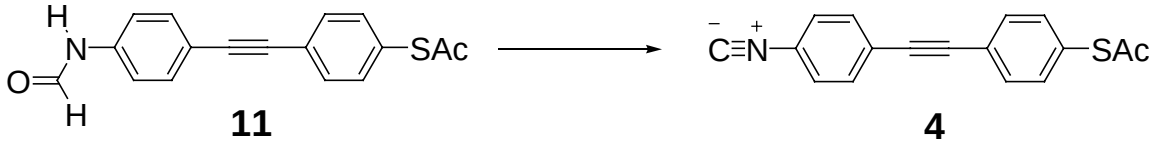

11 **4**

Thioacetic acid S- [4-[(4-isocyanophenyl)ethynyl]phenyl]ester (4) Into an oven-dried Schlenck flask, compound **11** (0.88 g, 2.99 mmol) and triphosgene (0.92 g, 3.11 mmol) were added. The flask was evacuated and back-filled with argon four times then cooled to 0°C. DCM (40 mL) and triethylamine (TEA, 16 mL) were then added followed by benzyltriethylammonium chloride (0.24 g, 1.04 mmol) in 16 mL of DCM. The flask was allowed to warm to room temperature and stirred for 5 hours. The solvents were removed on a rotatory evaporator and the residue was purified using flash chromatography (10:1 hexanes:ethyl acetate) to yield 0.21 g of the desired product (25%). IR (neat) 2124, 1711,

1508, 844, 820 cm^{-1}. FAB-MS (matrix: NBA); m/z Calcd 277.0561 (M+); found 277.0564 (Δ = 1.1 ppm).). ^{1}H NMR (400 MHz, $CDCl_3$) δ (ppm) 7.56 (d, *J* = 2.0 Hz, 2H), 7.54 (d, *J* = 2 Hz, 2H), 7.41 (d, *J* = 8.4 Hz, 2H), 7.37 (d, J = 8.8 Hz, 2H), 2.44 (s, 3H). ^{13}C NMR (400 MHz, $CDCl_3$) δ (ppm) 193.54, 166.03, 135.32, 134.53, 132.90, 132.69, 132.47, 131.38, 131.33, 129.05, 126.74, 124.62, 123.87, 91.56, 89.48, 30.59.

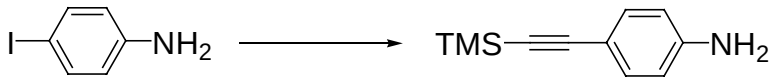

5 **6**

4-[trimethylsilyl)ethynyl]aniline (6) Inside a N_2-filled dry box, 4-iodoaniline (**5**) (5.15 g, 23.53 mmol), tris(dibenzylideneacetone) bispalladium (0) (0.53 g, 0.52 mmol), triphenylphosphine (0.58 g, 2.21 mmol), and copper iodide (0.61 g, 3.23 mmol) were added to an oven-dried Schlenck flask. THF (45 mL), diisopropylethylamine (15 mL), and trimethylsilylacetylene (8 mL, 62.86 mmol) then added. The flask was sealed, removed from dry box, and heated to 70°C with stirring for 48 hours. Flask cooled to room temperature and the solvents were removed on a rotatory evaporator. The remaining residue was dissolved in DCM and filtered through a silica plug. Filtrate was then dried and purified using flash chromatography (5:1 hexanes:ethyl acetate) to yield 3.87 g of the desired product (87%). ^{1}H NMR (400 MHz, $CDCl_3$) δ (ppm) 7.27 (d, *J* = 8.4 Hz, 2H), 6.59 (d, *J* = 8.8 Hz, 2H), 3.79 (bs, 2H), 0.23 (s, 9H).

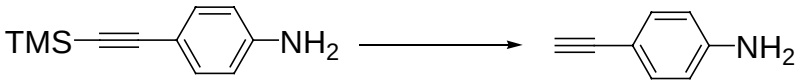

6 **7**

4-ethyynylaniline (7) In a round-bottom flask, compound **6** (3.87 g, 20.48 mmol) and potassium carbonate (3.66 g) were dissolved in methanol (150 mL). The solution was stirred at room temperature overnight, then diluted with water. The solution was extracted with ether, washed with brine, dried with magnesium sulfate, filtered, and the solvents removed on a rotatory evaporator to yield a red solid (2.37 g, 99%). ^{1}H NMR (400 MHz, $CDCl_3$) δ (ppm) 7.29 (d, *J* = 8.0 Hz, 2H), 6.60 (d, *J* = 8.4 Hz, 2H), 3.82 (bs, 2H), 2.95 (s, 1H).

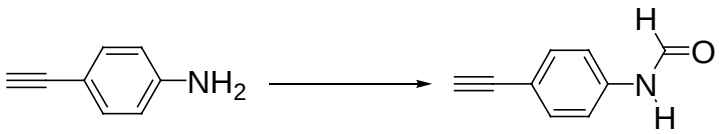

7 **8**

N-(4-ethynylphenyl)formamide (8) An oven-dried, round-bottomed flask was equipped with a reflux condenser and cooled to room temperature under nitrogen. Acetic anhydride (5 mL) was added to the flask and cooled to 0°C. Formic acid (3 mL) was then added dropwise. The mixture was heated to 60°C for 2.5 hours then cooled to room temperature. The solution was diluted with THF (15 mL) and cooled to -20°C. A solution of compound **7** (2.37 g, 20.26 mmol) in THF (15 mL) was added slowly and the resultant mixture was stirred at -20°C for 30 minutes. The solvents were removed on a rotatory evaporator and the residue dissolved in DCM. The organic phase was washed with water, dried with magnesium sulfate, filtered, and the solvents removed on a rotatory evaporator to yield a yellow solid. The residue was purified with flash chromatography eluting with 1:1 hexanes:ethyl acetate to produce a yellow solid (2.17 g, 74%). ^{1}H NMR (400 MHz, $CDCl_3$) δ (ppm) 8.73 (d, J = 11.6 Hz, 0.5H), 8.39 (d, J = 1.2 Hz, 0.5H), 7.49 (m, 5H), 7.04 (d, J = 8.8 Hz, 1H), 3.08 (d, 1H).

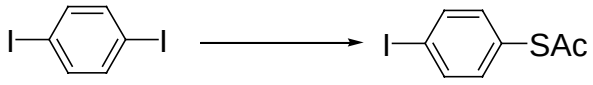

9 **10**

4-iodophenylthioacetate (10) Inside a N_2-filled dry box, diiodobenzene (**9**) (5.16 g, 15.63 mmol) was added to a Schlenck flask and dissolved in THF (40 mL). Into a second Schlenck flask, sulfur powder (0.44 g, 13.76 mmol) was suspended in THF (30 mL). The flasks were then sealed and removed from the dry box. The flask containing diiodobenzene was cooled to –78°C and the flask containing sulfur was cooled to 0°C. To the diiodobenzene solution, ^{t}BuLi (18 mL, 27.0 mmol) was added dropwise by syringe and the solution stirred vigorously for 5 minutes. The sulfur suspension was then added slowly to the first flask and the resultant solution was stirred at 0°C for 1 hour. Acetyl chloride (1.7 mL, 23.67 mmol) quickly added to the flask by syringe and the flask was allowed to warm to room temperature and stir overnight. The solution was then diluted with DCM, washed with water, dried with magnesium sulfate, filtered, and the solvents removed on a rotatory evaporator to yield a dark

yellow oil. The residue was purified with flash chromatography eluting with 25:1 hexanes:ethyl ether to produce a white solid (1.98 g, 46%). ^{1}H NMR (400 MHz, $CDCl_3$) δ (ppm) 7.74 (d, *J* = 8.4 Hz, 2H), 7.13 (d, *J* = 8.0 Hz, 2H), 2.43 (s, 3H).

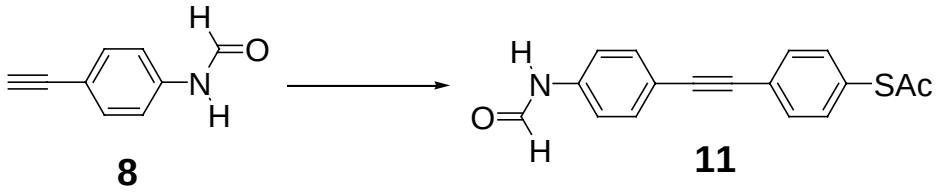

8 **11**

Thioacetic acid S-[4-[[4-(formylamino)phenyl]ethynyl]phenyl]ester (11) Inside a N_2-filled dry box, compound **10** (1.64 g, 5.90 mmol), compound **8** (0.70 g, 4.85 mmol), tris(dibenzylideneacetone) bispalladium (0) (0.10 g, 0.10 mmol), triphenylphosphine (0.16 g, 0.62 mmol), and copper iodide (0.09 g, 0.37 mmol) were added to an oven-dried Schlenck flask. THF (20 mL) and diisopropylethylamine (7 mL) were then added. The flask was sealed, removed from dry box, and heated to 90°C with stirring for 48 hours. The flask was then cooled to room temperature and the solvents were removed on a rotatory evaporator. The remaining residue was dissolved in DCM and filtered through a Celite plug. The filtrate was dried and purified using flash chromatography (1:1 hexanes:ethyl acetate) to yield 1.09 g of the desired product (76%). IR (neat) 1687, 1606, 1587, 1523, 1407, 1294, 1118, 831 cm^{-1}. FAB-MS (matrix: NBA); m/z Calcd 295.0667 (M+); found 295.0672 (Δ = 1.7 ppm). ^{1}H NMR (300 MHz, $CDCl_3$) δ (ppm) 8.75 (d, *J* = 11.7 Hz, 0.5H), 8.39 (d, *J* = 1.5 Hz, 0.5H), 7.75 (d, *J* = 11.4 Hz, 0.5 H), 7.42 (m, 7H), 7.05 (d, *J* = 8.7 Hz, 1H), 2.44 (s, 3H). ^{13}C NMR (400 MHz, $CDCl_3$) δ (ppm) 194.66, 194.34, 162.49, 159.44, 137.48, 137.19, 135.30, 134.57, 133.43, 133.36, 132.78, 132.72, 132.61, 132.40, 131.94, 131.83, 128.22, 127.95, 124.90, 124.65, 119.88, 119.84, 119.76, 119.07, 118.35, 118.29, 91.16, 90.57, 89.16, 88.60, 30.60.

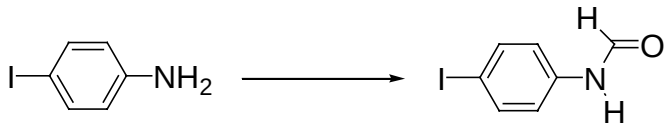

5 **12**

N-(4-iodophenyl)formamide (12) An oven-dried, round-bottomed flask was equipped with a reflux condenser and cooled to room temperature under nitrogen. Acetic anhydride

(60 mL, 0.64 mol) was added to the flask and cooled to 0°C. Formic acid (45 mL, 1.19 mol) was then added dropwise. The mixture was heated to 60°C for 30 minutes then cooled to room temperature. The solution was cooled to -0°C and a solution of 4-iodoaniline (**5**) (70.77 g, 0.32 mol) in THF (200 mL) was added slowly and the resultant mixture was allowed to gradually warm to room temperature and stir overnight. The solvents were removed on a rotatory evaporator and the residue was diluted with water. The precipitate was then filtered and recrystallized from dichloromethane with hexanes to yield an off-white solid (75.31 g, 94%). ^{1}H NMR (300 MHz, $CDCl_3$) δ (ppm) 8.66 (d, *J* = 11.1 Hz, 0.5H), 8.38 (d, *J* = 1.8 Hz, 1H), 7.63 (d, *J* = 6.9 Hz, 2H), 7.32 (d, *J* = 8.7 Hz, 1H), 6.85 (d, *J* = 8.7 Hz, 1H).

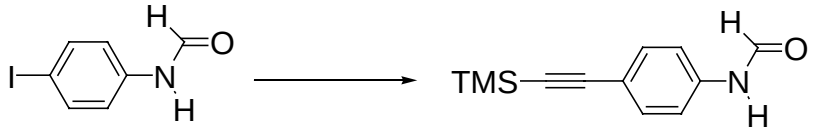

12 **13**

N-[4-[(trimethylsilyl)ethynyl]phenyl]formamide (13) Inside a N_2-filled dry box, compound **12** (10.17 g, 41.19 mmol), tris(dibenzylideneacetone) bispalladium (0) (1.09 g, 1.06 mmol), triphenylphosphine (1.04 g, 3.97 mmol), and copper iodide (0.85 g, 4.47 mmol) were added to an oven-dried Schlenck flask. THF (100 mL), diisopropylethylamine (30 mL), and trimethylsilylacetylene (7 mL, 55.0 mmol) then added. The flask was sealed, removed from dry box, and heated to 50°C overnight with stirring. The solution was cooled to room temperature, diluted with ammonium chloride, extracted with ether, dried with magnesium sulfate, filtered, and solvents were removed on a rotatory evaporator. The remaining residue was purified using flash chromatography (1:1 hexanes:ethyl acetate) to yield 7.98 g of the desired product (89%). ^{1}H NMR (400 MHz, $CDCl_3$) δ (ppm) 8.72 (d, *J* = 11.6 Hz, 0.5H), 8.37 (d, *J* = 1.6 Hz, 0.5H), 7.46 (m, 3H), 7.02 (d, *J* = 8.8 Hz, 1H), 0.24 (9H).

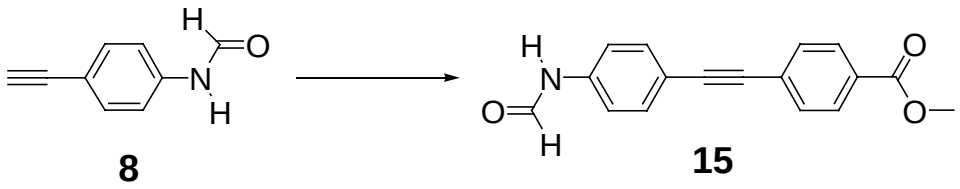

8 **15**

4-(4-formylamino-phenylethynyl)benzoic acid methyl ester (15) Inside a N_2-filled dry box, methyl-4-iodobenzoate (**14**) (2.79 g, 10.63 mmol), **8** (1.35 g, 9.31 mmol), tris(dibenzylideneacetone) bispalladium (0) (0.25 g, 0.24 mmol), triphenylphosphine (0.24 g, 0.93 mmol), and copper iodide (0.20 g, 1.04 mmol) were added to an oven-dried Schlenck flask. THF (20 mL) and diisopropylethylamine (8 mL) were then added. The flask was sealed, removed from dry box, and heated to 65°C with stirring for 48 hours. The flask was then cooled to room temperature and the solvents were removed on a rotatory evaporator. The remaining residue was dissolved in DCM and filtered through a Celite plug to yield a yellow-orange solid. The product was purified using flash chromatography (1:1 hexanes:ethyl acetate) followed by recrystallization in hot ethanol to yield 1.02 g of the desired product (39%). IR (neat) 1720, 1649, 1406, 1280, 1107 cm^{-1}. FAB-MS (matrix: NBA); m/z Calcd 279.0895 (M+); found 279.0891 (Δ = 1.4 ppm). ^1H NMR (400 MHz, $CDCl_3$) δ (ppm) 8.76 (d, *J* = 11.2 Hz 0.5H), 8.42 (d, *J* = 2.0 Hz, 0.5H), 8.02 (d, *J* = 8.4 Hz, 2H), 7.56 (m, 5H), 7.07 (d, *J* = 8.8 Hz, 1H), 3.93 (s, 3H). ^{13}C NMR (400 MHz, d_8-THF) δ (ppm) 165.69, 161.14, 158.78, 158.69, 139.51, 133.07, 132.40, 131.36, 129.75, 129.48, 128.26, 119.06, 118.99, 117.62, 117.08, 92.36, 87.89, 51.48.

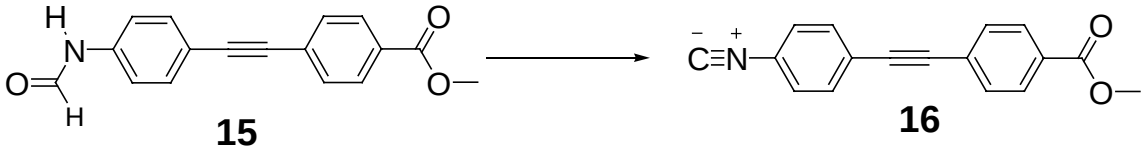

15 **16**

4-(4-isocyano-phenylethynyl)benzoic acid methyl ester (16) Into an oven-dried Schlenck flask, **15** (1.02 g, 3.66 mmol) and triphosgene (1.03 g, 3.46 mmol) were weighed. The flask was evacuated and back-filled with argon four times then cooled to 0°C. DCM (40 mL) and TEA (13 mL) were then added followed by benzyltriethylammonium chloride (0.52 g, 0.62 mmol) in 20 mL of dichloromethane. The flask was allowed to warm to room temperature and stir for 5.5 hours. The solvents were removed on a rotatory evaporator and the remaining residue was purified using flash chromatography (5:1 hexanes:ethyl acetate) to

yield 0.60 g of the desired product (63%). IR (neat) 2924, 2853, 2124, 1718, 1646, 1279, 1104 cm^{-1}. ^1H NMR (400 MHz, $CDCl_3$) δ (ppm) 8.04 (d, *J* = 8.4 Hz, 2H), 7.59 (d, *J* = 8.4 Hz, 2H), 7.56 (d, *J* = 8.8 Hz, 2H), 7.38 (d, *J* = 8.4 Hz, 2H), 3.94 (s, 3H). ^{13}C NMR (400 MHz, $CDCl_3$) δ (ppm) 166.64, 166.22, 132.95, 131.85, 130.28, 129.83, 127.31, 126.78, 124.40, 91.46, 90.64, 52.56.

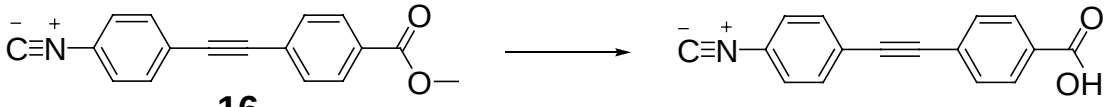

16 **17**

4-(4-isocyano-phenylethynyl)benzoic acid (17) In a round-bottom flask, compound **16** (0.59 g, 2.25 mmol) and lithium hydroxide (0.23 g, 8.52 mmol) were dissolved in methanol (50 mL), dichloromethane (30 mL), and water (15 mL). The solution was then stirred at room temperature for 48 hours. The solution was diluted with dichloromethane then extracted with water. The aqueous layer was acidified with concentrated hydrochloric acid to form a white precipitate, which was filtered to yield the desired product (0.54 g, 96%). ^1H NMR (400 MHz, d^6-DMSO) δ (ppm) 7.86 (d, *J* = 8.4 Hz 2H), 7.64 (dd, *J* = 6.8, 10.8 Hz, 4H), 7.46 (d, *J* = 8.4 Hz 2H). ^{13}C NMR (400 MHz, d^6-DMSO) δ (ppm) 168.83, 166.23, 133.38, 131.26, 130.97, 129.93, 127.60, 125.93, 124.70, 122.22, 93.08, 88.92.

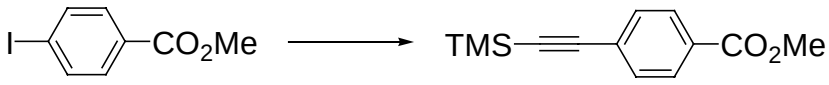

14 **18**

Methyl 4-(trimethylsilylethynyl)benzoate (18) Inside a N_2-filled dry box, methyl 4-iodobenzoate (**14**) (3.42 g, 13.05 mmol), tris(dibenzylideneacetone) bispalladium (0) (0.31 g, 0.30 mmol), triphenylphosphine (0.48 g, 1.84 mmol), and copper iodide (0.25 g, 1.33 mmol) were added to an oven-dried Schlenck flask. THF (25 mL), diisopropylethylamine (10 mL), and trimethylsilylacetylene (5 mL, 39.29 mmol) was then added. The flask was sealed, removed from dry box, and heated to 50°C with stirring for 48 hours. The flask was cooled to room temperature and the solvents were removed on a rotatory evaporator. The remaining residue was suspended in hexanes, sonicated, and filtered through a silica plug with 10:1 hexanes: ethyl acetate. Filtrate dried and purified using flash chromatography (20:1

hexanes:ethyl acetate) to yield 2.71 g of the desired product (89%). ^{1}H NMR (400 MHz, $CDCl_3$) δ (ppm) 7.97 (d, *J* = 8.0 Hz, 2H), 7.51 (d, *J* = 8.0 Hz, 2H), 3.91 (s, 3H), 0.26 (s, 9H). ^{13}C NMR (400 MHz, $CDCl_3$) δ (ppm) 166.73, 132.09, 129.90, 129.59, 127.99, 104.28, 97.91, 52.44, 0.21.

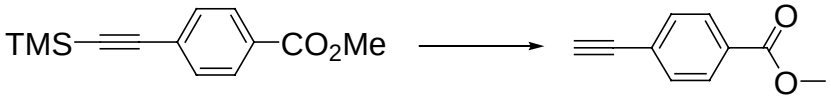

18 **19**

Methyl *p*-ethynyl benzoate (19) In a round-bottom flask, compound **18** (2.77 g, 11.94 mmol) and potassium carbonate (10.80 g) were dissolved in methanol (100 mL) and stirred at room temperature overnight. The solution was diluted with water, extracted with ether, dried with magnesium sulfate, filtered, and the solvents removed on a rotatory evaporator to yield a brown solid (1.42 g, 74%). ^{1}H NMR (400 MHz, d^{6}-DMSO) δ (ppm) 7.94 (d, *J* = 7.6 Hz, 1H), 7.88 (d, *J* = 8.0 Hz, 1H), 7.61 (d, *J* = 8.4 Hz 1H), 7.44 (d, *J* = 8.0 Hz, 1H), 3.84 (s, 1H), 2.49 (s, 3H).

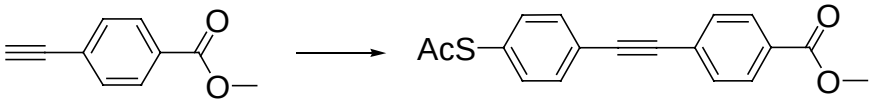

19 **20**

4-(4-acetosulfanyl-phenylethynyl)benzoic acid methyl ester (20) Inside a N_2-filled dry box, 4-iodophenylthioacetate (**10**) (0.98 g, 3.54 mmol), compound **19** (0.48 g, 3.01 mmol), tris(dibenzylideneacetone) bispalladium (0) (0.086 g, 0.08 mmol), triphenylphosphine (0.20 g, 0.46 mmol), and copper iodide (0.12 g, 0.63 mmol) were added to an oven-dried Schlenck flask. THF (7 mL) and diisopropylethylamine (3 mL) were then added. The flask was sealed, removed from dry box, and heated to 90°C for 48 hours. The flask was cooled to room temperature and the solvents were removed on a rotatory evaporator. The remaining residue was dissolved in dichloromethane and filtered through a Celite plug. The filtrate was dried and purified using flash chromatography (10:1 hexanes:ethyl acetate) to yield 0.19 g of the desired product (20%). ^{1}H NMR (400 MHz, $CDCl_3$) δ (ppm) 8.03 (d, *J* = 8.4 Hz, 2H), 7.59 (d, *J* = 8.4 Hz, 2H), 7.57 (d, *J* = 11.6 Hz, 2H), 7.41 (d, *J* = 8.4 Hz, 2H), 3.93 (s, 3H), 2.44 (s, 3H).

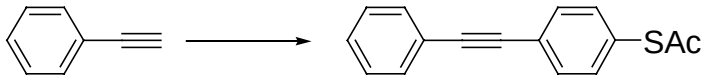

22 **23**

Thioacetic acid S-[4-(phenylethynyl)phenyl]ester (23) Inside a N_2-filled dry box, 4-iodophenylthioacetate (**10**) (1.97 g, 7.08 mmol), tris(dibenzylideneacetone) bispalladium (0) (0.26 g, 0.25 mmol), triphenylphosphine (0.19 g, 0.73 mmol), and copper iodide (0.13 g, 0.70 mmol) were added to an oven-dried Schlenck flask. THF (15 mL), diisopropylethylamine (5 mL), and phenylacetylene (**22**) (1.0 mL, 9.12 mmol) then added. The flask was sealed, removed from dry box, and heated to 60°C overnight with stirring. The solution was cooled to room temperature, the solvents removed on a rotatory evaporator, and the residue filtered through a Celite plug with dichloromethane. The remaining residue was purified using flash chromatography (10:1 hexanes:ethyl acetate) to yield an off-white solid (1.34 g, 75%). ^{1}H NMR (300 MHz, $CDCl_3$) δ (ppm) 7.55 (m, 4H), 7.37 (m, 5H), 2.44 (s, 3H).

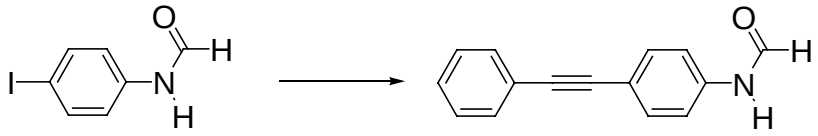

12 **24**

N-[4-(phenylethynyl)phenyl]formamide (24) Inside a N_2-filled dry box, **12** (2.06 g, 9.39 mmol), tris(dibenzylideneacetone) bispalladium (0) (0.21 g, 0.20 mmol), triphenylphosphine (0.26 g, 0.99 mmol), and copper iodide (0.28 g, 1.45 mmol) were added to an oven-dried Schlenck flask. THF (15 mL), diisopropylethylamine (6 mL), and phenylacetylene (**22**) (1.3 mL, 11.86 mmol) was then added. The flask was sealed, removed from dry box, and heated to 60°C for 24 hours with stirring. The solution was cooled to room temperature, the solvents removed on a rotatory evaporator, and the residue filtered through a Celite plug with methanol. The remaining residue was purified using flash chromatography (1:1 hexanes:ethyl acetate) to yield a tan solid (1.23 g, 59%). ^{1}H NMR (400 MHz, d^6-acetone) δ (ppm) 9.44 (bs, 0.5H) 8.92 (d, J = 11.2 Hz 0.5H), 8.40 (d, J = 1.6 Hz, 0.5H), 7.74 (m, 2H), 7.53 (m, 4H), 7.41 (m, 3H), 7.32 (d, 0.5H).

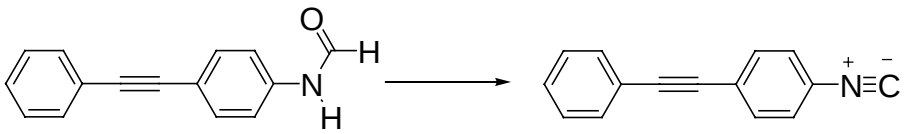

24 **25**

1-isocyano-4-(phenylethynyl)-benzene (25) Into an oven-dried Schlenck flask, **24** (0.94 g, 4.26 mmol) and triphosgene (1.65 g, 5.54 mmol) were weighed. The flask was evacuated and back-filled with argon four times then cooled to 0°C. DCM (25 mL) and TEA (20 mL) were then added followed by benzyltriethyl ammonium chloride (0.50 g, 2.20 mmol) in dichloromethane (15 mL). The flask was allowed to warm to room temperature and stir for 6 hours. The solution was washed with water, dried with magnesium sulfate, filtered, and the solvents removed on a rotatory evaporator. The remaining residue was purified using flash chromatography (10:1 hexanes:ethyl acetate) to yield 0.35 g of the desired product (40%). ^{1}H NMR (300 MHz, $CDCl_3$) δ (ppm) 7.53 (m, 4H), 7.37 (m, 4H).

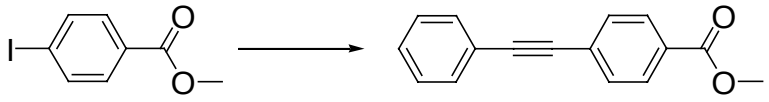

14 **26**

Methyl 4-(phenylethynyl)benzoate (26) Inside a N_2-filled dry box, methyl 4-iodobenzoate (**14**) (1.90 g, 7.60 mmol), tris(dibenzylideneacetone) bispalladium (0) (0.17 g, 0.17 mmol), triphenylphosphine (0.23 g, 0.90 mmol), and copper iodide (0.21 g, 1.12 mmol) were added to an oven-dried Schlenck flask. THF (15 mL), diisopropylethylamine (5 mL), and phenylacetylene (**22**) (1.1 mL, 10.0 mmol) then added. The flask was sealed, removed from dry box, and heated to 60°C for 24 hours with stirring. The solution was cooled to room temperature, the solvents removed on a rotatory evaporator, and the residue filtered through a Celite plug with dichloromethane. The remaining residue was purified using flash chromatography (10:1 hexanes:ethyl acetate) to yield an orange solid (1.50 g, 84%). ^{1}H NMR (400 MHz, $CDCl_3$) δ (ppm) 8.02 (d, J = 8.4 Hz, 2H), 7.59 (d, J = 8.4 Hz, 2H), 7.55 (m, 2H), 7.37 (m, 3H), 3.93 (s, 3H).

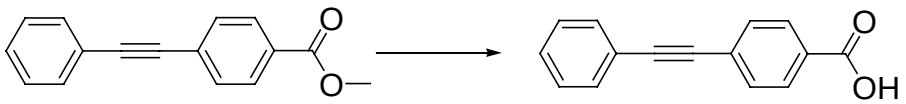

26 **27**

4-(phenylethynyl) benzoic acid (27) In a round-bottom flask, compound **26** (1.45 g, 6.14 mmol) and lithium hydroxide (0.72 g, 26.67 mmol) were dissolved in methanol (150 mL), dichloromethane (90 mL), and water (45 mL). The solution was then stirred at room temperature for 4 days. The solution was then extracted diluted with 2N NaOH. The aqueous layer was acidified with concentrated hydrochloric acid, extracted with dichloromethane, dried with magnesium sulfate, filtered, and the solvent removed with a rotatory evaporator to yield an off-white solid (1.06 g, 76%). ^{1}H NMR (400 MHz, d^{6}-DMSO) δ (ppm) 7.95 (d, *J* = 8.0 Hz, 2H), 7.65 (d, *J* = 8.4 Hz, 2H), 7.58 (m, 2H), 7.43 (m, 3H).

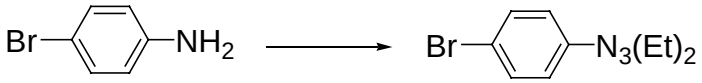

28 **29**

1-(4-bromophenyl)-3,3-diethyl-1-triazene (29) In a 500-mL flask, bromoaniline (**28**) (20.70 g, 120 mmol) was dissolved in 1.3 M HCl (200 mL) and cooled to 0°C. Sodium nitrite (12.35 g, 179 mmol) was dissolved in water (40 mL), cooled to 0°C, and added dropwise to the bromoaniline solution over one hour. The solution was then stirred at 0°C for one hour. In a 1-L flask, potassium carbonate (27.86 g) was dissolved in water (150 mL). Diethylamine (19 mL) was added then the solution was cooled to 0°C. Bromoaniline/sodium nitrite solution was added dropwise to the potassium carbonate solution and stirred at 0°C for two hours. The solution was extracted with ether, dried with magnesium sulfate, filtered, and the solvents removed on a rotatory evaporator. The residue was dissolved in ether and filtered through a silica plug. The solvents were removed on a rotatory evaporator to yield 25.15 g of a dark brown oil (82%). ^{1}H NMR (400 MHz, $CDCl_3$) δ (ppm) 7.42 (d, *J* = 8.8 Hz, 2H), 7.29 (d, *J* = 8.8 Hz, 2H), 3.75 (q, *J* = 7.2 Hz, 4H), 1.26 (t, *J* = 6.4 Hz, 6H).

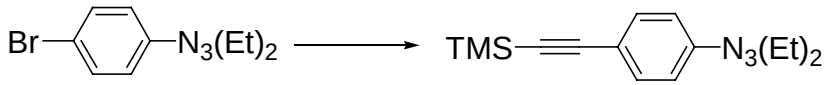

29 **30**

1-[4-[(trimethylsilyl)ethynyl]phenyl]-3,3-diethyl-1-triazene (30) Into an oven-dried Schlenck flask, compound **29** (20.55 g, 80.3 mmol), tris(dibenzylideneacetone) bispalladium (0) (1.51 g, 1.65 mmol), triphenylphosphine (4.16 g, 15.9 mmol), and copper iodide (1.56 g, 8.21 mmol) were added. The flask was evacuated and backfilled with argon three times. THF (150 mL) and diisopropylethylamine (45 mL) were then added and contents mixed well. Trimethylsilylacetylene (13.5 mL, 96.4 mmol) was then added. The flask was sealed and heated to 80°C for 72 hours. The flask was cooled to room temperature and the solvents were removed on a rotatory evaporator. The remaining residue was suspended in petroleum ether, sonicated for 20 minutes, and then filtered through a plug filter of silica under Celite. The solvents were removed on a rotatory evaporator to yield 20.82 g of a dark brown oil (95%). ^{1}H NMR (400 MHz, $CDCl_3$) δ (ppm) 7.43 (d, J = 8.4 Hz, 2H), 7.34 (d, J = 8.4 Hz, 2H), 3.76 (q, J = 7.2 Hz, 4H), 1.27 (t, 6H), 0.25 (s, 9H).

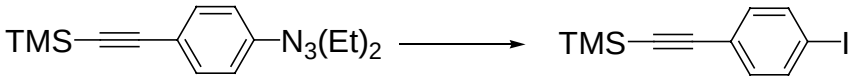

30 **31**

[(4-iodophenyl)ethynyl]trimethylsilane (31) Compound **30** (9.86 g, 36.12 mmol) was added to a heavy-walled tube and purged well with nitrogen. Methyl iodide (20 mL, 324 mmol) was then added by syringe. The flask was then heated to 120°C overnight. The flask was cooled to room temperature and excess methyl iodide was distilled off. The remaining residue was dissolved in petroleum ether and filtered through a silica plug. The solvents were removed on a rotatory evaporator to yield a yellow brown solid (8.81 g, 81%). ^{1}H NMR (400 MHz, $CDCl_3$) δ (ppm) 7.63 (d, J = 8.0 Hz, 2H), 7.17 (d, J = 8.0 Hz, 2H), 0.24 (s, 9H).

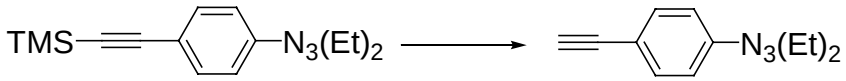

30 **32**

1-(4-ethynylphenyl)-3,3-diethyl-1-triazene (32) In a round-bottom flask, compound **30** (9.22 g, 33.8 mmol) and a catalytic amount of potassium carbonate were dissolved in methanol (50 mL). The solution was stirred at room temperature overnight then the solvents were removed on a rotatory evaporator. The remaining residue was dissolved in DCM and filtered through a silica plug. The solvents were removed on a rotatory evaporator to yield 6.61 g of a dark brown oil (97%). ^{1}H NMR (400 MHz, $CDCl_3$) δ (ppm) 7.44 (d, J = 8.4 Hz, 2H), 7.35 (d, J = 8.4 Hz, 2H), 3.76 (q, J = 7.2 Hz, 4H), 3.06 (s, 1H), 1.25 (t, 6H).

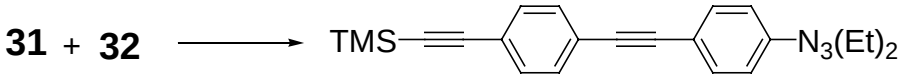

33

1-[4-[[4-[(trimethylsilyl)ethynyl]phenyl]ethynyl]phenyl]-3,3-diethyl-1-triazene (33) Into an oven-dried Schlenck flask, compound **31** (4.10 g, 13.67 mmol), compound **32** (2.26 g, 11.24 mmol), tris(dibenzylideneacetone) bispalladium (0) (0.27 g, 0.26 mmol), triphenylphosphine (0.33 g, 1.26 mmol), and copper iodide (0.30 g, 1.58 mmol) were added. The flask was evacuated and backfilled with argon four times. Inside a N_2-filled dry box, THF (25 mL) and diisopropylethylamine (8 mL) were then added and contents mixed well. The flask was sealed, removed from the dry box, and heated to 60°C for 48 hours. The flask was cooled to room temperature and the solvents were removed on a rotatory evaporator. The remaining residue was dissolved in DCM and filtered through a silica plug. The solvents were removed on a rotatory evaporator and the remaining residue was purified using flash chromatography (50:1 hexanes:ethyl acetate) to yield 2.87 g of the desired product (93%). ^{1}H NMR (400 MHz, $CDCl_3$) δ (ppm) 7.43 (m, 8H), 3.78 (q, J = 7.2 Hz, 4H), 1.28 (t, J = 7.2 Hz, 6H), 0.28 (s, 9H).

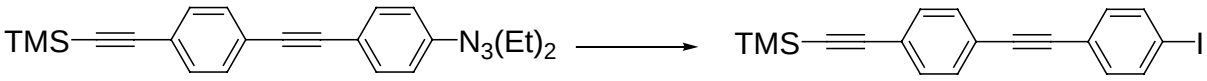

33 **34**

[4-[(4-iodophenyl)ethynyl]phenylethynyl]trimethylsilane (34) To a heavy-walled flask, compound **33** (2.89 g, 7.70 mmol) was added and purged well with nitrogen. Freshly-distilled methyl iodide (10 mL, 225 mmol) was then added by syringe. The flask was then heated to 120°C for 48 hours. The flask was cooled to room temperature and excess methyl iodide was distilled off. The remaining residue was dissolved in ethyl ether and filtered through a silica plug. The solvents were removed on a rotatory evaporator to yield a bright yellow solid, which was purified using flash chromatography (100% hexanes) to yield (2.82 g, 91%). ^{1}H NMR (400 MHz, $CDCl_3$) δ (ppm) 7.69 (d, J = 8.0 Hz, 2H), 7.44 (s, 4H), 7.24 (d, J = 8.4 Hz, 2H), 0.25 (s, 9H).

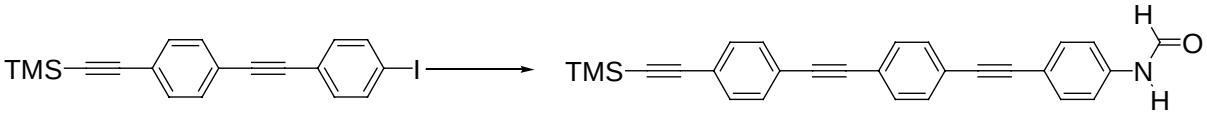

34 **35**

N-{[4-[4-(4-trimethylsilaneethynyl-phenylethynyl)-pehnylethynyl]-phenyl}formamide (35) Inside a N_2-filled dry box, **34** (0.72 g, 1.80 mmol), **7** (0.31 g, 2.14 mmol), tris(dibenzylideneacetone) bispalladium (0) (0.075 g, 0.07 mmol), triphenylphosphine (0.084 g, 0.32 mmol), and copper iodide (0.077 g, 0.40 mmol) were added to an oven-dried Schlenck flask. THF (5 mL) and diisopropylethylamine (2 mL) were then added. The flask was sealed, removed from dry box, and heated to 70°C for 48 hours. The flask was cooled to room temperature and the solvents were removed on a rotatory evaporator. The remaining residue was dissolved in methanol and filtered through a silica plug. The filtrate was dried and purified using flash chromatography (1:1 hexanes:ethyl acetate) to yield 0.13 g of the desired product (17%). ^{1}H NMR (300 MHz, d^6-DMSO) δ (ppm) 10.35 (s, 1H), 8.24 (s, 1H), 7.515 (m, 12H), 0.25 (s, 9H).

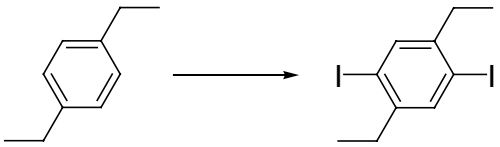

36 **37**

1,4-diethyl-2,5-diiodobenzene (37) Periodic acid (2.81 g, 12.34 mmol), iodine (5.64 g, 22.19 mmol), and 1,4-diethylbenzene (**36**) (3.33 g, 24.82 mmol) were weighed into a round-bottomed flask and dissolved in acetic acid (23 mL), water (7 mL), and sulfuric acid (0.7 mL). The flask was equipped with a condenser and the solution stirred under nitrogen at 100°C for 22 hours. The solution was cooled to room temperature, diluted with water, and the excess iodine was quenched with sodium thiosulfate. The solution was then extracted with dichloromethane, washed with sodium carbonate, dried with magnesium sulfate, filtered, and the solvents removed on rotary evaporator to yield a yellow solid. The product was purified by recrystallization from hot ethanol/acetone to give an off-white crystalline solid (5.93 g, 62%). ^{1}H NMR (300 MHz, $CDCl_3$) δ (ppm) 7.62 (s, 2H), 2.64 (q, J = 8.4 Hz, 4H), 1.18 (t, J = 8.4 Hz, 6H).

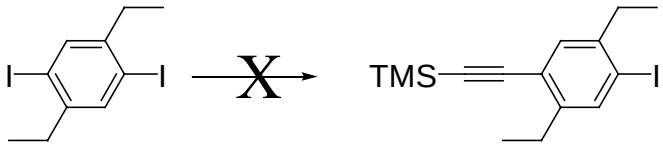

37 **38**

Attempt at 2,5-diethyl-4-[(trimethylsilyl)ethynyl]iodobenzene (38) Inside a N_2-filled dry box, compound **37** (1.31 g, 3.39 mmol), tris(dibenzylideneacetone) bispalladium (0) (0.07 g, 0.07 mmol), triphenylphosphine (0.14 g, 0.53 mmol), and copper iodide (0.12 g, 0.61 mmol) were added to an oven-dried Schlenck flask followed by dry THF (7 mL) and dry *i*Pr_2Net (3 mL). The solution was mixed well then TMS-acetylene (0.33 g, 3.38 mmol) was added. The flask was sealed and removed from the dry box and stirred at 40°C for 23 hours. The flask was cooled to room temperature and the solvents was removed on a rotatory evaporator. The remaining residue was filtered through a silica plug with DCM. The solvents were removed on a rotatory evaporator to yield a tan crystalline solid, which was purified using flash chromatography (100% hexanes). NMR of the product did not show the expected TMS peak at ~0.25 ppm.

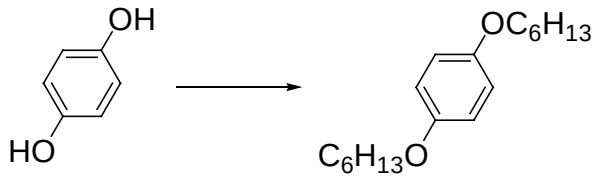

39 **40**

1,4-dihexyloxybenzene (40) To a solution of *p*-hydroquinone (**39**) (8.41 g, 76.45 mmol) in acetone (600 mL) was added bromohexane (32.5 mL, 0.23 mol) and potassium carbonate (26.44 g, 0.19 mol). The solution was refluxed under nitrogen for 72 hours, at which point an additional aliquot of potassium carbonate (8.41 g, 60.94 mmol) was added. The solution was refluxed an additional 48 hours then diluted with toluene and filtered hot. The solvents were removed on a rotatory evaporator to yield a brown crystalline solid, which was recrystallized from hot ethanol to give an off-white crystalline solid (14.45 g, 68%). ^{1}H NMR (300 MHz, $CDCl_3$) δ (ppm) 6.77 (s, 4H), 3.84 (t, *J* = 6.3 Hz, 4H), 1.70 (quint., *J* = 7.5 Hz, 4H), 1.40 (m, 4H), 1.29 (m, 8H), 0.86 (t, *J* = 6.6 Hz, 6H).

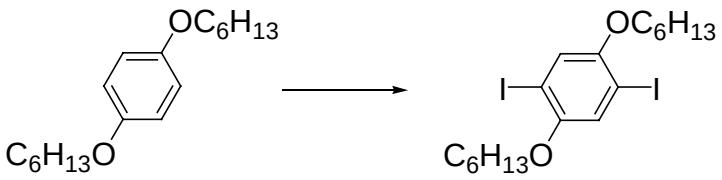

40 **41**

1,4-bis(hexyloxy)-2,5-diiodobenzene (41) Periodic acid (2.87 g, 12.60 mmol), iodine (7.64 g, 30.08 mmol), and 1,4-dihexyloxybenzene (**40**) (7.10 g, 25.55 mmol) were weighed into a round-bottomed flask and dissolved in acetic acid (50 mL), water (20 mL), and sulfuric acid (1.25 mL). The flask was equipped with a condenser and the solution stirred under nitrogen at 100°C for 24 hours. The solution was cooled to room temperature, diluted with water, and the excess iodine was quenched with sodium thiosulfate. The solution was then extracted with dichloromethane, washed with sodium carbonate, dried with magnesium sulfate, filtered, and the solvents removed on rotary evaporator. The product was purified by recrystallization from hot ethanol/acetone to give a yellowish crystalline solid (12.70 g, 94%). ^{1}H NMR (300 MHz, $CDCl_3$) δ (ppm) 7.17 (s, 2H), 3.92 (t, *J* = 6.6 Hz, 4H), 1.80 (quint., *J* = 6.6 Hz, 4H), 1.50 (quint., *J* = 8.1 Hz, 4H), 1.35 (m, 8H), 0.91 (t, *J* = 6.9 Hz, 6H).

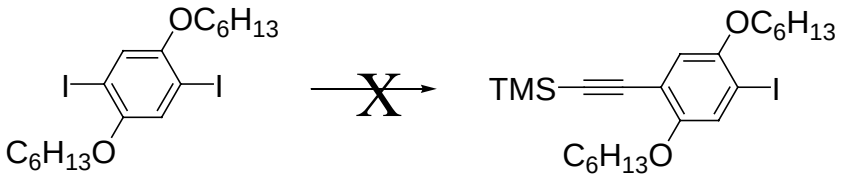

41 **42**

Attempt at 2,5-dihexyloxy-4-[(trimethylsilyl)ethynyl]iodobenzene (42) Inside a N_2-filled dry box, compound **41** (1.00 g, 1.88 mmol), tris(dibenzylideneacetone) bispalladium (0) (0.06 g, 0.06 mmol), triphenylphosphine (0.06 g, 0.23 mmol), and copper iodide (0.08 g, 0.40 mmol) were added to an oven-dried vial followed by 8 mL of dry TEA. The solution was mixed well then TMS-acetylene (0.19 g, 1.96 mmol) was added. The vial was stirred in the dry box at 50°C for 48 hours. The vial was cooled to room temperature and the TEA was removed on a rotatory evaporator. The remaining residue was filtered through a silica plug with 1:1 hexanes:ethyl acetate. The solvents were removed on a rotatory evaporator to yield a yellow solid. Examination by TLC revealed a large amount of un reacted starting material. Also, NMR of the crude product did not show the expected TMS peak at ~0.25 ppm. The synthesis was not pursued any furthur.

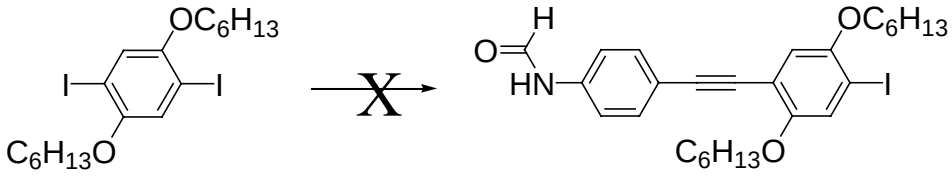

41 **43**

Attempt at [4-(2,5-Bis-hexyloxy-4-iodo-phenylethynyl)-phenyl]formamide (43) Inside a N_2-filled dry box, compound **41** (1.02 g, 1.93 mmol), compound **8** (0.25 g, 1.72 mmol), tris(dibenzylideneacetone) bispalladium (0) (0.04 g, 0.04 mmol), triphenylphosphine (0.06 g, 0.23 mmol), and copper iodide (0.08 g, 0.42 mmol) were added to an oven-dried vial followed by 20 mL of dry TEA. The vial was stirred in the dry box at 50°C for 48 hours. The vial was cooled to room temperature and the TEA was removed on a rotatory evaporator. The remaining residue was filtered through a silica plug with 1:1 hexanes:ethyl acetate. The filtrate was dried and checked by TLC. A large amount of unreacted starting material was still present as determined by TLC thus the synthesis was not pursued further.

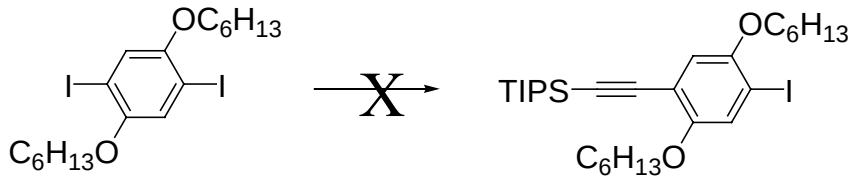

41 **44**

Attempt at 2,5-dihexyloxy-4-[(triisopropylsilyl)ethynyl]iodobenzene (44) Inside a N_2-filled dry box, compound **41** (1.03 g, 1.94 mmol), tris(dibenzylideneacetone) bispalladium (0) (0.06 g, 0.06 mmol), triphenylphosphine (0.06 g, 0.24 mmol), and copper iodide (0.03 g, 0.17 mmol) were added to an oven-dried vial followed by 20 mL of dry TEA. The solution was mixed well then TIPS-acetylene (0.34 g, 1.87 mmol) was added. The vial was stirred in the dry box at 70°C for 72 hours. The vial was cooled to room temperature and the TEA was removed on a rotatory evaporator. The remaining residue was filtered through a silica plug with dichloromethane. The solvents were removed on a rotatory evaporator to yield an orange brown solid, which was purified using flash chromatography (4:1 hexanes:ethyl acetate). Two fractions were collected and examined by NMR. The most intense spot on the TLC plate was starting material and the weaker spot was shown not to be the desired product. The synthesis was not pursued any further.

2.5 REFERENCES

(26) Martin, B. R.; Dermody, D. J.; Reiss, B. D.; Fang, M. M.; Lyon, L. A.; Natan, M. J.; Mallouk, T. E. *Adv. Mater.* **1999**, *11*, 1021-1025.

(27) Ahmadi, T. S.; Wang, Z. L.; Henglein, A.; ElSayed, M. A. *Chem. Mater.* **1996**, *8*, 1161-1163.

(28) Bauer, L. A.; Reich, D. H.; Meyer, G. J. *Langmuir* **2003**, *19*, 7043-7048.

(29) Price, D. W.; Dirk, S. M.; Maya, F.; Tour, J. M. *Tetrahedron* **2003**, *59*, 2497-2518.

(30) Tour, J. M.; Jones, L.; Pearson, D. L.; Lamba, J. J. S.; Burgin, T. P.; Whitesides, G. M.; Allara, D. L.; Parikh, A. N.; Atre, S. *J. Am. Chem. Soc.* **1995**, *117*, 9529-9534.

(31) Tour, J. M.; Rawlett, A. M.; Kozaki, M.; Yao, Y. X.; Jagessar, R. C.; Dirk, S. M.; Price, D. W.; Reed, M. A.; Zhou, C. W.; Chen, J.; Wang, W. Y.; Campbell, I. *Chem. Eur. J.* **2001**, *7*, 5118-5134.

(32) Flatt, A. K.; Yao, Y. X.; Maya, F.; Tour, J. M. *J. Org. Chem.* **2004**, *69*, 1752-1755.

(33) Arcoya, A.; Seoane, X. L.; Figoli, N. S.; Largentiere, P. C. *Appl. Catal.* **1990**, *62*, 35-45.

(34) Cassar, L. *J. Organomet. Chem.* **1975**, *93*, 253-257.

(35) Appel, R.; Kleinstu.R; Ziehn, K. D. *Angew. Chem.* **1971**, *10*, 132-133.

CHAPTER 3

Examination of the Binding of Bifunctional Molecules to Metal Surfaces and Nanoparticles

3.1 INTRODUCTION

Once the synthesis of the bifunctional test molecule **4** was finalized, as described in Chapter 2, it then became necessary to determine an analytical method for studying the binding of the linker molecules to metal nanoparticles. It has previously been indicated[36,37] that thiols bind selectively to gold over platinum and isonitriles bind selectively to platinum over gold. These conclusions were based on observations on the competition of two types molecules for a given type of surface. A method was needed to verify the selectivity of a molecule with two functional groups to a specific metal. This specificity is the driving force behind our proposed orthogonal self-assembly.

Previous research has shown that upon binding to platinum, there is a ~70-100 cm^{-1} shift in the isonitrile group stretch.[38-41] This shift when bonded to Pt is due to a loss of electron density on the bonded terminal carbon atom that then causes an increase in electron donation from the nitrogen. The increase in frequency also indicates that little π back-bonding is occurring from the metal since back-bonding would increase the electron density in the antibonding orbitals of the isonitrile and thus lower the vibration frequency.[40] This shift to lower wavenumber has been observed for isonitriles bonding to palladium[41] and was explained as being due to a strong back-bonding by the Pd metal. The authors did not observe a shift to lower wavenumber when the isonitrile was bonded to Au, which indicated to them that the isonitrile-Au bond was solely σ in character.

Polarization modulation infrared reflection-adsorption spectroscopy (PM-IRRAS) was chosen to initially examine the isonitrile groups binding preference to the two substrates by comparing its stretching energy. PM-IRRAS is used for characterization of thin films or monolayers on metal surfaces. The sample spectrum produced is the differential IR absorption between the p-component (perpendicular) and the s-component (parallel) reflected off the surface. It has the advantage of high surface sensitivity as the result of the surface selection rules. In brief, s-polarized light will not give any vibrational information about what is on the surface due to an oscillating image charge in the metal that cancels any transition moment excited by the light in the molecule on the surface (Figure 3.1). However, p-polarized light tends to enhance the signal from transition moments with at least some component perpendicular to the surface. PM-IRRAS creates a dichroic difference that is (p-

s)/(p+s) to obtain the spectrum of absorbed molecules on metal surfaces without the need for a separate background/reference slide.

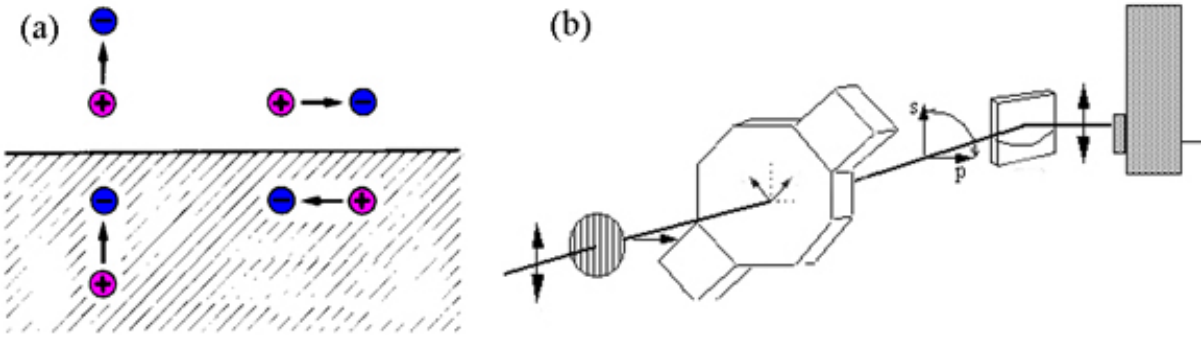

Figure 3.1. a) Surface selection rule [image from www.chembio.uoguelph.ca/educmat/chm729/eels/link3.htm] b) PM-IRRAS instrumentation [image from www.biophyreasearch.com/ftir.htm]

3.2 RESULTS AND DISCUSSION

3.2.1 PM-IRRAS of linker molecule on Au and Pt

The purpose of the initial IR experiment was to verify that the isonitrile shift described above could be observed with the bifunctional molecule **4**. A gold slide and a piece of platinum foil were prepared with a monolayer of bifunctional molecule **4**. For the initial experiment, only the solution exposed to the gold was deprotected with NH_4OH.[42] Since the solution exposed to the platinum sample did not contain any base to deprotect the thioacetate group, this experiment was not expected to show any competition between the isonitrile group and the thiol group to bind to the platinum. As can be seen in Figure 3.2, the PM-IRRAS for the gold substrate shows an isonitrile stretch at 2116 cm^{-1}, which compares well with the isonitrile stretch of 2124 cm^{-1} in solution. These results suggest the bifunctional linker molecule is bound to the Au slide via the exposed thiol terminal group. Upon examining the platinum substrate, the isonitrile stretch shifted to 2210 cm^{-1}, indicative of the linker molecule binding through the isonitrile. These data indicates that IR can indeed provide a good measurement of the selective binding of the bifunctional molecule **4**. Though there was good evidence of the isonitrile binding to the platinum, the test was biased in that only the linker solution for the Pt sample was deprotected. To observe the binding affinity of each terminus of the molecule, it would be necessary to deprotect both sample solutions. Also, the high absorbance of the samples indicates the formation of multilayers. To

minimize multilayers and to enhance solubility of the molecule, the concentration of the linker should be decreased.

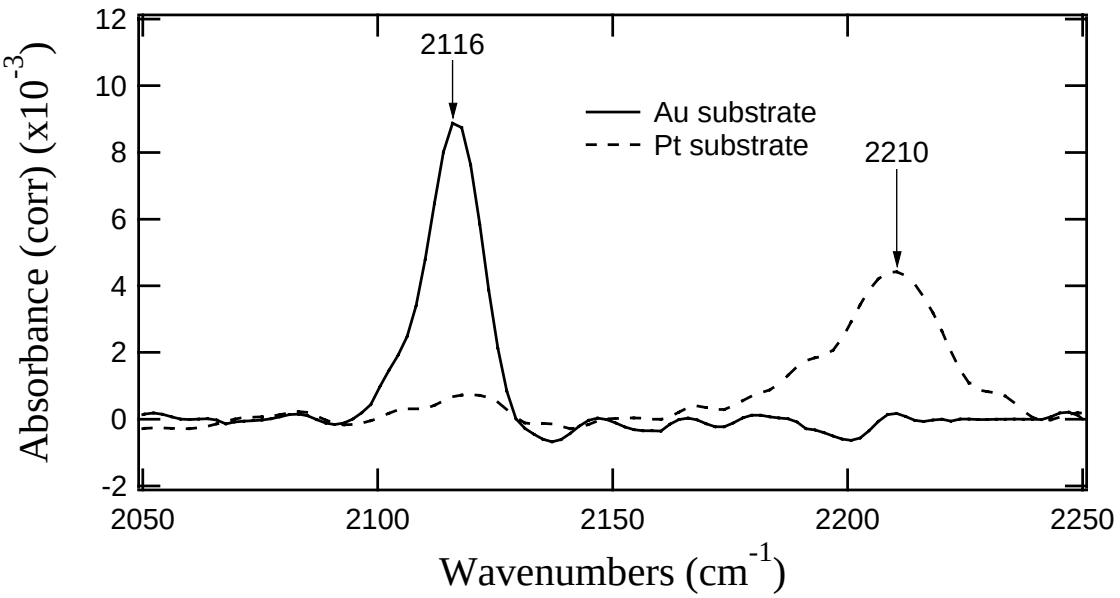

Figure 3.2. PM-IRRAS of molecule **4** on Au (deprotected) and Pt (protected).

A solution of **4** was prepared at a concentration of 0.4 mM in 7:2 toluene/EtOH and the thioacetate was deprotected using NH_4OH. This solution was used to separately incubate a Au and a Pt sample followed by examination by PM-IRRAS. The decreased absorbance of the samples is more consistent with what is expected upon monolayer formation. While not as distinctive as the results previous, Figure 3.3 indicates that the affinities of the functional groups for Au and Pt appear to be similar, which is not unexpected given the results published by Wrighton and Whitesides.[37] Further experiments using the PM-IRRAS were not possible due to instrument difficulties requiring a switch to the less sensitive grazing angle FTIR.

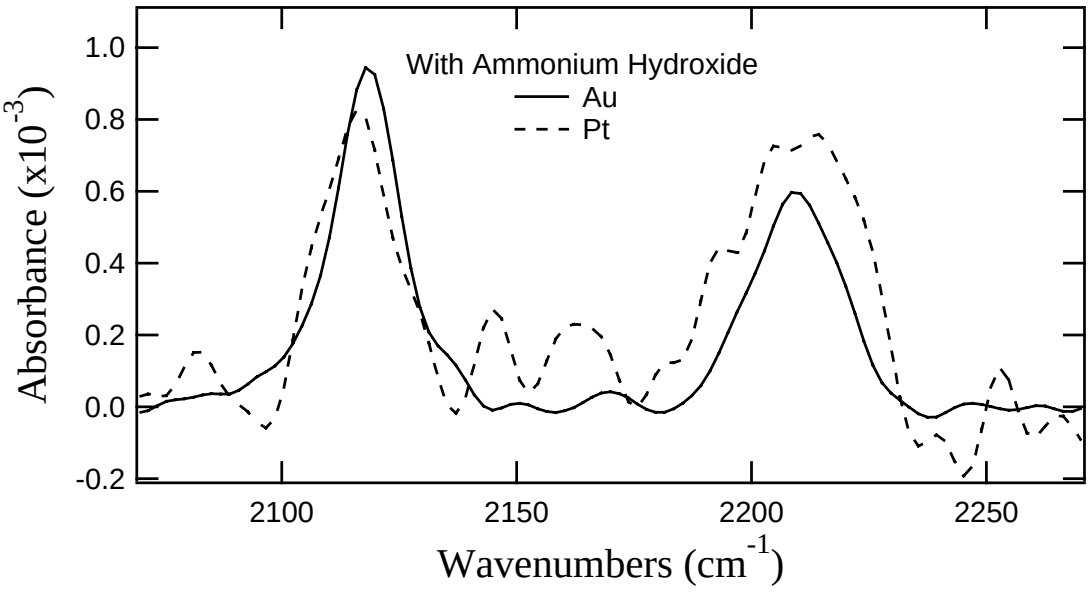

Figure 3.3. PM-IRRAS of molecule **4** on Au and Pt (both deprotected).

3.2.2 Reflectance IR of linker and monofunctional molecules on Au and Pt

The binding of molecule **4** to Au and Pt substrates was analyzed using grazing-angle reflectance FTIR. Ellipsometric thicknesses of 13.8 (3.7 Å (on Au) and 14.1 (5.1 Å (on Pt) indicated that monolayers of these molecules formed on each substrate (given an estimated molecular length of 14 Å from AM1-level geometry optimization). These monolayers were then evaluated using grazing angle infrared reflectance spectroscopy (Figure 3.4). An enhanced acetylene stretch at ca. 2216 cm^{-1} was observed in these monolayers and in spectra subsequently taken on nanoparticles. More importantly, the isonitrile stretch of the molecule on both gold and platinum indicated mostly unbound isonitrile, suggesting that these molecules were bound via the thiol groups. As a control, a monolayer of molecule **25** was formed on Pt. This molecule lacks a thiol, and the monolayer composed of it showed a broad stretch centered around 2158 cm^{-1} corresponding mostly to bound isonitrile. Thus, it is concluded that isonitrile binding to Pt occurs, but not under the competing influence of a thiol group.

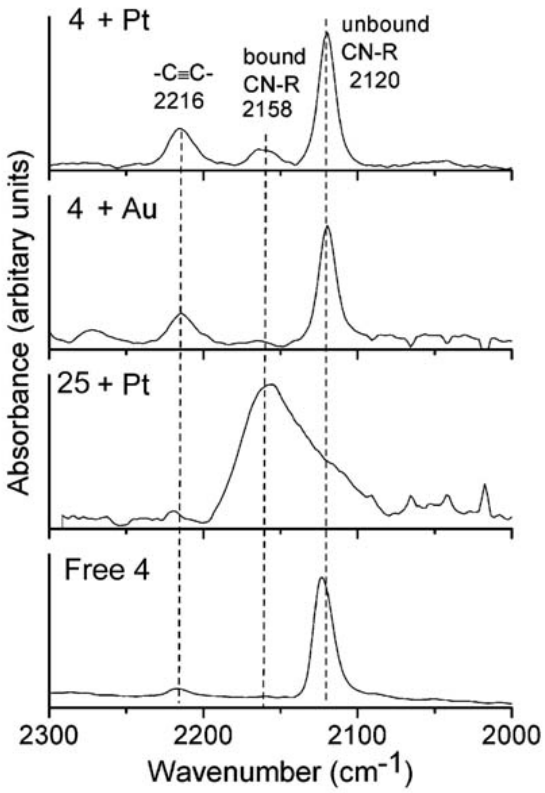

Figure 3.4. Grazing angle IR spectra of **4** (after deprotection) and **25** incubated with gold and platinum substrates.

3.2.3 Transmission FTIR of monofunctional molecules binding to AuNPs and PtNPs

While the above experiments displayed promising results for using IR for determination of binding, the ultimate goal of the project was to use nanoparticles as the metal substrates. The monofunctional isonitrile molecule **25** (1.0 mM in THF) was incubated for 30 minutes with dodecanethiol-capped AuNP and hexanethiol-capped PtNP in separate solutions to determine the relative preferences that the molecule has for each metal. The solutions were then evaporated on a salt plate and examined by FTIR (128 scans). It was expected that only a bound isonitrile peak would be present for the PtNP sample. It was also hoped that the AuNP sample would only show unbound isonitrile, but there is evidence in the literature that isonitriles will bind to Au, though not as strongly as they do to Pt.[43,44] As seen in Figure 3.5, the IR spectrum shows a signal indicative of only bound isonitrile while the Au sample displays signal indicative of a mixture of both bound and unbound isonitrile. These results indicate that the isonitrile favors the PtNP over the AuNP when no competing thiol is present.

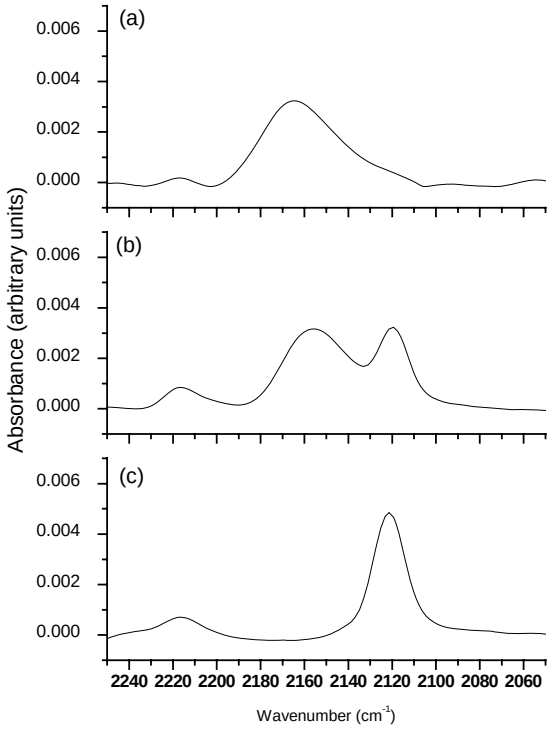

Figure 3.5. Transmission FTIR of monofunctional isonitrile molecule **25**: a) incubated with PtNP, b) incubated with AuNP, c) in solution.

3.2.4 Transmission FTIR of linker molecule binding to AuNPs and PtNPs

The previous experiment was then repeated using the bifunctional linker **4**. With both functional groups present, there is a competition between which terminus will bind to the metal. It was hoped that in the presence of both functional groups there would be a bias for the thiol group to bind to the AuNP (thus showing only a free isonitrile signal) and the isonitrile group to bind to the PtNP (thus showing only a bound isonitrile signal). A solution of molecule **4** (1.4 mM in THF) was deprotected with a few drops of NH_4OH (confirmed by FTIR) and incubated for 30 minutes with hexanethiol-capped AuNPs and PtNPs in separate solutions. The solutions were then evaporated on a salt plate and examined by FTIR (128 scans). The carbonyl peak observed in the spectrum of free **4** at 1711 cm^{-1} was shifted to lower wavenumber (Figure 3.6), consistent with deprotection to form free acetic acid and thiol. The binding of molecule **4** to the PtNP showed the expected shift of the isonitrile peak from 2120 to 2169 cm^{-1} indicating that the isonitrile was bound to the nanoparticle. When

the molecule was incubated with Au-NP, no change in the position of the isonitrile stretch was observed. This result is consistent with a lack of binding between isonitrile and gold.

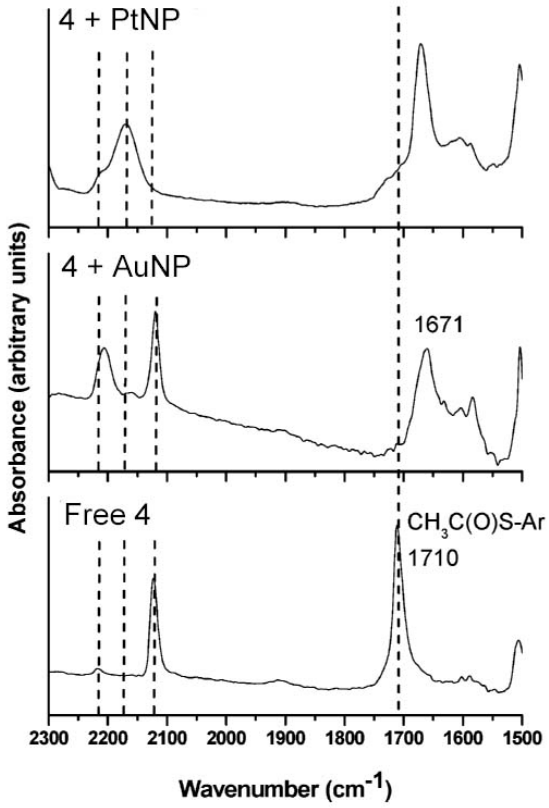

Figure 3.6. Transmission FTIR of linker molecule **4** deprotected and incubated with AuNP and PtNP.

3.2.5 Binding to Surfaces versus Nanoparticles

The results of these two experiments (e.g., binding to a nominally bare substrate versus binding to a nanoparticle where the molecule may have to displace hexanethiol or insert into a defect site in the thiol coating) are quite different. Further, the apparent selectivities for binding in these cases do not follow those observed by Wrighton and Whitesides[37] in which separate, thiol-containing and isonitrile-containing molecules competed for a bare metal substrate. Thus, these results indicate a new dimension when thinking about orthogonal self-assembly and indicate the relative selectivity in two cases for the archetypal thiol/isonitrile on Au/Pt interactions.

On a surface-bound sample, there is a large area of exposed sites for the linker molecule to bind without interference. On the nanoparticle substrates, it is necessary for the linker molecule to either insert into a defect site in the capping-ligand layer or undergo a place exchange reaction to displace a capping-ligand. There are several factors that will affect the ability of the linker molecule to displace a ligand molecule, including the affinity of the ligand for the nanoparticle, the affinity of the linker for the nanoparticle, and the concentration of the linker molecule relative to the nanoparticles.

Murray et al. have provided evidence for a model of thiol place exchange on Au nanoparticles. [45] At low concentrations, the incoming thiol quickly displaces a capping thiol at an easily accessible vertex site. There are relatively few of these and once they have been displaced the remaining incoming thiol prefers to stay in solution. It is necessary to significantly increase the concentration of the incoming thiol as well as use stronger reaction conditions to place exchange on the more protected edge and terrace sites of the nanoparticle, but even then conversions of <100% occurred.

3.3 CONCLUSION

In order to establish by IR that the bifunctional molecule **4** is capable of orthogonal self-assembly, it is necessary to prove that each terminal group will bind exclusively to its preferred metal. Thus when exposed to gold, the molecule is expected to bind via the free thiol leaving a free isonitrile group that would not show a shift in the IR spectra. When exposed to a Pt substrate, the molecule should bind exclusively through the isonitrile group seen as a shifted peak in the IR spectrum. The experiments performed above were limited in that each solution was only exposed to one metal, and thus not a true example of orthogonal self-assembly. While the Au samples did show evidence of isonitrile binding, the linker in those particular samples was not given the opportunity to bind to Pt. It has been shown in the literature that isonitriles on Au can be displaced by thiols,[43,44] clearly indicating a higher preference of the thiols for Au. This research also shows that isonitriles can readily bind to Au making it difficult to determine if the bound isonitrile peak seen by IR is a result of binding to Au or Pt.

Thus, the IR experiments were helpful in determining the general binding affinity of the end groups for Au and Pt, but the results were not definitive since it could not be

determined to which metal each functional group was bound. Also, these methods did not allow for quantifiable results such as percent conversion of the individual particles into heterodimers. To remedy this problem, alternate analytical techniques were required and will be the topic of the next chapter.

3.4 EXPERIMENTAL

General Considerations

PM-IRRAS samples were analyzed using a Digilab (Randolph, MA) FTS6000 FTIR with a PM-IRRAS attachment. Reflectance IR samples were run using a Digilab (Randolph, MA) FTS3000 FTIR with a PIKE Technologies (Madison, WI) VeeMax Reflectance attachment. Transmission FTIR samples were run on a Perkin Elmer (Waltham, MA) Spectrum RX 1 FTIR Spectrometer. Alkane-capped AuNP were prepare as according to the method by Brust et al.[46] Alkane-capped PtNP were prepare as according to the method by Cliffel and Eklund.[47]

PM-IRRAS IR of linker molecule on Au and Pt

A solution of **4** was prepared at a concentration of 5.1 mM in 5:2 EtOH/THF. To deprotect the thioacetate to the free thiol, 25 μL of NH_4OH was added and the solution was stirred vigorously. A gold slide was cleaned with fresh Piranha solution (3:1 H_2SO_4:H_2O_2), rinsed with EtOH, and dried. The slide was placed immediately into the sample solution and allowed to incubate for 2 days. A second solution of **4** was prepared at a concentration of 5.1 mM in 5:2 EtOH/THF. A piece of platinum foil was cleaned with fresh Aqua Regia (3:1 HCl/HNO_3), rinsed with EtOH, and dried with N_2. The Pt foil was placed immediately into the solution and allowed to incubate for 2 days. Both slides were then removed from solution, rinsed with EtOH, dried, and examined by PM-IRRAS.

The experiment was repeated using a deprotected thiol for both samples. A solution of **4** was prepared at a concentration of 0.4 mM in 7:2 toluene/EtOH. Again, 25 μL of NH_4OH was used to deprotect the thioacetate. This solution was split equally into two separate vials. A freshly cleaned gold slide was placed in one and a freshly cleaned platinum foil was placed in the other. The substrates were allowed to incubate for 20 hours, removed from solution, rinsed with EtOH, dried with N_2, and examined with PM-IRRAS.

Grazing Angle Reflectance IR of linker and monofunctional molecules on Au and Pt

A solution of **4** was prepared at a concentration of 10.5 mM in THF and deprotected with 1% of NH_4OH. Solution was stirred for 20 minutes. The solution was split equally between two vials. A gold slide and piece of Pt foil were UV/Ozone cleaned for 20 minutes then soaked in EtOH for 15 minutes. The Au slide and Pt foil were placed into the sample solutions and allowed to incubate overnight. Two control slides were prepared in a similar manner using a solution of **23** (9 mM in THF) for the Au slide and **25** (13.3 mM in THF) for the Pt foil. A gold slide and Pt foil were cleaned and examined immediately to act as blanks. Samples were analyzed using a grazing angle reflectance FTIR.

3.5 REFERENCES

(36) Gardner, T. J.; Frisbie, C. D.; Wrighton, M. S. *J. Am. Chem. Soc.* **1995**, *117*, 6927-6933.

(37) Hickman, J. J.; Laibinis, P. E.; Auerbach, D. I.; Zou, C. F.; Gardner, T. J.; Whitesides, G. M.; Wrighton, M. S. *Langmuir* **1992**, *8*, 357-359.

(38) Avery, N. R.; Matheson, T. W. *Surf. Sci.* **1984**, *143*, 110-124.

(39) Shih, K. C.; Angelici, R. J. *Langmuir* **1995**, *11*, 2539-2546.

(40) Horswell, S. L.; Kiely, C. J.; O'Neil, I. A.; Schiffrin, D. J. *J. Am. Chem. Soc.* **1999**, *121*, 5573-5574.

(41) Murphy, K. L.; Tysoe, W. T.; Bennett, D. W. *Langmuir* **2004**, *20*, 1732-1738.

(42) Tour, J. M.; Jones, L.; Pearson, D. L.; Lamba, J. J. S.; Burgin, T. P.; Whitesides, G. M.; Allara, D. L.; Parikh, A. N.; Atre, S. *J. Am. Chem. Soc.* **1995**, *117*, 9529-9534.

(43) Kovtyukhova, N. I.; Mallouk, T. E. *Chem. Eur. J.* **2002**, *8*, 4355-4363.

(44) Martin, B. R.; Dermody, D. J.; Reiss, B. D.; Fang, M. M.; Lyon, L. A.; Natan, M. J.; Mallouk, T. E. *Adv. Mater.* **1999**, *11*, 1021-1025.

(45) Hostetler, M. J.; Templeton, A. C.; Murray, R. W. *Langmuir* **1999**, *15*, 3782-3789.

(46) Brust, M.; Walker, M.; Bethell, D.; Schiffrin, D. J.; Whyman, R. *J. Chem. Soc., Chem. Commum.* **1994**, 801-802.

(47) Eklund, S. E.; Cliffel, D. E. *Langmuir* **2004**, *20*, 6012-6018.

CHAPTER 4

Characterization of Nanoparticles and Nanoparticle Heterodimers

4.1 INTRODUCTION

The techniques used in Chapter 3 provided a sound basis for determining the binding affinity of the thioacetate and isonitrile groups to metal nanoparticles and surfaces, but these techniques had some limitations. For example, from the data, one could only determine if the isonitrile was binding to some particle but could not verify that the isonitrile was bound to a platinum nanoparticle. To determine if discrete heterodimers form using two, different metal nanoparticles and a bifunctional linker molecule, a technique was needed that could confirm that a single gold (Au) nanoparticle was linking with single platinum (Pt) nanoparticle. Transmission Electron Microscopy (TEM) has been used extensively in the literature to examine nanoparticles and nanoparticle assemblies.[48-50] This technique can provide a useful method to study the formation of heterodimers since it allows for visual inspection of the heterodimer. Also, with high-resolution TEM, it is possible to distinguish between different nanoparticle materials based on the lattice-spacing of the atoms in the particle.[51-54]

To characterize nanoparticle heterodimers by TEM, the ideal combination of nanoparticles would be a spherical particle linked to a non-spherical particle. There have been numerous papers involving the synthesis of nanoparticles of non-spherical shapes,[49,55-58] but the usefulness of some of these procedures is hindered by the need for purification due to a mixture of shapes. Another option that would enhance visual comparison of nanoparticle solutions and allow for clear distinction between nanoparticles of different materials is to use particles of significantly different sizes.

Given the strategy where two nanoparticles of different sizes are used to form nanoparticle heterodimers that can be characterized by TEM, one must find methods to prepare these two, differently sized particles. When considering a procedure for the synthesis of nanoparticles, there are several factors that must be considered. These include the average size of the particle, the size distribution of particles in the sample, the concentration of particles that will be in the sample, the capping ligand on the particles, and the solubility of the particles. While the Brust synthesis[59] of the AuNP used for the FTIR experiments in Chapter 3 was straightforward, the nanoparticle size and size distribution using this method can be difficult to control. Another convenient way to acquire nanoparticles is purchase through various vendors. Gold nanoparticles (AuNP) have been extensively employed in the literature,[60-65] and thus, there are many varieties of AuNP

available for purchase with known size, size distribution, and concentration. In contrast, platinum nanoparticles (PtNP) have a more limited commercial availability. There are several synthetic reports for the preparation of PtNP with various capping ligands, but the maximum diameter of these particles are limited to approximately 10 nm.[49,51,52,66,67] Thus, the range of size of these particles is limited compared to that of AuNP. In the case of AuNP, one can obtain these commercially with diameters ranging from 2 to 250 nm with a variety of capping ligands.

Another method that has been used to distinguish between nanoparticles of varying sizes as well as various shapes is size-exclusion chromatography (SEC). This method is highly attractive due to its ability to analyze the sample as a whole whereas TEM is limited to a very small portion of the sample and can be biased by the choice of which portions of the sample to examine. SEC utilizes a column filled with a packing material that contains pores of a known size. Molecules that are small enough to fit in the pores interact with the stationary phase more than the larger molecules and thus elute at longer retention times. This technique has been used to separate nanoparticles of different size[68,69] as well as separating nanorods and nanoparticle assemblies from individual nanoparticles.[48,70]

In this chapter, we will explore two methods for the determination of heterodimer formation. As mentioned above, a definitive method for characterizing the formation of discrete heterodimers was very important. We will show that while TEM does provide confirmation for dimer formation, its usefulness is somewhat limited. SEC also showed promise in providing a more overall examination of the sample, but there were several variables related to instrumentation that had to be examined and optimized for SEC to be a viable technique.

4.2 RESULTS AND DISCUSSION

Since commercially available AuNP allowed for precise choice of nanoparticle size, it was decided to purchase AuNP from Ted Pella, Inc. These particles are water-soluble and contain excess citrate anion in the solution, which helps to stabilize the nanoparticles. It was initially decided to use large AuNP (30 nm) to couple with smaller PtNP (~3 nm) to allow for easier visual identification via TEM. For the PtNP, a polyacrylate-capped particle was

chosen.[71] The synthesis was simple and, as was discovered during the course of experiments, adjustment of certain parameters allowed for size control of the particles.

There is the possibility that a AuNP will settle directly next to a PtNP on the TEM sample grid during preparation. By keeping the concentration of the samples low, the probability of this happening was minimized. Also, the ratio of particles to linker molecule was kept at approximately 1:1 to minimize the formation of multiple particle aggregates. Even if the selectivity of binding of each end of the molecule for only one particle is high, only the particle/linker stoichiometry biases the number of particles that aggregate together. Thus, even at a 1:1:1 AuNP/linker/PtNP stoichiometry, some aggregates with three, four or more particles are expected statistically to form.

To form AuNP-PtNP heterodimers, a solution of 30 nm AuNP and 3 nm PtNP was incubated with a solution of the bifunctional linker molecule **4** (Sample BRW-5-64), and then analyzed by TEM. BRW-5-64 is the notebook page number associated with the sample and is used here, as well as throughout this chapter, as a sample's or set of samples' unique identifier. In the experimental section at the end of this chapter, these same notebook page numbers are used to identify the preparation conditions for set of sample.

As can be seen in Figure 4.1, it is easy to discern the difference between the two types of nanoparticles. From just the particles shown in Figure 4.1, 45% are heterodimers. This value is calculated as the number of heterodimers (i.e. the number of large AuNP with a small PtNP directly beside it) divided by the total number of AuNP in the image. As this value is solely based on the image shown in Figure 4.1, it is only an approximation of the whole sample and not necessarily a statistically accurate count.

While results of the previous experiment indicated a reasonable proportion of heterodimers in the sample, it was necessary, as a control experiment, to determine if the gold and platinum particles would link together without the presence of the bifunctional linker molecule. Thus, particles were mixed in the presence of a molecule similar to the linker **4**, but with only one binding functional group (BRW-5-80). To this end, a mixture AuNP and PtNP were incubated with compound **25,** which contains an isonitrile group but not a thioacetate group. If the binding of the two particles is due solely to the presence of the bifunctional linker molecule **4**, then the particles incubated with compound **25** should not produce any heterodimers or homodimers.

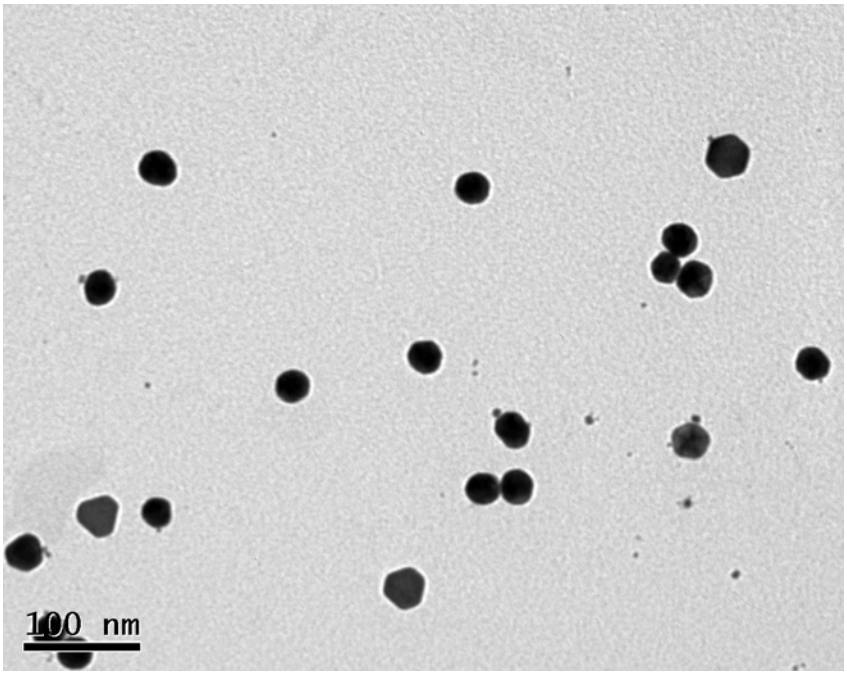

Figure 4.1. TEM image of 30 nm AuNPs and 3 nm PtNPs incubated with a solution of Compound 4.

This experiment yielded a heterodimer to single particle ratio of 6/50 (12%) when the bifunctional molecule **4** was used. However, when a solution of molecule **25** was used, no dimers were observed out of 50 AuNP examined. These data thus support the hypothesis that a bifunctional molecule is necessary to form the AuNP-PtNP heterodimers. The percentage of heterodimers is much lower in this experiment as compared to the 45% from the previous one. These results may be due to the fact that TEM can only examine a very small portion of the sample and thus different observations of the same sample may give large variations in the apparent yield. Alternatively, the result may reflect large variations in the true yield between preparations. Nevertheless, an important point to be taken from these data is that the sample incubated with a monofunctional molecule does not yield any heterodimers.

In an attempt to increase the yield of heterodimers formed, the amount of linker molecule **4** added to the nanoparticles was increased from 2 equivalents to 4 equivalents relative to the AuNP concentration (BRW-5-81). The results of this preparation were characterized by TEM. The TEM showed mostly large aggregates of the nanoparticles with ca. > 20 particles in each aggregate. Thus, it was not possible to calculate a percentage of heterodimers. This aggregation does indicate that a close to stoichiometric (1:1) amount of

linker molecule as compared to the nanoparticles is desirable and necessary for heterodimer formation.

Another way that was investigated to increase the number of heterodimers formed was to increase the incubation time (BRW-5-83). As characterized by TEM, this experiment yielded a heterodimer to single particle ratio of 16/30 (53%) indicating that an increase in incubation time does yield a higher percentage of heterodimers. Though there is an increase in the percentage of heterodimers, there were multiple PtNPs observed bound to a single AuNP (e.g. as shown in Figure 4.2). This result suggests that, under these conditions, formation of larger aggregates competed with formation of heterodimers. It is possible that this result could be avoided by decreasing the concentration of the PtNP solution but also incubating for the longer time. However, these conditions were not evaluated.

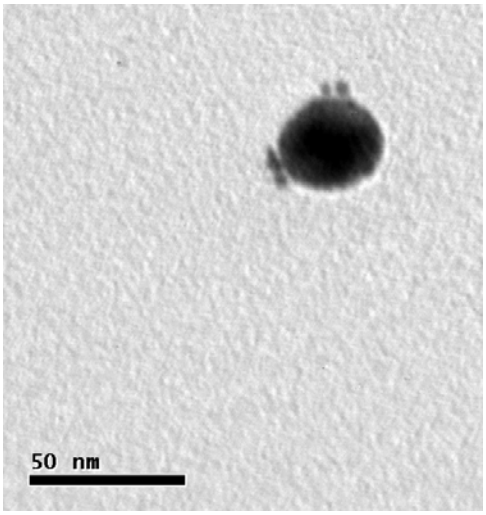

Figure 4.2. TEM image of 30 nm AuNP with multiple 4 nm PtNPs bound.

While TEM provided a good method for characterizing the percentage of heterodimers formed in a preparation, it was not amenable to performing multiple observations quickly and was not convenient for monitoring the evolution of samples over time. Because of this, an alternate method was sought that would allow monitoring of a sample solution over the course of a few hours to several days. One option for this was size-exclusion chromatography (SEC).

It was thought that SEC columns with pore sizes comparable to those of the particles might separate them and potentially allow individual particles, dimers and aggregates to be

distinguished. The available SEC column had a pore size of 300Å. Thus, the upper limit for the size of the nanoparticles was reckoned to be on the size of the pore (300 Å or 30 nm). To avoid particles that were too big to be fractionated by the columns, the 30 nm AuNP used previously were abandoned in favor of 20 nm AuNP.

Two solutions were prepared for the initial SEC experiment (BRW-5-84). The first solution contained a mixture of 20 nm AuNP and 4 nm PtNP incubated with the bifunctional linker molecule **4**. The second solution contained only 20 nm AuNP and 4 nm PtNP. Samples were analyzed on a Macrosphere SEC column (300Å pore size) using 40 mM sodium dodecylsulfate (SDS) in water as the mobile phase with a flow of 1 mL/min, an injection volume of 20 μL, and a detection wavelength of 520 nm. SDS was used in the mobile phase to minimize irreversible adsorption to the column following procedures described previously.[70]

As can be seen in Figure 4.3, the sample with linker molecule **4** shows a small peak that appeared preceding the large peak assigned to the AuNP. This peak with the lower retention time indicates that there is something larger than the 20 nm AuNP present in the sample as, in SEC, larger analytes elute first from the column. The smaller analytes have greater interaction with the column due to their ability to move into the pores of the packing material and thus elute later. These results do not directly prove that heterodimers have been formed, but they do imply that a nanoparticle assembly is present in the sample that is slightly larger than the 20 nm AuNP.

In order to determine an optimum nanoparticle heterodimer size that was most easily distinguished from the two, individual nanoparticles, mixtures containing several different sizes of AuNP and PtNP were examined by SEC (BRW-6-10). It was hoped that a combination of particles that showed some resolution in SEC would also have a clear size difference when viewed using TEM. A set of four samples was made using combinations of 10 nm and 20 nm AuNP and 8 nm and 18 nm PtNP (Table 4.1).

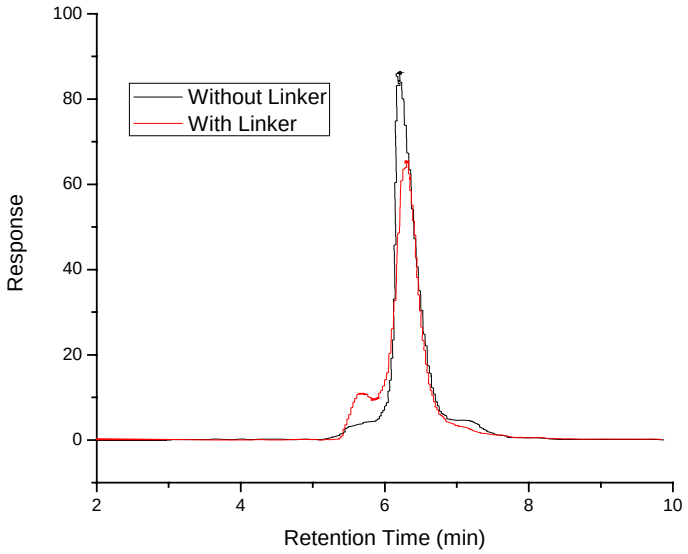

Figure 4.3. SEC chromatogram of 20 nm AuNP and 4 nm PtNP with linker (red) and without linker (black).

Table 4.1. Size combinations of AuNPs and PtNPs

Sample	AuNP	PtNP
A	20 nm (1.16 nM)	8 nm (6 nM)
B	20 nm (1.16 nM)	18 nm (0.8 nM)
C	10 nm (9.5 nM)	8 nm (6 nM)
D	10 nm (9.5 nM)	18 nm (0.8 nM)

One of the difficulties inherent in using prepared nanoparticles is the determination of the concentration of the nanoparticle solution. Accurately knowing the concentration of the nanoparticle solution is particularly important for preparing the sample solutions at the correct stoichiometric ratio. To determine the nanoparticle concentration, the average diameter of the nanoparticles was measured using TEM. Then, the initial amount of metal salt used for the preparation was assumed to be converted completely into nanoparticles. This calculation gives the assumed total number of nanoparticles formed in the preparation. By dividing by the final volume of the solution, it is possible to calculate an approximation of the nanoparticle concentration.

While this calculation gives a reasonable estimate of concentration, there are several concerns associated with this estimation. The first is that all of the metal salt is completely converted to nanoparticles. This is a reasonable assumption but difficult to check. If not all of the salt is consumed, then the actual concentration will be lower than the calculated value. Second, as mentioned above, it is difficult to accurately examine enough of the TEM grid to arrive at a statistical value for the average diameter of the nanoparticles.

Of the four nanoparticle combinations examined, samples B and D displayed the greatest change in the SEC chromatograms when samples with linker molecule **4** were compared to those samples without linker. As can be seen in Figure 4.4a, the sample with linker shows a small peak that appeared preceding the large peak due to the AuNP. As in the previous experiment, the peak with the shorter retention time indicates that there is something larger than the 20 nm AuNP present in the sample. When the particles are changed to 10 nm AuNP and 18 nm PtNP, there was no additional peak that was easily discernable, but a greater increase in total absorbance intensity was observed for the peak at ~11 min (Figure 4.4b).

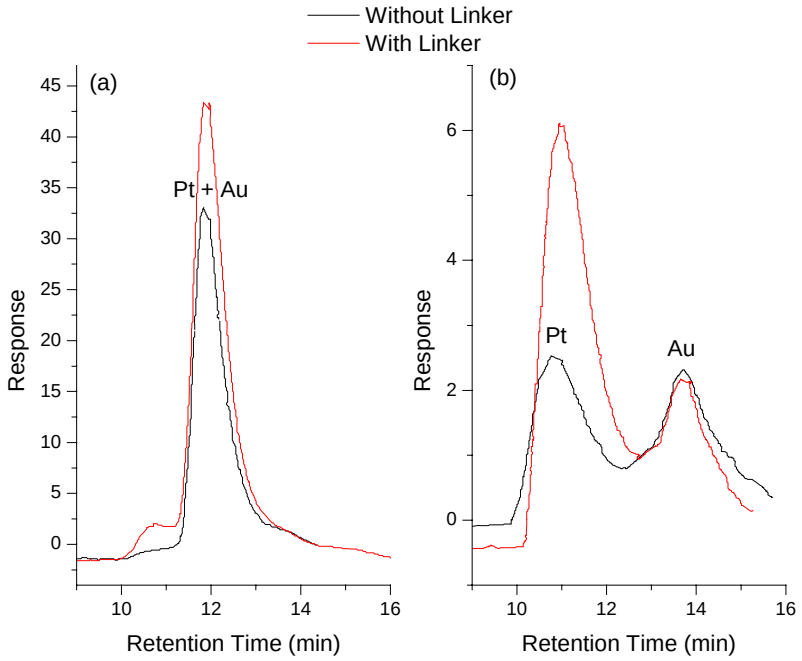

Figure 4.4. SEC chromatogram of (a) Sample B and (b) Sample D.

It is necessary to pause and explain the appearance of the peaks in these SEC chromatograms. In previous experiments, smaller PtNP were used (~3-4 nm) to couple to larger AuNP (30 nm). In general, larger particles of a given type have a greater molar absorptivity than smaller ones at a given wavelength.[72,73] This phenomenon is due to the plasmon absorption band that results from the oscillation of free electrons in the conduction band of the metal nanoparticles and is dependent on the size of the particle.[74] Because of the greater absorption, the 20 nm AuNP peak is expected to be much larger than and partially obscure the smaller peak assigned to the 3-4 nm PtNPs. The appearance of the chromatogram in Figure 4.3 is consistent with this interpretation. In addition to the expectation that the PtNP would have a lower molar absorptivity due to their smaller size, PtNP absorb much more weakly at 520 nm compared to AuNP.

For Sample D (Figure 4.4b), the combination of 18 nm PtNP and 10 nm AuNP resulted in a large peak due to the PtNP, presumably as the result of an increase in absorptivity because of the PtNP was larger than that in Sample B. Also, the peak due to AuNP was observed to be much smaller as expected as the result of a decrease in size of the AuNP and the necessary decrease in the amount of AuNP added to keep the AuNP:PtNP concentrations close to 1:1.

It was first hypothesized that coupling a 18 nm PtNP with a 10 nm AuNP would result in a ~29 nm heterodimer (the sum of the two particle dimers and the linker) that should elute at a much earlier retention time than the individual AuNPs and PtNPs. Aggregation could be one possibility for the increase in response at 11 min, but each sample was filtered using a 0.2 μm filter that should serve to eliminate any aggregates larger than 200 nm. Also, any aggregates larger than ~30 nm would have eluted at the void volume of the column, as they were not expected to be retained in the pores.

To determine the size of the nanoparticle that would have a retention time of 11 min, a calibration curve was created (BRW-6-29) by running AuNP of 2, 5, 10, 20 and 40 nm and PtNP of 3, 8, 15, and 18 nm on the SEC and plotting the log of the nanoparticle size versus retention time (Figure 4.5). Previous research has shown that the relationship between the logarithm of the nanoparticle size and the elution time is expected to be linear if the separation is only based on steric exclusion.[69] From the AuNP plot, the peak retention time of 11 minutes corresponds to a nanoparticle size of 22.6 nm indicating a small array of

nanoparticles. Since this retention time corresponds to a collection of only a few nanoparticles, there is the possibility that the increased response at 11 min is due to the heterodimer coeluting with the individual PtNPs. This result could only be observed if the effective diameter of the heterodimer is not 29 nm.

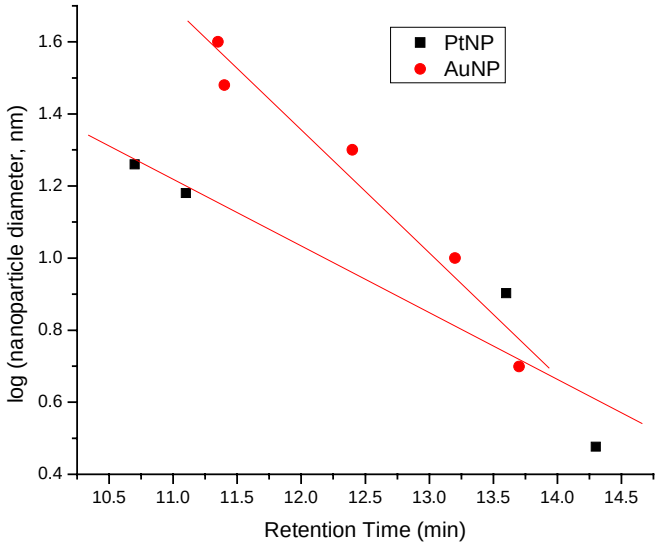

Figure 4.5. Plot of log (NP diameter, nm) versus retention time. PtNP (slope = -0.185, r^2 = 0.88); AuNP (slope = -0.341, r^2 = 0.96).

While the simplest estimate of the diameter of the heterodimer is just the sum of the two particle sizes (29 nm), it was soon realized that this assumption is not valid. If the geometry of the heterodimer is approximated as that of a cylinder, as it moves through the SEC column, it can travel parallel to the column or perpendicular to the column. These modes of travel yield different apparent sizes, ~18 nm or ~29 nm respectively. Also, if the heterodimer is traveling parallel to the column, its interaction with the 30 nm pores is much greater as compared to the larger perpendicular heterodimer. The peak that results in the SEC chromatogram is thus an average of all the modes of travel. Thus, the correct heterodimer size in a SEC experiment is its hydrodynamic radius. Hydrodynamic radius of a cylinder can be calculated using Equation 1.[75] Based on this equation, the hydrodynamic radius of the 10 nm AuNP + 18 nm PtNP heterodimer was calculated in three ways (Table 4.2). The first calculation assumed that the radius of the cylinder (R) was that of the AuNP.

The second calculation used the radius of the PtNP for R. The final calculation used an average of the two particle radii for R. These calculations suggest that the expected hydrodynamic radius (and thus retention time) of the heterodimer (ca. 20 nm) is not too different than that of the PtNP. The increase in the size of the peak at ca. 11 min in Figure 4.4 might be because it is the result of co-elution of the unlinked PtNP with the PtNP-AuNP heterodimers.

$$R_H = \sqrt[3]{\frac{3LR^2}{4}} \qquad \text{(Eq. 1)}$$

Table 4.2. Calculations of Apparent Diameter of Heterodimers

Radius for Calculation	Apparent Diameter (nm)
5 nm (10 nm AuNP)	16.32
9 nm (18 nm PtNP)	24.16
7 nm (Average of AuNP and PtNP)	20.43

If the new peak at 11 min is due to the heterodimer, one would expect an equal decrease in the height/area of the peak assigned to free AuNPs. However, this is not observed. One possible hypothesis for this is that only a small amount of the AuNPs are actually being linked together to form heterodimers. Since there is such a significant increase in the peak height at 11 min, this hypothesis is only valid if the linking of the particles together causes an enhancement of the AuNP signal. It has been shown in previous research that when 12 nm AuNPs are linked to form dimers, there is a shift in the wavelength of maximum absorption of the Au plasmon peak from 525 nm to 535 nm.[76] Also, as the size of the AuNP is increased, the wavelength of maximum absorption changes.[77] This effect was verified with the AuNPs used for experiments in this chapter and the results are shown in Table 4.3. Finally, as the size of AuNP increases, the molar absorptivity at 520 nm also increases (Table 4.3). Since the intensity of the Au 520 nm plasmon absorbance is related to nanoparticle size, it is possible that there is an increase in the molar absorptivity of the AuNP in the heterodimer as compared to free AuNPs. Also, the wavelength of maximum of

absorbance for the 10 nm AuNP is 518 nm, which means that at 520 nm, the absorbance would be lower. When the particles link to form a heterodimer, the wavelength of maximum absorbance is expected to shift to longer wavelengths which could lead to higher absorbance at 520 nm.

Table 4.3. Wavelength of maximum absorption and calculated extinction coefficient for AuNP

Diameter (nm)	λ_{max}	ε_{520}
5	514	1.21×10^{7}
10	518	8.14×10^{7}
15	518	4.81×10^{8}
20	522	1.01×10^{9}
30	524	2.13×10^{9}
60	534	2.18×10^{10}

Sample D from the experiment shown in Figure 4.4b resulted in the largest observable change in the SEC chromatogram when comparing samples with and without linker. Though the heterodimer peak overlaps with free PtNP peak, the nanoparticle combination for Sample D displays the best resolution between the heterodimer peak and the free AuNP peak of the samples examined as well as having a large increase in response. Therefore, the combination of 10 nm AuNP and 18 nm PtNP was chosen for further investigation. Samples were prepared and monitored over the course of 24 hours in an attempt to observe the appearance and changes of the new heterodimer peak (BRW-6-13). As in the previous experiment, there was a dramatic increase in peak height at a retention time of ~11.5 minutes (Figure 4.6) indicating the possibility of heterodimer formation. Examination by TEM confirmed that dimers were present but due to the small difference in the average sizes of the AuNP compared to the PtNP, it was difficult to determine if the dimers observed were AuNP-AuNP and/or PtNP-PtNP homodimers or AuNP-PtNP heterodimers (Figure 4.7).

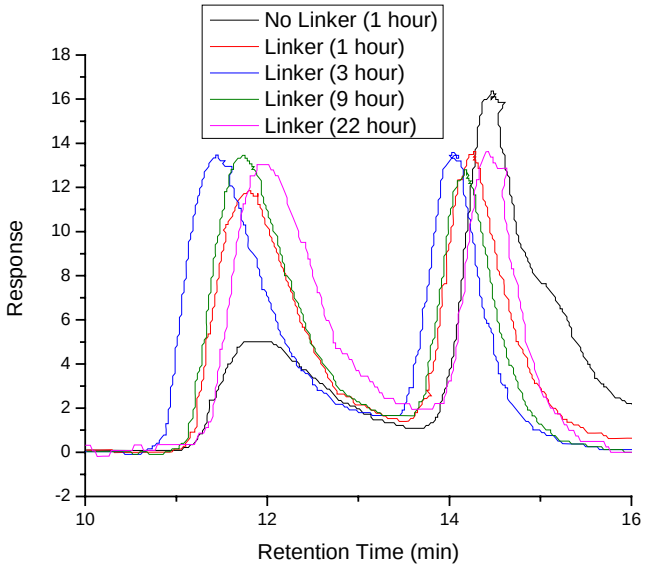

Figure 4.6. SEC chromatograms monitoring heterodimer formation over time.

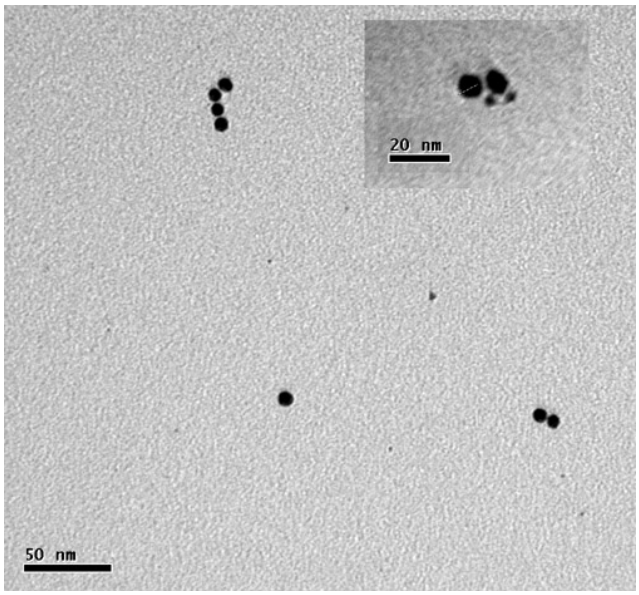

Figure 4.7. TEM image of AuNPs and PtNPs incubated with linker.

After considering the results of these previous experiments, it was thought that an ideal pairing of particles would be a large PtNP (18 nm) and a small AuNP (5 nm). This

thinking was based on the idea that, using 520 nm detection observation of the AuNP over the PtNP would be favored due to their relative absorbencies at this wavelength. Thus, binding a small AuNP to a large PtNP could give the most noticeable change in the relative peak sizes in SEC as the result of heterodimer formation. Moreover, the large difference in the sizes of the two particles should facilitate visual identification by TEM. This pairing of particles yields a calculated apparent hydrodynamic diameter of 21.5 nm, which should yield a peak in the SEC that should be well separated from that of the individual 5 nm AuNP peak.

In order to prepare a 1:1 solution of 18 nm PtNP and 5 nm AuNP, it was necessary to significantly dilute the concentration of the AuNPs from 83 nM to ~0.8 nM as this latter concentration was the practical maximum obtainable for PtNP. To determine the lowest acceptable concentration for observation of a peak in SEC, two solutions of 5 nm AuNP were prepared at 20.8 nM and 41.5 nM (BRW-6-18). In addition, three samples of larger 10 nm AuNPs were prepared at concentrations of at 0.95 nM, 2.38 nM, and 4.75 nM. From SEC chromatograms on these solutions shown in Figure 4.8b, it can be seen that the 5 nm AuNPs showed a moderate response at 20.8 nM, but if intensity is proportional to concentration as expected, dilution down to 0.8 nM would not yield a strong enough signal to detect the particles at that concentration. The SECs of the 10 nm AuNP solutions yielded better results (Figure 4.8a). Dilution to of 10 nm AuNP to 0.95 nM gave sufficient peak response and could likely be diluted further and still provide an acceptable signal. Thus, based on these results, the use of 5 nm AuNP turned out not to be practical. The combination of 10 nm AuNP and 18 nm PtNP was retained in the remaining experiments.

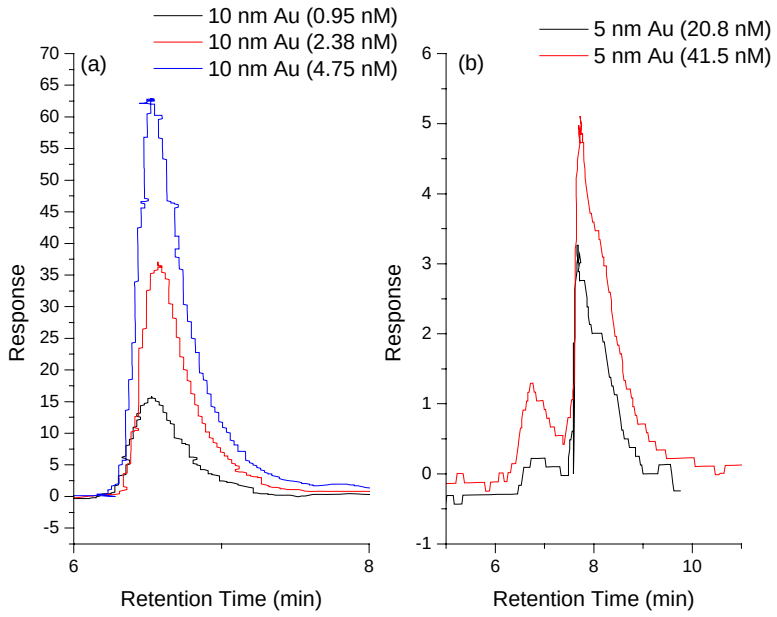

Figure 4.8. SECs showing (a) 10 nm AuNPs at 0.95, 2.38 and 4.75 nM concentrations and (b) 5 nm AuNPs at 20.8 and 41.5 nM concentrations.

It is well documented in the literature that interactions in solution between individual nanoparticles and interactions between nanoparticles and column packing materials depends significantly on the presence of electrolytes.[78-81] Increasing electrolyte concentration decreases the size of the electrical double layer surrounding the nanoparticles allowing for adsorption to the stationary phase or aggregation between the particles.[68,82] To determine the effects of the ionic strength of the citrate buffer on the appearance of SECs of AuNP-PtNP samples, two samples of AuNPs and PtNPs were prepared with buffer concentrations of 1 mM and 100 mM citrate ion (BRW-6-19). The sample containing 1 mM buffer yielded a chromatogram similar to the above experiments with 10 nm AuNP + 18 nm PtNP in solution with no added citrate buffer. The sample containing 100 mM buffer, however, showed a drastically decreased signal of only ~10% response as compared to the sample containing 1 mM buffer (Figure 4.9). These results are mostly likely due to significant aggregation of the nanoparticles in the sample that were then retained in the 0.2 μm filter before the filtered solution was injected into the SEC. Because of these results, it was decided to use a low

sample buffer concentration of 1mM citrate ion to help stabilize the particles without causing aggregation.

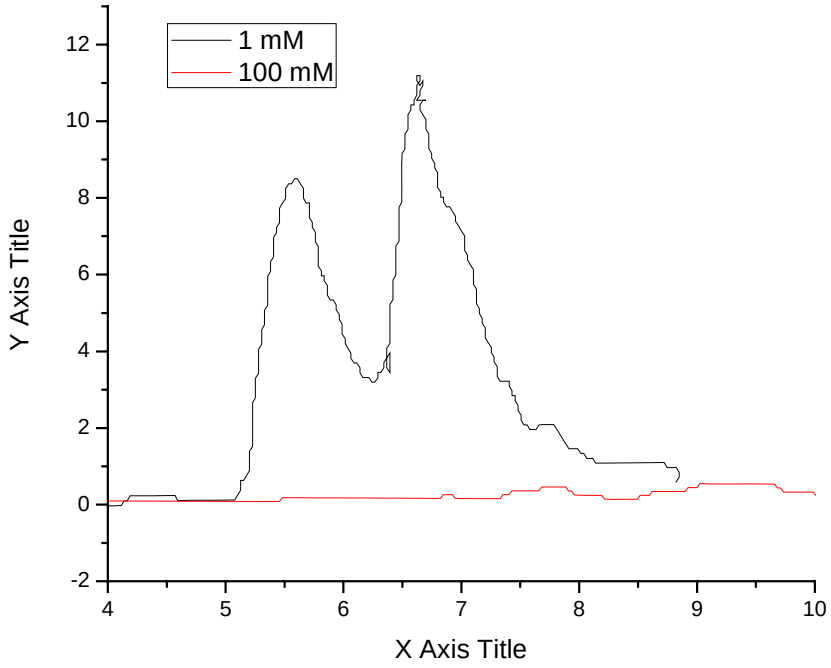

Figure 4.9. Comparison of AuNP + PtNP sample using 1 mM and 100 mM citrate sample buffers.

As can be seen in Figure 4.6, there is some variability in retention times of peaks observed when the same nanoparticle solution was injected repeatedly into the column. Since this variability will obfuscate small differences between the retention times of heterodimers with those of free nanoparticles, experiments were preformed to quantify the variability of the retention time of SEC peaks on nanoparticle samples. A sample of 10 nm AuNP and 18 nm PtNP was prepared with a citrate buffer concentration of 1 mM (BRW-6-20). A second sample was also prepared without buffer (BRW-6-26). Each sample was injected five times on the SEC system using a mobile phase containing 40 mM SDS and 1 mM citrate buffer for the buffered sample and only 40 mM SDS for the unbuffered sample. The percent relative standard deviations (%RSD) of the retention time and response of the peak assigned to the AuNP are shown in Table 4.4. The presence of the 1 mM citrate buffer

appears to somewhat improve the reproducibility of the retention and response as compared to the sample without buffer.

Table 4.4. Calculations for samples with and without 1 mM citrate buffer

	With buffer		Without buffer	
	Retention Time (min)	Peak Height (A/D units)	Retention Time (min)	Peak Height (A/D units)
Average	6.64	11.46	6.76	14.16
Standard Deviation	0.016	0.39	0.035	0.58
%RSD	0.24	3.44	0.52	4.12

A set of experiments similar to those above were performed to test the effect of column heating. Elevating the temperature of the column has been shown to decrease retention time variability as well as affect peak shape in some chromatographic techniques due to the increase in diffusion of the analytes.[83] The two samples from the prior experiments were injected on the SEC using the same conditions as previously but with a column temperature of 35°C (BRW-6-21, BRW-6-27). Six injections were made to calculate the reproducibility of the retention time and response of the peak assigned to the AuNP. The percent relative standard deviations (%RSD) are shown in Table 4.5. When compared to the data in Table 4.4 running at room temperature, heating the column to 35ºC does not appear to improve the reproducibility of the samples.

Table 4.5. Calculations for samples with and without 1 mM citrate buffer run at 35ºC

	With buffer		Without buffer	
	Retention Time (min)	Peak Height (A/D units)	Retention Time (min)	Peak Height (A/D units)
Average	6.72	9.88	6.63	13.79
Standard Deviation	0.047	1.32	0.053	1.00
%RSD	0.70	13.38	0.80	7.28

Originally, the ratio of linker molecule to nanoparticles was kept at 1:1 in an attempt to minimize more than two nanoparticles binding together. To verify that this ratio was optimum, several samples (BRW-6-22) were prepared with increasing equivalents of linker relative to the nanoparticles (1, 2, 5, and 10 equivalents). Another change to the experimental protocol was also made. In previous experiments, it was thought that the pH of the sample solutions was basic enough to deprotect the thioacetate group. To make sure that the thioacetate was deprotected and thus maximize binding, a small amount of NH_4OH was added to deprotect the thioacetate in situ.[84] The samples were injected on the SEC at 1, 4.5, and 22 hours after preparation to observe any changes in the peaks over time.

Considering the effect of particle:linker ratio (Figure 4.10), the samples with linker show an increased peak at a retention time of ~5.6 minutes when compared to the sample without linker. As stated above, it is believed that a peak due to heterodimer formation would be present at this time in the SEC chromatogram. The samples with higher equivalents of linker did not show significant improvement of heterodimer formation when examined after 1 hour. When the samples were reexamined at 4 and 22.5 hours (Figure 4.11 and Figure 4.12, respectively), the samples with higher equivalents of linker begin to show decreased response of both peaks as well as peak broadening. These results could indicate aggregation of several particles together rather than the expected heterodimer formation. Since no benefits were found upon increasing the ratio of linker to particles used for heterodimer formation, it was kept at 1 equivalent relative to the AuNP concentration.

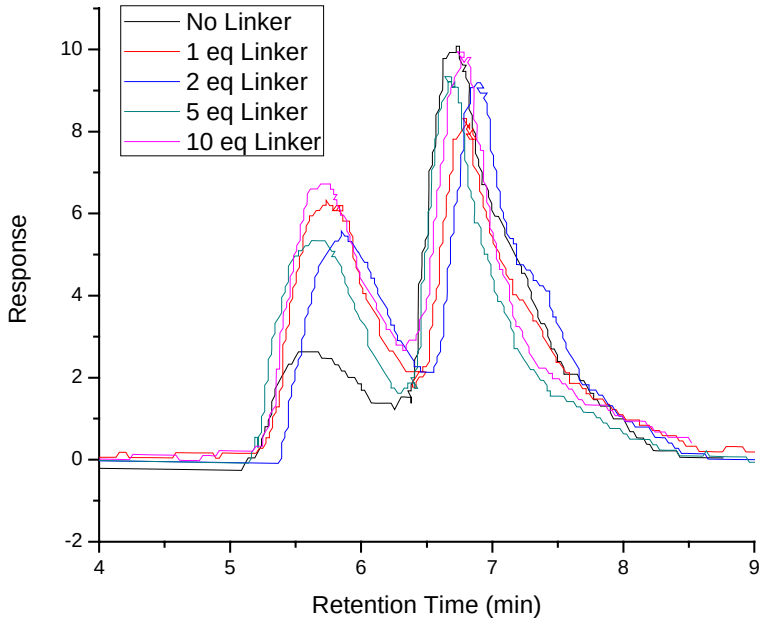

Figure 4.10. Comparison of heterodimer formation using increasing linker equivalents after 1 hour incubation.

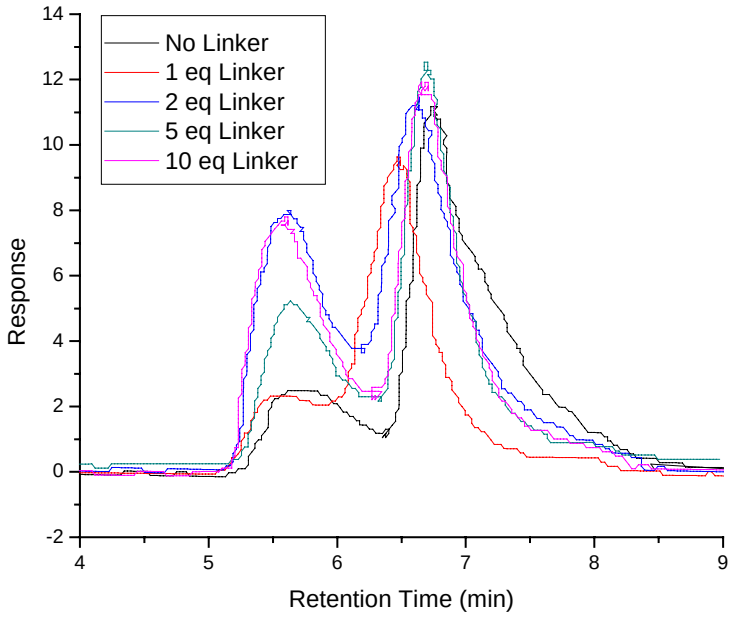

Figure 4.11. Comparison of heterodimer formation using increasing linker equivalents after 4 hour incubation.

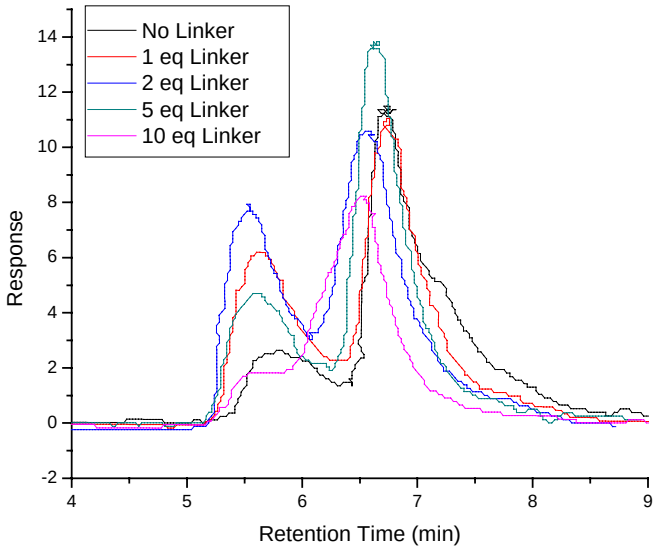

Figure 4.12. Comparison of heterodimer formation using increasing linker equivalents after 22.5 hour incubation.

Previously, the effect of buffer strength on the SEC chromatograms was examined briefly using only two sample buffer strengths. This investigation was expanded to include the effect of the mobile phase buffer strength on the nanoparticle peak reproducibility and shape. A sample of 10 nm AuNP and 14 nm PtNP was examined by SEC using mobile phases containing 0, 2.5, 5, and 25 mM citrate buffer (BRW-6-42). Three injections of each solution were made and the %RSDs of the retention time and response of the nanoparticle peak were calculated. As shown in Table 4.6, the mobile phases with buffer yielded better reproducibility in retention time and response as compared to the mobile phase with no buffer. However, as the buffer strength was increased, the response of the peak dramatically decreased (Figure 4.13). As mentioned above,[68,82] this behavior may be due to the decreased electric double layer that screens the nanoparticles from each other and the column stationary phase. When this double layer decreases, the particles are more likely to stick to each other and the column, which is seen as peak broadening and increased amount of irreversible adsorption on the column. This behavior would manifest itself as a decreased detector response. Based on these concerns, a mobile phase buffer strength of 1 mM was chosen to increase reproducibility as well as maximize peak response.

Table 4.6. Reproducibility of the nanoparticle peak with varying mobile phase buffer strength

Buffer Strength	0 mM		2.5 mM	
	Retention Time (min)	Peak Height (A/D units)	Retention Time (min)	Peak Height (A/D units)
Average	5.933	700	5.996	628
Standard Deviation	0.024	130.1	0.0144	81.0
%RSD	0.40	18.6	0.2	12.9
Buffer Strength	5 mM		25 mM	
	Retention Time (min)	Peak Height (A/D units)	Retention Time (min)	Peak Height (A/D units)
Average	6.009	462	6.271	137
Standard Deviation	0.021	52.1	0.017	12.7
%RSD	0.3	11.3	0.3	9.3

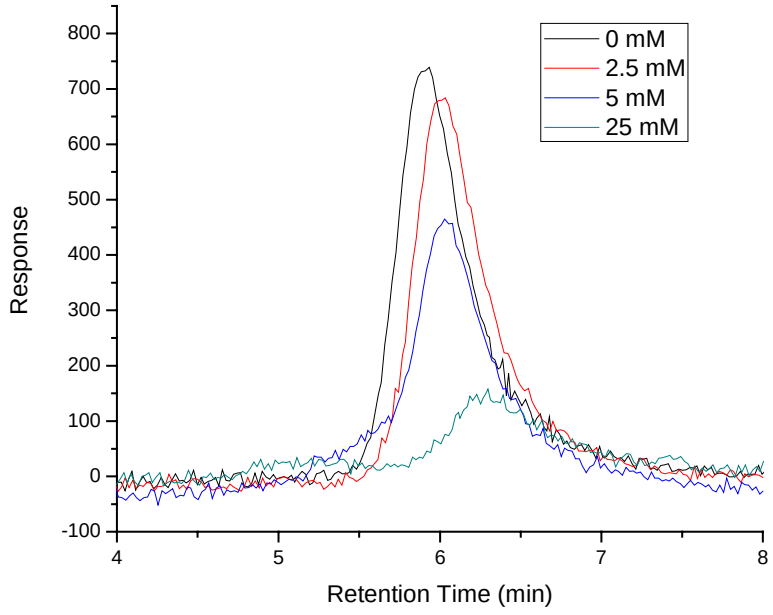

Figure 4.13. SEC chromatograms of AuNP + PtNP sample with varying mobile phase buffer strength.

Since the effect of buffer has been shown to be very important to the SEC results, it was decided to determine if there is an effect due to the buffer concentration in the sample prior to injection. In the previous experiment, although the mobile phase was buffered, the samples were not buffered. Because of this, there is a significant change in environment of the nanoparticles from the sample (no buffer) to the column (buffer). To perform this experiment, three samples of 10 nm AuNP and 14 nm PtNP were prepared using 2.5, 12.5, and 25 mM citrate buffer (BRW-6-44). Each buffered sample was examined using the corresponding buffered mobile phase. Due to a sample dilution error, the 12.5 mM sample was run using the 5 mM mobile phase. The 2.5 and 12.5 mM samples were injected three times while the 25 mM sample was injected twice. The %RSDs of the retention time and response of the nanoparticle peak were calculated and are shown in Table 4.7.

Table 4.7. Results of varying sample buffer strength

Buffer Strength	2.5 mM		12.5 mM		25 mM	
	Time (min)	Peak Height (A/D units)	Time (min)	Peak Height (A/D units)	Time (min)	Peak Height (A/D units)
Average	6.328	460	6.416	253	6.722	68
SD	0.0127	81.1	0.0561	35.3	0.099	12
%RSD	0.20	17.6	0.9	14.0	1.5	17.6

The data collected suggests that the presence of buffer in the sample did not improve the reproducibility at low concentrations (2.5 mM). At higher buffer strengths (Figure 4.14), the peak response was drastically reduced as compared to an unbuffered sample. Also, a second peak appeared at a shorter retention time (5.25 min) that could be attributed to aggregation of the particles to form small aggregates of 2-4 particles. The response of this peak at 5.25 min also decreases significantly at higher buffer strengths. This decrease in peak response for both peaks at 25 mM buffer is attributed to irreversible adsorption to the stationary phase due to a decrease in the electrical double layer. Since low sample buffer strength did not affect reproducibility substantially, it was decided to use a sample buffer of 1 mM. In this way, the sample buffer strength was kept the same as the mobile phase strength

and was envisioned to minimize any unforeseen problems due to a change in buffer concentration from an unbuffered sample to a buffered mobile phase in the SEC column.

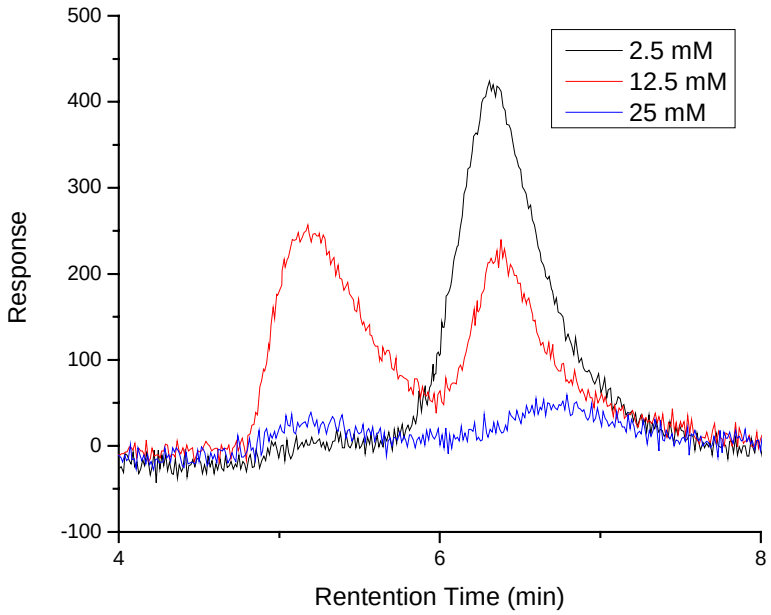

Figure 4.14. SEC chromatograms of AuNP + PtNP with varying sample buffer strengths.

Another variable that could affect the sample reproducibility is the pH of the buffered mobile phase. The pH of nanoparticle solutions has been shown to affect the degree of aggregation.[85] The pKa values of the citrate ion employed in the previous buffer solutions are 3.13, 4.76, and 6.40. Since the effective buffering capacity of any buffer is limited to the pKa ± 1 pH unit, it was necessary to choose a different buffer to allow for examination above pH 7. A phosphate buffer was chosen instead as phosphate ion has pKa values of 2.15, 7.20, and 12.33. Samples of 10 nm AuNP and 14 nm PtNP (BRW-6-46) were prepared at three buffer concentrations (1, 5, and 10 mM phosphate) and examined by SEC at three different pH values (3, 7, and 11) using the corresponding buffer concentrations (1, 5, and 10 mM phosphate). The results for the samples containing 1 mM buffer are shown in Table 4.8. The data from the 5 and 10 mM samples (Figure 4.15) showed significantly decreased response and new peaks similar to that seen previously when using elevated buffer concentrations.

Thus, no quantitative analysis was made of these data. The samples containing 1 mM pH 7 phosphate buffer yield the best reproducibility as well as the highest response.

Table 4.8. Results of varying 1 mM phosphate

pH	4		7		11	
	Time (min)	Peak Height (A/D units)	Time (min)	Peak Height (A/D units)	Time (min)	Peak Height (A/D units)
Average	6.283	464	6.172	662	6.253	484
SD	0.108	23.4	0.0354	37.5	0.0742	16.8
%RSD	1.7	3.5	0.60	5.7	1.2	3.5

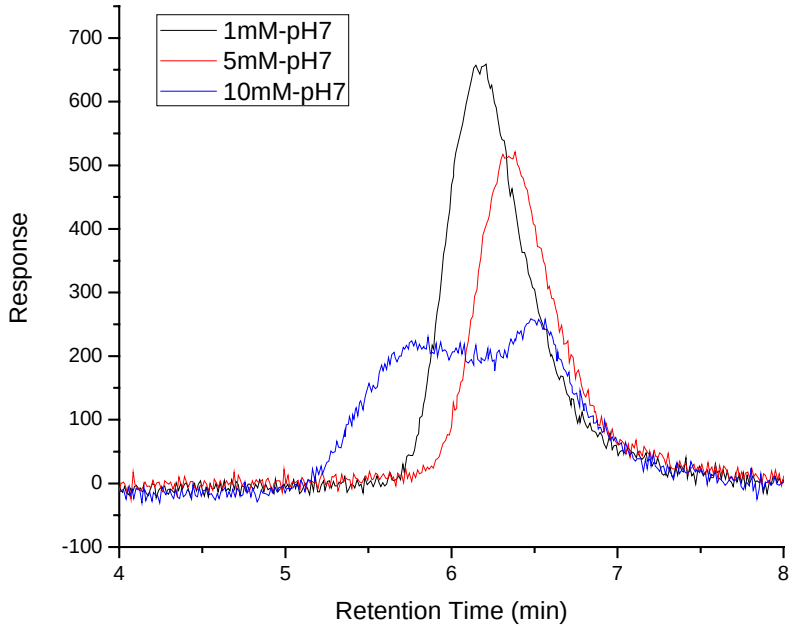

Figure 4.15. Effect of pH on peak reproducibility.

4.3 CONCLUSION

The early results showing that there was some heterodimer formation were illustrated nicely using TEM. However, as mentioned above, TEM does not allow for quantitative analysis of heterodimer formation. The results are extremely variable due to the small area of the sample being examined. Nevertheless, by using particles with a significant size difference, it was possible to easily tell the nanoparticles apart.

Once it was determined that TEM could not provide the necessary quantitative data, it was hoped that SEC would provide a convenient method for analyzing the formation of heterodimers. The goal was to have a quick method for observing the change of individual nanoparticles into linked heterodimers. Originally, the assumption seemed valid that these goals were possible. While promising results were collected, it has now become clear that several factors frustrate the use of SEC for the separation of nanoparticle arrays. The results shown here are not explained using only simple size-exclusion principles.

One problem that arose was limitations in the range of sizes of nanoparticles that could be used. For TEM, the best results were attained by using nanoparticles with a large size difference. This choice allowed for easier identification of heterodimers since they should have one large nanoparticle beside one small nanoparticle. Once the switch to SEC was made, it was necessary to adjust the size of the nanoparticles. The column size limited the total hydrodynamic radius of particles/assemblies that could be characterized to around 30 nm. Also, due to the resolution of the column, the combination of 30 nm and 4 nm particles was not viable since the total size of the heterodimer was too close to the size of the large particle. Because of this, the nanoparticles diameters had to be closer in size (10-15 nm). This choice allowed for a larger distinction between nanoparticles and the heterodimer. Unfortunately, since the nanoparticles were closer in size, it was difficult to tell by TEM if the dimers formed were homodimers or heterodimers.

The data also suggests that there are other variables responsible for the separation of the nanoparticles and heterodimers besides size-exclusion. If this were the case, the plots of the AuNP and PtNP retention times versus diameter (Figure 4.5) should have a similar shape. This is not the case indicating there are other factors involved. The most obvious is the capping-ligand of the nanoparticle. The AuNP are capped with citrate ion while the PtNP have a polyacrylate coating. This difference can create difficulties when trying to calculate

the apparent size of the heterodimer based from a SEC chromatogram. Since the heterodimer is made up of both types of particles, it should interact with the column like both individual nanoparticles. This behavior would cause error when the retention time is compared to a calibration curve of either individual nanoparticle.

In developing the methods necessary to analyze the test heterodimer by SEC, many other variables were examined for their significance. The largest concern when working with nanoparticles in a chromatographic system is aggregation. Another problem is irreversible adsorption to the column. Both of these problems can result in lower signal and broadened peaks. It was determined that high sample buffer strengths, high mobile phase buffer strengths, and mobile phase pH extremes were to be avoided due to aggregation/adsorption. In conclusion, SEC shows promise as useful technique for analyzing nanoparticles and nanoparticle arrays. In order to be a routine technique, several of the limitations mentioned above need to be resolved.

4.4 EXPERIMENTAL

Materials

Unconjugated gold nanoparticles in sizes of 2 nm (250 nM), 5 nm (83 nM), 10 nm (9.5 nM), 15 nm (2.32 nM), 20 nm (1.16 nM), 30 nm (0.33 nM), 40 nm (0.15 nM), and 60 nm (0.043 nM) were purchased from Ted Pella, INC. (Redding, CA). Polyacrylate-capped platinum nanoparticles were synthesized using a method modified from El-Sayed et. al.[49] except solutions of the Pt salt were aged anywhere from 1 hour to 4 days to increase the size of the final PtNPs. TEM grids were purchased from Ted Pella, INC. (Redding, CA).

Transmission Electron Microscopy

TEM samples were prepared by placing a few drops of sample solution on a Type A, 300 mesh, carbon/formvar-coated copper grid and wicking the solvent away with a Kimwipe from below the grid. The samples were analyzed using a Philips (FEI Company, Hillsboro, OR) CM12 Transmission Electron Microscope at an accelerating voltage of 100 kV.

Size Exclusion Chromatography

SEC samples were analyzed on an Alltech Macrosphere SEC column (300Å pore size) using 40 mM SDS in water as the mobile phase with a flow of 1 mL/min, an injection volume of 20 μL, and a detection wavelength of 520 nm unless otherwise indicated in the individual experiment description. The SEC instrumentation consisted of a Series III Isocratic HPLC Pump, a Model 500 Variable UV/VIS Detector, a Rheodyne 7512 Manual Injector, and either a Linear Instruments Chart Recorder or a Remote Measurements Systems ADC-1 Analog-to-Digital Converter running on a Power Mac 7200/90.

Preparation of AuNP + PtNP (+ Linker) Solutions

BRW-5-64 A solution of compound **4** (40 μL, 2.25 nM in 2:3 THF:EtOH) was added to 0.25 mL of AuNP (30 nm, 0.33 nM purchased from Ted Pella) in 10 μL aliquots every 20 minutes. The solution was allowed to incubate for 4 hours then 0.25 mL of PtNP (~3 nm, ~10 nM) was added followed by stirring overnight. The sample solution was then examined by TEM.

BRW-5-80 A sample with the bifunctional linker was prepared by adding 40 μL of linker solution (Compound **4**, 5.3 nM in 2:3 THF:EtOH) to 0.25 mL of 30 nm AuNP in 10 μL aliquots every 15 minutes. The solution was allowed to incubate for 8 hours then 0.25 mL of PtNP (~4 nm, ~12.4 nM) was added followed by stirring for 16 hours. For comparison, a sample using the monofunctional molecule was prepared by adding 80 μL of compound **25** (2.67 nM in 2:3 THF:EtOH) to 0.25 mL of 30 nm AuNP in 20 μL aliquots every 15 minutes. The solution was allowed to incubate for 9 hours then 0.25 mL of PtNP (~4 nm, ~12.4 nM) was added followed by stirring for 15 hours. The sample solutions were then examined by TEM.

BRW-5-81 An 80 μL portion of linker solution (compound **4**, 5.3 nM in 2:3 THF:EtOH) was added to 0.25 mL of 30 nm AuNP in 20 μL aliquots every 15 minutes. The solution was allowed to incubate for 9 hours then 0.25 mL of PtNP (~4 nm, ~12.4 nM) was added followed by stirring for 15 hours. As in the previous experiment, a sample using the monofunctional molecule was prepared by adding 80 μL of compound **25** (5.4 nM in 2:3

THF:EtOH) to 0.25 mL of 30 nm AuNP in 20 μL aliquots every 15 minutes. The solution was allowed to incubate for 9 hours then 0.25 mL of PtNP (~4 nm, ~12.4 nM) was added followed by stirring for 15 hours. The sample solutions were then examined by TEM.

BRW-5-83 Four 20 μL aliquots of linker solution (compound **4**, 5.3 nM in 2:3 THF:EtOH) was added to 0.5 mL of 30 nm AuNP in 15 minute intervals. The solution was allowed to incubate for 24 hours then 0.5 mL of PtNP (~4 nm, ~12.4 nM) was added in 0.1 mL aliquots every 15 minutes followed by stirring for 48 hours. A sample using the monofunctional molecule was prepared by adding 80 μL of compound **25** (5.4 nM in 2:3 THF:EtOH) to 0.5 mL of 30 nm AuNP in 20 μL aliquots every 15 minutes. The solution was allowed to incubate for 24 hours then 0.5 mL of PtNP (~4 nm, ~12.4 nM) was added in 0.1 mL aliquot every 15 minutes followed by stirring for 48 hours. The sample solutions were then examined by TEM.

BRW-5-84 Two solutions were prepared for SEC analysis. The first was prepared by adding 250 μL of linker solution (compound **4**, 5.3 nM in 2:3 THF:EtOH) to 0.5 mL of 20 nm AuNP in 50 μL aliquots every 10 minutes. The solution was allowed to incubate for 24 hours then 0.5 mL of PtNP (~4 nm, ~12.4 nM) was added in 0.1 mL aliquots every 15 minutes followed by stirring for 3 days. The second solution was prepared by mixing 0.5 mL of AuNP with 0.5 mL of PtNP and stirring for 4 days. The samples were then analyzed by SEC.

BRW-6-10 A set of four samples was made using combinations 10 nm and 20 nm AuNP and 8 nm and 18 nm PtNP. Samples A-C were prepared by stirring 0.5 mL of AuNP with 0.5 mL of PtNP for 30 minutes followed by adding 100 μL of linker solution (compound **4**, 5.3 nM in 2:3 THF:EtOH) in 20 μL aliquots every 15 minutes. The solutions were then stirred for 4 hours. Due to concentration issues, Sample D was prepared by stirring 0.1 mL of AuNP with 1.0 mL of PtNP for 30 minutes followed by adding 20 μL of linker solution (compound **4**, 5.3 nM in 2:3 THF:EtOH) in 4 μL aliquots every 15 minutes. The solution was then stirred for 4 hours. The combinations of nanoparticles for each sample are listed in

Table 4.1. Four more solutions were prepared as above, except no linker was added. The samples were then analyzed by SEC column at a flow of 0.5 mL/min.

BRW-6-13 Two samples were prepared for analysis by SEC. The first was prepared by stirring 0.1 mL of 10 nm AuNP with 1.0 mL of PtNP (~18 nm, ~0.8 nM) for 1 hour followed by adding 200 μL of linker solution (compound **4**, 5.2 nM in 2:3 THF:EtOH) to a mixture of in 40 μL aliquots every 10 minutes. A second solution was prepared in the same manner, but no linker molecule was added. The samples were then analyzed by SEC column at a flow of 0.5 mL/min.

BRW-6-18 Three samples of 10 nm AuNP and two samples of 5 nm AuNP were prepared at varying concentrations. Three dilutions of 10 nm AuNP were made at 0.95 nM, 2.38 nM, and 4.75 nM. Solutions of 5 nm AuNP were also prepared at concentrations of 20.8 nM and 41.5 nM. The samples were then analyzed by SEC.

BRW-6-19 Two samples of AuNP and PtNP were prepared with buffer concentrations of 1 mM and 100 mM citrate. The 1 mM buffered sample was prepared by adding 10 μL of 100 mM citrate buffer stock solution to 1.0 mL of PtNP (~18 nm, ~0.8 nM) and 0.1 mL of 10 nm AuNP. The 100 mM buffered sample was prepared by adding citric acid (0.105 g) and sodium citrate (0.144 g) directly to 10 mL of PtNP (~18 nm, ~0.8 nM). After stirring, 1 mL of this buffered PtNP solution was transferred to another vial and 0.1 mL of 10 nm AuNP was added. The samples were then analyzed by SEC using 40 mM SDS and 1 mM citrate in water as the mobile phase.

BRW-6-20, 26 The 1 mM buffered sample of Au and PtNP was prepared by adding 10 μL of 100 mM citrate buffer stock solution to 1.0 mL of PtNP (~18 nm, ~0.8 nM) and 0.1 mL of 10 nm AuNP (BRW-6-20). A second sample was prepared without the buffer solution (BRW-6-26). The samples were then analyzed by SEC. For the buffered sample, a 40 mM SDS and 1 mM citrate mobile phase was used. Five injections were made to calculate the reproducibility of the retention time and response of the peak assigned to AuNP.

BRW-6-21, 27 To test the effect of column heating, the two reproducibility samples from above were also injected on the SEC using the conditions above (BRW-6-20, 26) but with a column temperature of 35°C. Six injections were made to calculate the reproducibility of the retention time and response of the peak assigned to AuNP.

BRW-6-22 A stock solution of AuNP and PtNP was prepared by mixing 5 mL of PtNP (~18 nm, ~0.8 nM), 0.5 mL of 10 nm AuNP, and 50 μL of 100 mM citrate buffer. The solution was stirred for 45 minutes then four 1 mL aliquots were transferred into separate vials. To these vials, various amounts of linker molecule **4** (50 nM in 2:3 THF:EtOH) and buffer were added according to Table 4.9. The linker was deprotected in situ using 100 μL of 0.5 mM NH_4OH and stirred for 40 minutes before addition to the nanoparticles. The equivalents of linker added were calculated at stoichiometric ratio of 1:1 with the AuNP. The samples were injected on the SEC at 1, 4.5, and 22 hours after preparation using 40 mM SDS and 1 mM citrate in water as the mobile phase.

Table 4.9. Preparation of samples for linker equivalent analysis

Equivalents	μL of Linker (50 nM, compound **4**)	μL of 100 mM citrate buffer
1	20	180
2	40	160
5	100	100
10	200	0

BRW-6-29 Five AuNPs solutions (2, 5, 10, 20 and 40nm) were analyzed by SEC using 40 mM SDS and 1 mM citrate in water as the mobile phase.

BRW-6-42 A sample solution was prepared by mixing 0.1 mL of 10 nm AuNP with 1.0 mL of PtNP (~14 nm, ~1.15 nM). The sample was then analyzed by SEC. The mobile phases used contained 40 mM SDS in water with varying concentrations of citrate buffer (0, 2.5, 5, 25, 63, and 125 mM). Three injections of the sample solution were made.

BRW-6-44 Three samples were prepared for SEC analysis using varying citrate buffer concentrations. The 10 nm AuNP and 14 nm PtNP (~1.15 nM) samples were prepared using the amounts shown in Table 4.10. The samples were then analyzed by SEC. The mobile phases used contained 40 mM SDS in water with varying concentrations of citrate buffer (2.5, 12.5, and 25 mM). Each buffered sample was run using the corresponding buffered mobile phase. Due to a sample dilution error, the 12.5 mM sample was run using the 5 mM mobile phase. The 2.5 and 12.5 mM samples were injected three times while the 25 mM sample was injected twice.

Table 4.10. Preparation of samples for sample buffer strength analysis

Sample Buffer Strength	PtNP (mL)	AuNP (μL)	125 mM citrate (μL)	H_2O (μL)
2.5	0.5	50	18	282
12.5	0.5	50	90	210
25	0.5	50	180	120

BRW-6-46 Three samples were prepared at different buffer (Table 4.11). The samples were examined by SEC with mobile phases of three different pH values (4, 7, and 11) as well as three different buffer concentrations (1, 5, and 10 mM phosphate). The buffered samples were run using the corresponding mobile phase buffer concentration. Three injections of each solution were made.

Table 4.11. Preparation of buffered samples for pH analysis

Buffer Strength	PtNP (mL)	AuNP (mL)	50 mM phosphate (mL)	H_2O (uL)
1	1.0	0.1	30	370
5	1.0	0.1	150	250
10	1.0	0.1	300	100

4.5 REFERENCES

(48) Novak, J. P.; Nickerson, C.; Franzen, S.; Feldheim, D. L. *Anal. Chem.* **2001**, *73*, 5758-5761.

(49) Ahmadi, T. S.; Wang, Z. L.; Henglein, A.; ElSayed, M. A. *Chem. Mater.* **1996**, *8*, 1161-1163.

(50) Xu, X. Y.; Rosi, N. L.; Wang, Y. H.; Huo, F. W.; Mirkin, C. A. *J. Am. Chem. Soc.* **2006**, *128*, 9286-9287.

(51) Huang, J. C.; He, C. B.; Liu, X. M.; Xiao, Y.; Mya, K. Y.; Chai, J. W. *Langmuir* **2004**, *20*, 5145-5148.

(52) Yee, C.; Scotti, M.; Ulman, A.; White, H.; Rafailovich, M.; Sokolov, J. *Langmuir* **1999**, *15*, 4314-4316.

(53) Nagesha, D. K.; Liang, X.; Mamedov, A. A.; Gainer, G.; Eastman, M. A.; Giersig, M.; Song, J.-J.; Ni, T.; Kotov, N. A. *J. Phys. Chem. B* **2001**, *105*, 7490-7498.

(54) Epifani, M.; Carlino, E.; Blasi, C.; Giannini, C.; Tapfer, L.; Vasanelli, L. *Chem. Mater.* **2001**, *13*, 1533-1539.

(55) Wang, Z. L.; Petroski, J. M.; Green, T. C.; El-Sayed, M. A. *J. Phys. Chem. B* **1998**, *102*, 6145-6151.

(56) Herricks, T.; Chen, J. Y.; Xia, Y. N. *Nano Lett.* **2004**, *4*, 2367-2371.

(57) Yuan, H.; Cai, R. X.; Pang, D. W. *Chin. Chem. Lett.* **2003**, *14*, 1163-1166.

(58) Jin, R. C.; Cao, Y. W.; Mirkin, C. A.; Kelly, K. L.; Schatz, G. C.; Zheng, J. G. *Science* **2001**, *294*, 1901-1903.

(59) Brust, M.; Walker, M.; Bethell, D.; Schiffrin, D. J.; Whyman, R. *J. Chem. Soc., Chem. Commum.* **1994**, 801-802.

(60) Srivastava, S.; Frankamp, B. L.; Rotello, V. M. *Chem. Mater.* **2005**, *17*, 487-490.

(61) Kim, T.; Lee, K.; Gong, M. S.; Joo, S. W. *Langmuir* **2005**, *21*, 9524-9528.

(62) Link, S.; El-Sayed, M. A. *J. Phys. Chem. B* **1999**, *103*, 4212-4217.

(63) Guo, R.; Song, Y.; Wang, G. L.; Murray, R. W. *J. Am. Chem. Soc.* **2005**, *127*, 2752-2757.

(64) Brewer, S. H.; Glomm, W. R.; Johnson, M. C.; Knag, M. K.; Franzen, S. *Langmuir* **2005**, *21*, 9303-9307.

(65) Kiang, C. H. *Physica a* **2003**, *321*, 164-169.

(66) Henglein, A.; Ershov, B. G.; Malow, M. *J. Phys. Chem.* **1995**, *99*, 14129-14136.

(67) Horswell, S. L.; Kiely, C. J.; O'Neil, I. A.; Schiffrin, D. J. *J. Am. Chem. Soc.* **1999**, *121*, 5573-5574.

(68) Liu, F. K.; Wei, G. T. *Chromatographia* **2004**, *59*, 115-119.

(69) Wei, G. T.; Liu, F. K. *J. Chromatogr. A* **1999**, *836*, 253-260.

(70) Wei, G.-T.; Liu, F.-K.; Wang, C. R. C. *Anal. Chem.* **1999**, *71*, 2085-2091.

(71) Rampino, L. D.; Nord, F. F. *J. Am. Chem. Soc.* **1941**, *63*, 2745-2749.

(72) Link, S.; El-Sayed, M. A. *J. Phys. Chem. B* **1999**, *103*, 8410-8426.

(73) Maye, M. M.; Han, L.; Kariuki, N. N.; Ly, N. K.; Chan, W. B.; Luo, J.; Zhong, C. J. *Anal. Chim. Acta.* **2003**, *496*, 17-27.

(74) Bohren, C. F.; Huffman, D. R. *Absorption and Scattering of Light by Small Particles*; John Wiley: New York, 1983.

(75) Atkins, A. W. *Physical Chemistry*; 5th ed.; Oxford University Press: Oxford, 1994.

(76) Brousseau, L. C.; Novak, J. P.; Marinakos, S. M.; Feldheim, D. L. *Adv. Mater.* **1999**, *11*, 447-449.

(77) Kreibig, U.; Vollmer, M. *Optical Properties of Metal Clusters*; Springer: Berlin, 1995.

(78) Wang, L. H.; Liu, X. F.; Hu, X. F.; Song, S. P.; Fan, C. H. *Chem. Commun.* **2006**, 3780-3782.

(79) Rosi, N. L.; Mirkin, C. A. *Chem. Rev.* **2005**, *105*, 1547-1562.

(80) Hunter, R. J. *Foundations of Colloid Science*; Oxford University Press, Inc.: New York, 2001.

(81) Shaw, D. J. *Colloid and Surface Chemistry*; Butterworth-Heinemann Ltd.: Oxford, 1991.

(82) Fischer, C. H.; Kenndler, E. *J. Chromatogr. A* **1997**, *773*, 179-187.

(83) Katz, E. *Handbook of HPLC*; Marcel Dekker, Inc.: New York, 1998; Vol. 78.

(84) Tour, J. M.; Jones, L.; Pearson, D. L.; Lamba, J. J. S.; Burgin, T. P.; Whitesides, G. M.; Allara, D. L.; Parikh, A. N.; Atre, S. *J. Am. Chem. Soc.* **1995**, *117*, 9529-9534.

(85) Su, C. H.; Wu, P. L.; Yeh, C. S. *Bull. Chem. Soc. Jpn.* **2004**, *77*, 189-193.

APPENDIX

Selected NMR Spectra

^{1}H NMR for 4

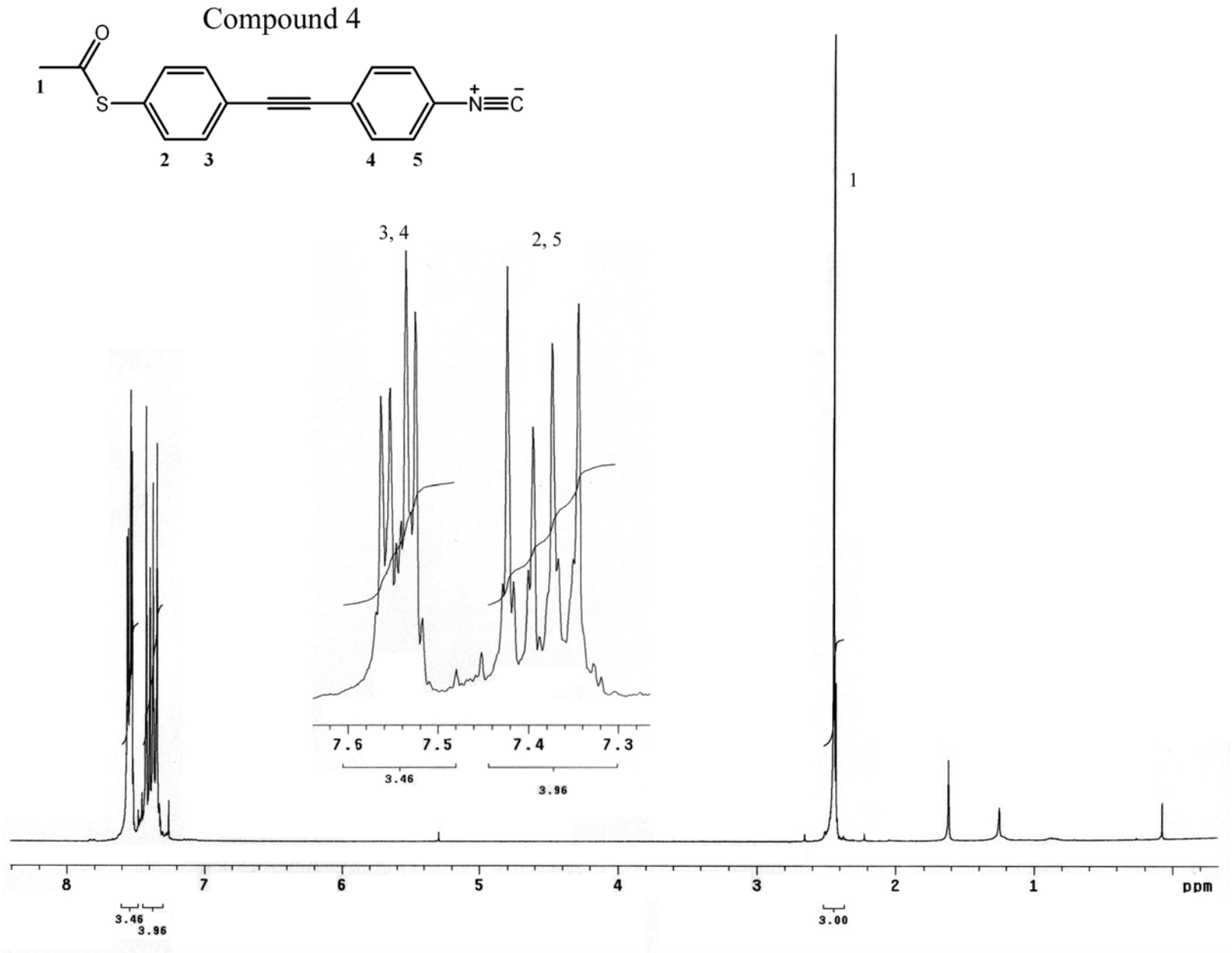
Compound 4
O
1
S
2 3
4 5
+
N≡C
−
3, 4
2, 5
1
7.6
7.5
7.4
7.3
3.46
3.96
8
7
6
5
4
3
2
1
ppm
3.46
3.96
3.00

^{13}C NMR for 4

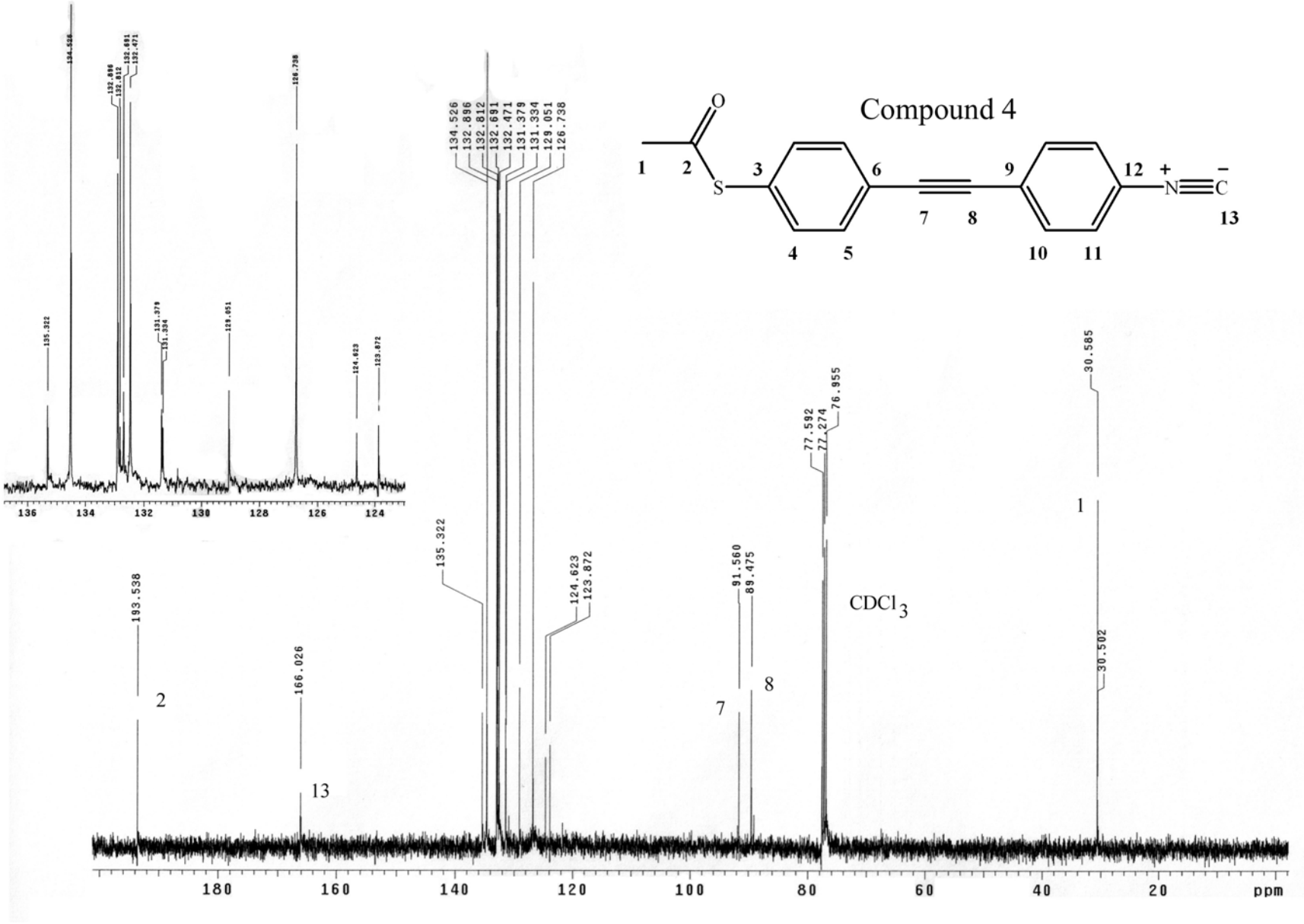
Compound 4
O
S
N
C
1
2
3
4
5
6
7
8
9
10
11
12
13
134.526
132.896
132.812
132.691
132.471
131.379
131.334
129.051
126.738
135.322
124.623
123.872
91.560
89.475
77.592
77.274
76.955
30.585
30.502
193.538
166.026
CDCl3
ppm

^{1}H NMR for 11

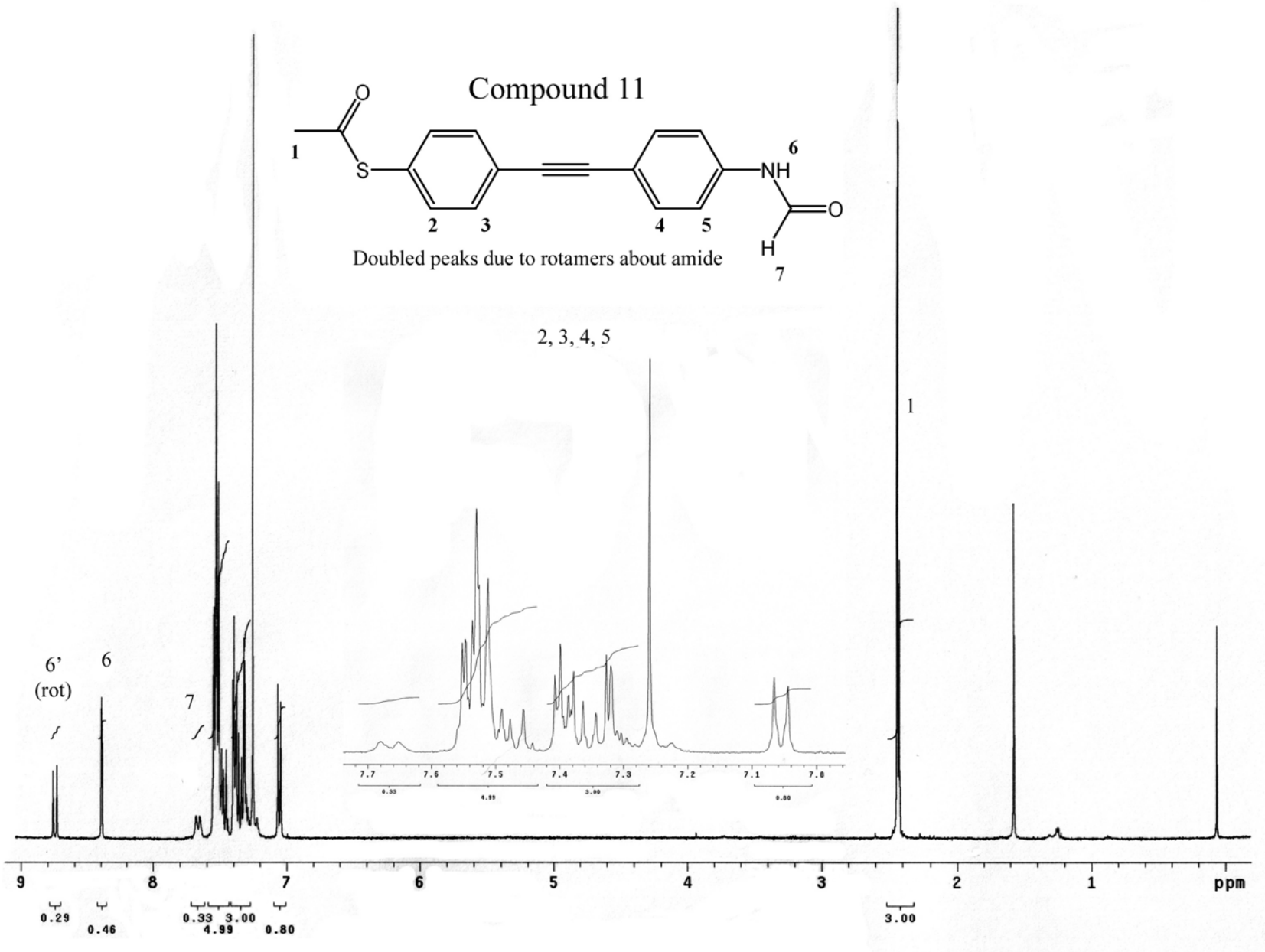
Compound 11
O
1
S
2
3
4
5
NH
6
O
H
7
Doubled peaks due to rotamers about amide
2, 3, 4, 5
1
6'
(rot)
6
7
9
8
7
6
5
4
3
2
1
ppm
0.29
0.46
0.33
3.00
4.99
0.80
3.00

^{13}C NMR for 11

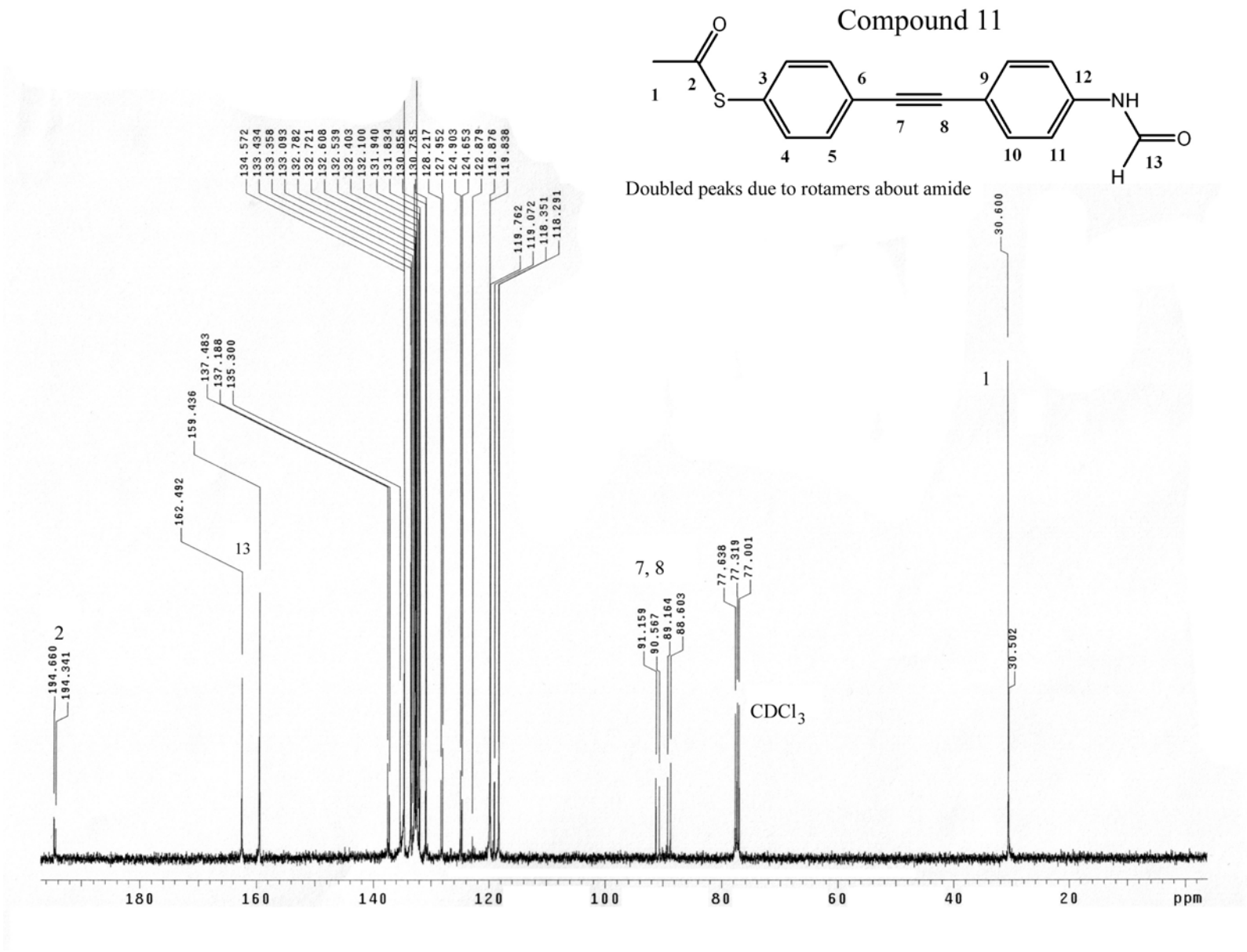

^{1}H NMR for 15

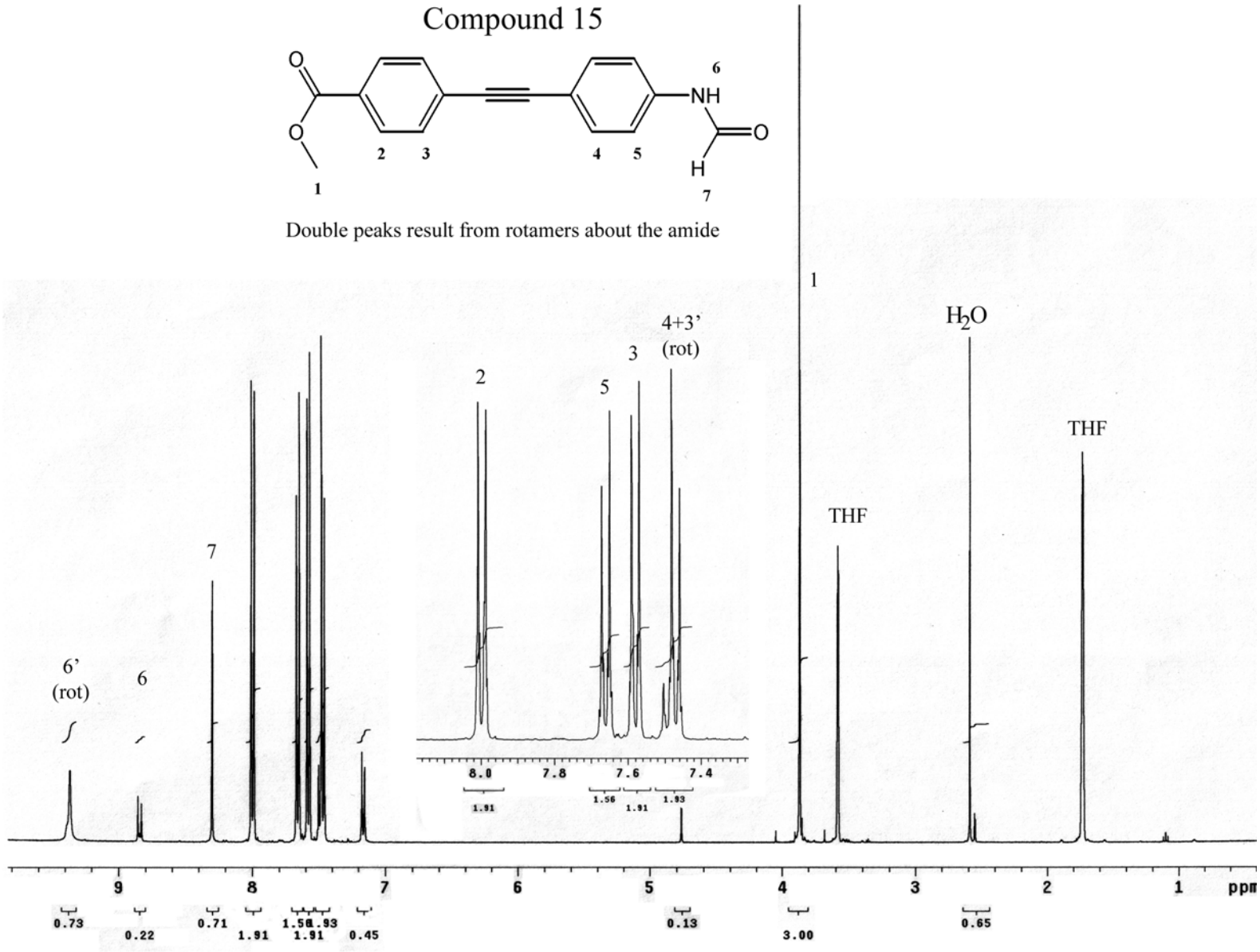
Compound 15
O
O
1
2
3
4
5
NH
6
O
H
7
Double peaks result from rotamers about the amide
6'
(rot)
6
7
2
5
3
4+3'
(rot)
1
THF
H2O
THF
8.0
7.8
7.6
7.4
1.91
1.56
1.91
1.93
9
8
7
6
5
4
3
2
1
ppm
0.73
0.22
0.71
1.91
1.91
0.45
0.13
3.00
0.65

^{13}C NMR for 15

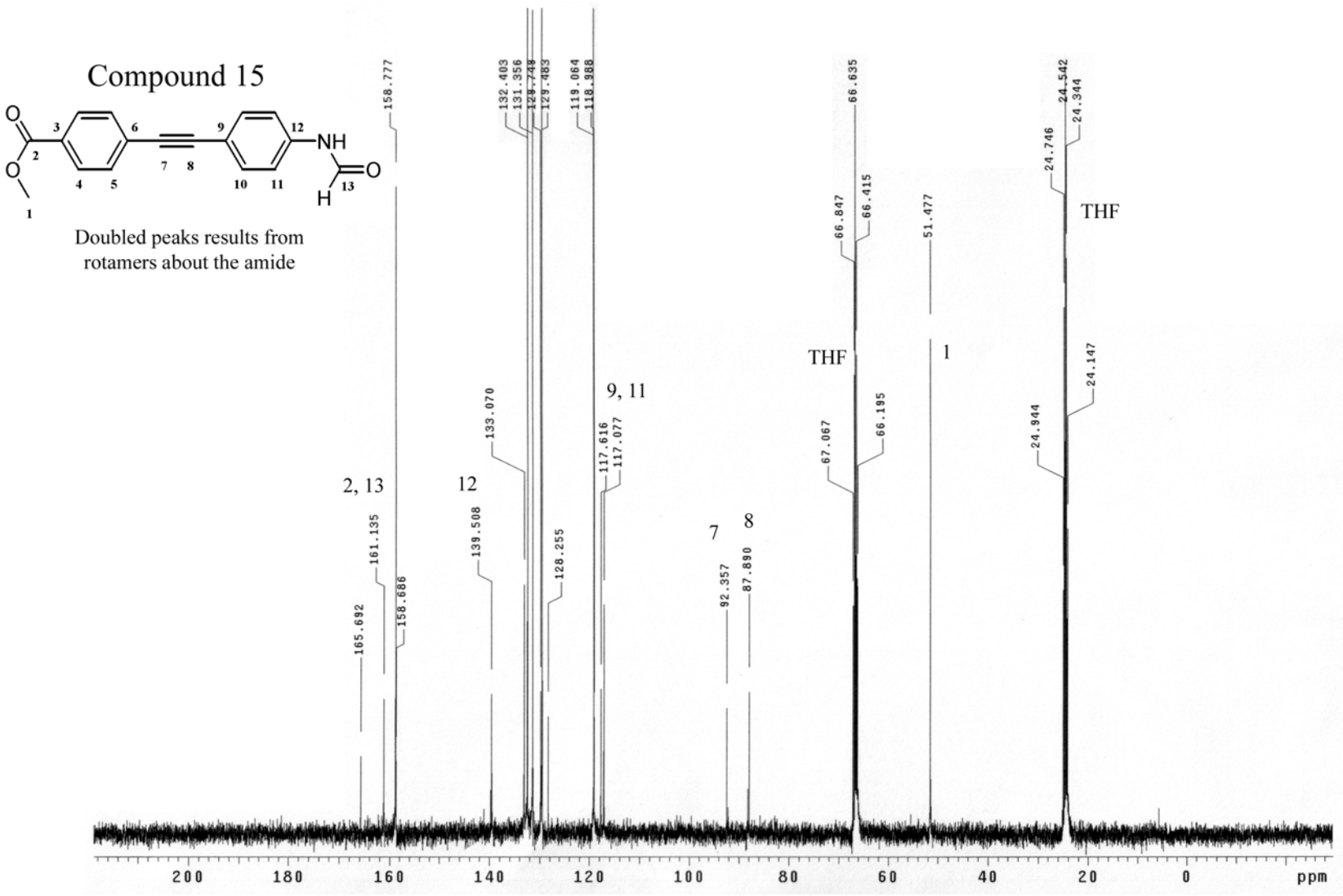

^{1}H NMR for 16

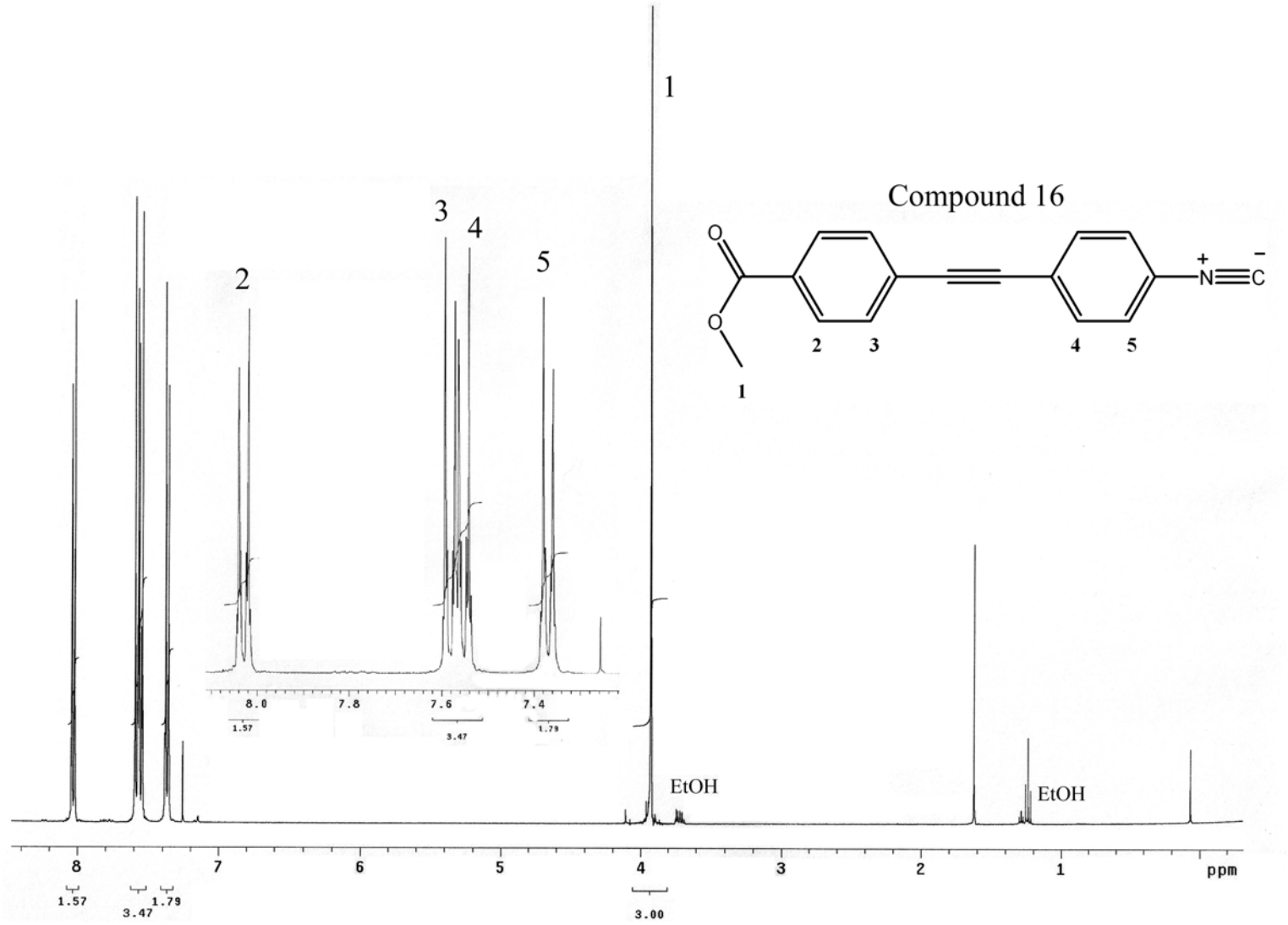

^{13}C NMR for 16

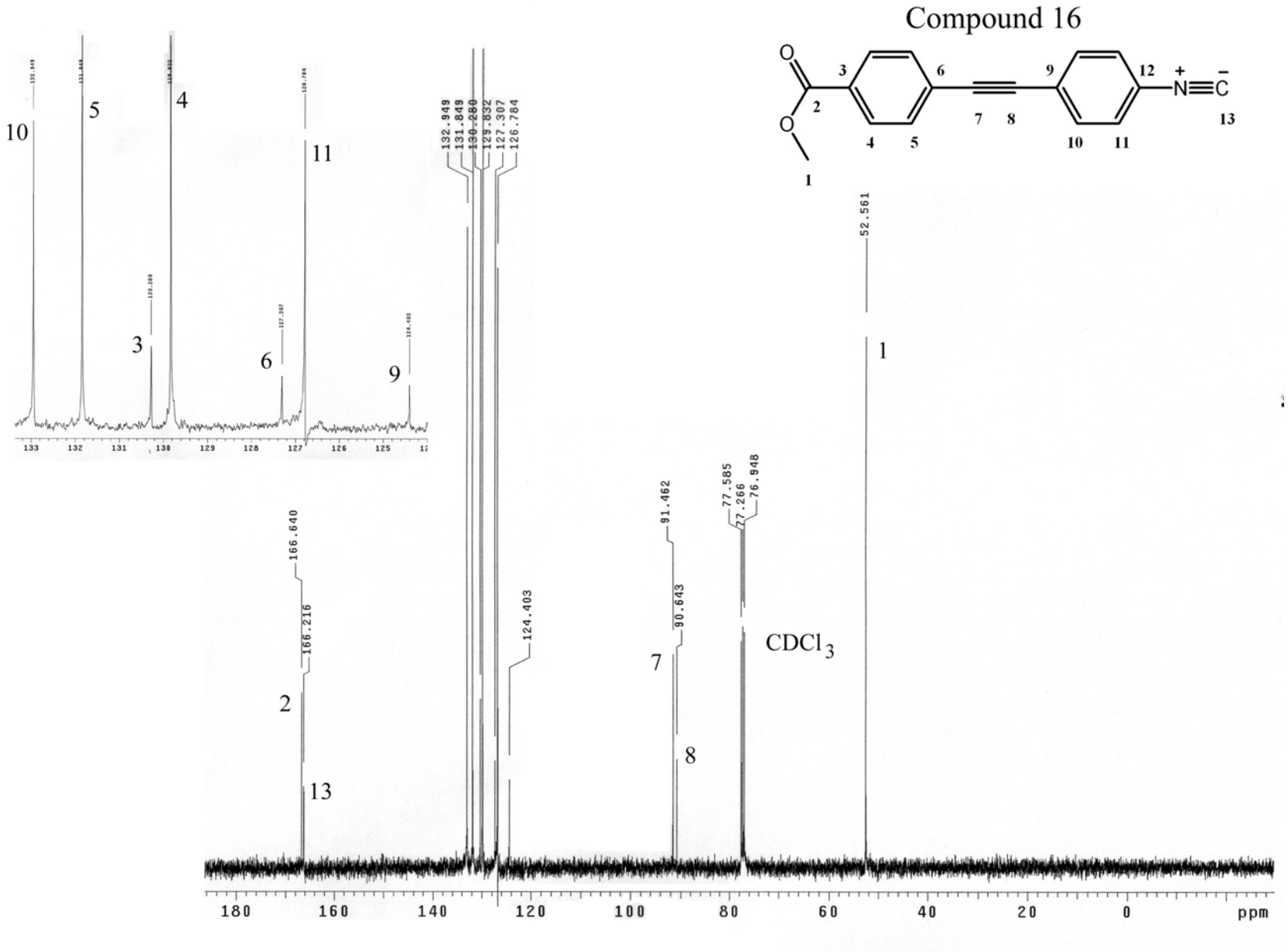

^{1}H NMR for 17

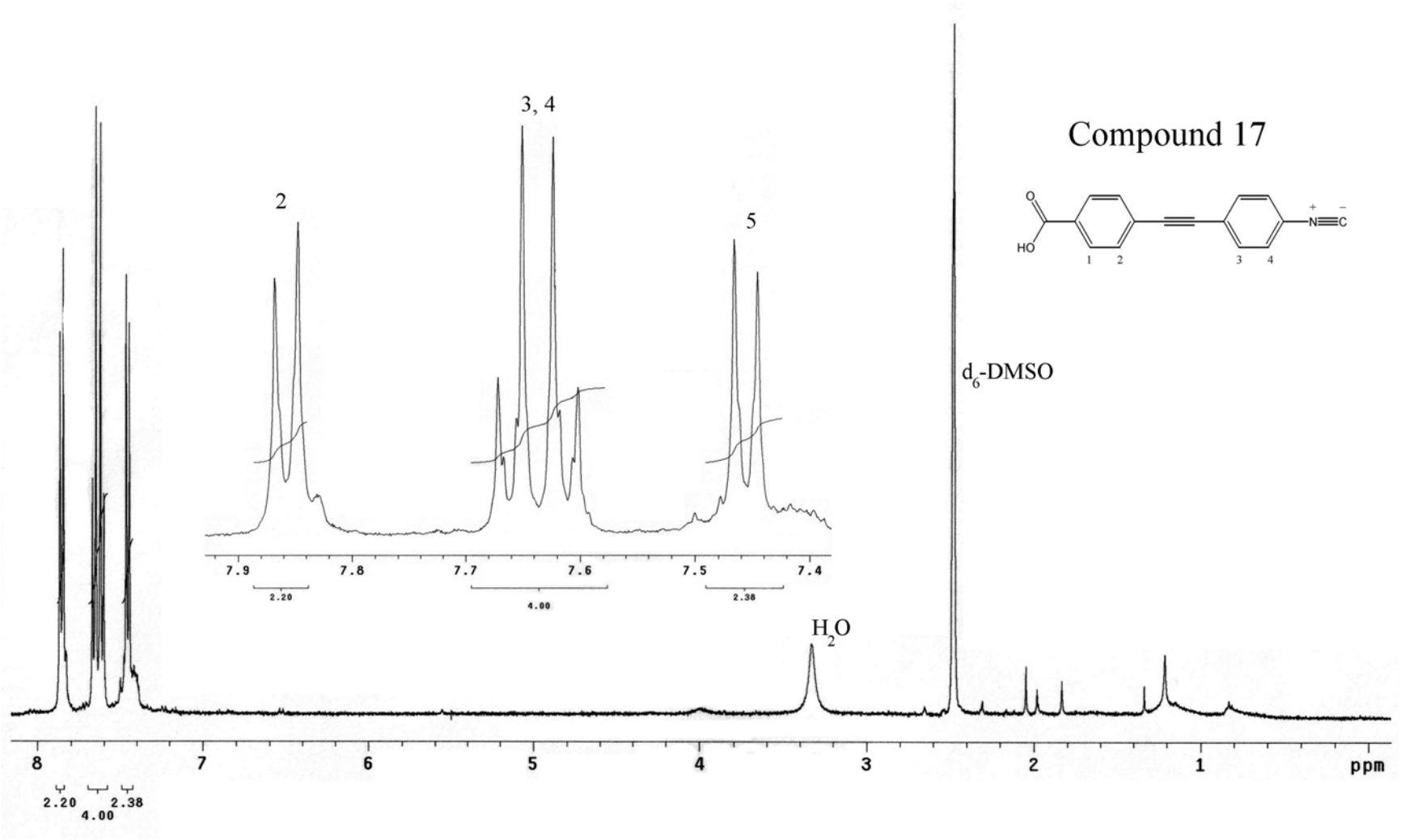

^{13}C NMR for 17